Production of Bio-Composite Filament using Lignin, Polylactic Acid and High Impact Polystyrene for Additive Manufacturing (3D Printing)

by

Sanjita Wasti

A thesis submitted to the Graduate Faculty of
Auburn University
in partial fulfillment of the
requirements for the Degree of
Master of Science

Auburn, Alabama
August 8, 2020

Keywords: 3D printing, fused deposition modeling (FDM), bio-composites, polylactic acid (PLA), lignin, high impact polystyrene (HIPS)

Approved by

Sushil Adhikari, Chair, Professor, Department of Biosystems Engineering
Maria Auad, Professor, Department of Chemical Engineering
Brian Via, Professor, School of Forestry and Wildlife Sciences
Eldon Triggs, Lecturer, Department of Aerospace Engineering

Abstract

Petroleum-based plastics, which are excessively used, are non-biodegradable, and lead to environmental pollution. Plant-based bio-products, on the other hand, are abundantly present, sustainable but are less exploited and valued. Lignin is the most promising plant-based polymer which is obtained relatively in a large amount as by-product from pulp-paper industry but have low market value. Additive manufacturing, also known as 3D printing, is rapidly growing manufacturing technology where a three-dimensional object is created by the application of material layer by layer. The main objective of this study was to incorporate lignin in two different polymers namely polylactic acid (PLA) and high impact polystyrene (HIPS) to develop composite filaments that can be used for 3D printing and to study the effect of lignin on the properties of filaments.

In the first part of this study, lignin and PLA were added at different ratios to develop filaments. Characterization of those PLA-lignin filaments were performed using thermogravimetric analysis, differential scanning calorimetry, tensile test of filaments, scanning electron microscopy and dynamic mechanical analysis. Till 20 wt.% lignin was incorporated in PLA matrix; however, there was significant decrease in tensile strength and elongation at maximum load compared to that of pure PLA filaments. To further improve the mechanical properties of those filaments, two plasticizers namely PEG 2000 and struktol® TR451 were added separately in varying ratio in PLA and 20 wt.% lignin mixture (PLA_L20 hereafter) and similar characterizations were done. A 2 wt% of PEG in PLA_L20 showed significant improvement in mechanical properties. On the other hand, struktol did not show significant enhancement in tensile stress at maximum load of PLA_L20 composite.

In the second part of the study with HIPS and lignin, 5, 10, 15 and 20 wt.% of lignin were extruded with HIPS to develop the filaments. Similar to the first part of the study, thermal, mechanical, and morphological properties were studied in addition to the flame-retardant. Filaments till 10 wt.% addition of lignin had similar mechanical properties as that of lignin; however, on further increasing lignin to 20wt.%, tensile strength and elongation at break were degraded. Additionally, adding unmodified lignin did not contribute to flame resistance of HIPS.

Overall, this research provides the prospect of utilizing lignin as a filler material for 3D printing when mixed with polymers such as PLA and HIPS. This could contribute to the lignin valorization. However, lignin cannot be blended at higher amount without compromising mechanical properties of biocomposites.

Acknowledgments

I would like to express my deepest gratitude towards my supervisor, Dr. Sushil Adhikari, for providing an opportunity to pursue master's degree in his research group. His support, encouragement and guidance have helped me take better decision and grow as a researcher throughout my study. I am really grateful to have him as my mentor. Besides, I would also like to thank my committee members: Dr. Maria Auad, Dr. Brian Via, and Dr. Eldon Triggs for sharing their expertise and knowledge in the research topic.

I must acknowledge Dr. Maria Auad and Dr. Ramsis Farag for letting me use their laboratories as well as helping me to operate different instruments used for this research. I would also like to acknowledge Dr. Oladiran Fasina for allowing and training me to use his particle sizer analyzer and differential scanning calorimeter. I am thankful to Dr. Dilpreet Bajwa for letting me use his extruder at North Dakota State University, and Dr. Jamileh Shojaeiarani for helping and training me to use the extruder to prepare initial samples from polylactic acid and lignin. I am grateful to my colleagues and friends at Biological Engineering Research Laboratory (BERL) and Center for Polymer and Advanced Composites (CPAC) for their help and support during my research. I must acknowledge Attis Innovation, LLC for providing organosolv lignin required for the research. Furthermore, this research would have been incomplete without the support of funding agency. Therefore, I would like to acknowledge Auburn University- Intramural Grant Program (IGP) grant for supporting this research.

Last but not the least I would like to thank the most important people of my life: my mom, dad and my brother for their unconditional love, care, and support. You guys always had faith on me, supported each step that I took in my life and encouraged me to follow my dreams.

Table of Contents

List of Tables

List of Figures

List of Abbreviations

FDM	Fused deposition modeling
PLA	Polylactic acid
HIPS	High impact polystyrene
ABS	Acrylonitrile butadiene styrene
DSC	Differential scanning calorimetry
TGA	Thermogravimetric analysis
SEM	Scanning electron microscopy
DMA	Dynamic mechanical analysis
FTIR	Fourier transform infrared spectroscopy
PEG	Polyethylene glycol
ASTM	American society for testing and materials
STL	Standard tessellation language
CAD	Computer-aided design
s	Second
wt%	Weight percent
mm	Millimeter
μm	Micrometer
mm/s	Millimeter per second
mg	Milligram
mL/min	Milliliter per minute
°C/min	Degree Celsius per minute

Tg	Glass transition temperature
Tcc	Cold crystallization temperature
Tm	Melting temperature
Hcc	Cold crystallization enthalpy
Hm	Melting enthalpy
kN	Kilonewton
mm/min	Millimeter per minute
E’	Storage modulus
E”	Loss modulus
kV	Kilovolt
MPa	Megapascal
GPa	Gigapascal

Chapter 1

Introduction

Additive manufacturing is a rapidly growing manufacturing technology that is expected to grow form $6 billion in 2016 to $21 billion by 2021 [1]. It is a sustainable and efficient manufacturing technology in which any shape of three dimensional object is created by depositing materials layer by layer [2–4]. Among different 3D printing techniques, fused deposition modeling (FDM) is the most commonly used techniques that requires solid thermoplastic filament as a feedstock for printing purpose [5]. Most of the thermoplastic filaments used are petroleum-based, and emit greenhouse gases which are hazardous to environment as well as human health [6]. Different biomaterials such as wood flour [7], rice straw [8], lignin [9–11], cocoa shell [5] have been added in polymer matrix as a filler to reduce the usage of polymer, to decreases the cost of filaments and to improve the properties of filaments. Among those biomaterials, lignin is the second most abundant plant-based polymer, obtained relatively in large amount as the byproduct from pulp-paper and potentially from the 2nd generation bio-ethanol industries. The main problem of incorporating unmodified lignin in polymer matrix is that increase in lignin content leads to the decrease in mechanical properties of filaments [9–11].

The first part of this study was to incorporate lignin in polylactic acid (PLA) matrix; an environment friendly biopolymer; and to develop a composite filament for 3D printing that has better properties and printability. Several studies were done on developing biocomposite filaments using different types of lignin with PLA [11–13]. From the studies carried out, it was found that mechanical properties of PLA were degraded on adding lignin. The degraded properties of PLA-lignin composite filaments were the reason behind lack of successful commercialization of such

filaments. Studies have shown that adding different additives such as plasticizers, carbon fibers, compatibilizers helps in improving the properties of composite filaments. The main hypothesis of this study is that plasticizer can improve mechanical properties of PLA-lignin composite filaments.

The second part of this study was to incorporate lignin in high impact polystyrene (HIPS) to develop composite filaments for 3D printing. Several studies were carried out focusing on incorporating lignin with petroleum-based polymers however none of them were on HIPS. The main hypothesis of the study with HIPS-lignin is that lignin can improve the fire-retardant properties of HIPS filaments.

1.1 Objectives

The main objective of this research was to incorporate lignin in polymer matrix to develop composite filaments for 3D printing. Two different polymer matrices, PLA and HIPS, were selected for developing composite filaments. This main objective was achieved by accomplishing four specific objectives mentioned below.

1.1.1 To determine the effect of organosolv lignin in PLA filaments and object printed from the filament.

A 5, 10, 15 and 20 wt% of lignin was added in the PLA and the PLA-lignin mixtures were extruded to obtain the filaments. The effect of lignin in thermal, mechanical, and morphological properties of PLA were determined using differential scanning calorimetry (DSC), thermogravimetric analysis (TGA), tensile test of filaments and scanning electron microscopy (SEM), respectively. Dynamic mechanical analysis (DMA) was performed to determine the viscoelastic properties of 3D printed samples. Fourier transform infrared spectroscopy (FR-IR) was performed with the samples to determine the change in molecular structure on adding lignin.

1.1.2 To determine the effect of PEG 2000 in PLA-lignin composite filament and in the object printed from that filament.

Different amounts of polyethylene glycol (PEG-0.25, 0.5, 0.75, 1, 2, 3, 4 and 5 wt%) were added in PLA-20wt% lignin mixer, and the sample were extruded to obtain filaments. To determine the effect of PEG in mechanical properties of PLA-lignin composite, tensile test of filaments was carried out. DSC and TGA of filaments were performed to determine the effect in thermal properties whereas the effect of PEG in the morphology of PLA-lignin composite filaments was determined using SEM. To determine the effect of PEG in viscoelastic properties of 3D printed samples, DMA was performed.

1.1.3 To investigate the effect of struktol® TR451 in the PLA-lignin composite filament and in the object printed from that filament.

Varying composition of struktol from 0.25 to 1 wt% was added in PLA-lignin (20 wt%) composite and the mixers were extruded through twin extruder to obtain the filaments. Tensile test of filaments, DSC, TGA and SEM were carried out to determine the effect of struktol in mechanical, thermal, and morphological properties. As in the case of PEG, filaments were printed, and DMA was performed to determine the viscoelastic properties of the PLA-lignin-struktol composites.

1.1.4 To determine the effect of organosolv lignin in HIPS filaments and object printed from the filaments.

Varying concentration of lignin (5, 10, 15 and 20wt%) were added in HIPS and the manually mixed samples were extruded through twin extruder to develop filaments for 3D printing. The effect of lignin in mechanical properties of HIPS were determined by performing tensile test of the filaments. Effect on thermal and morphological properties on adding lignin were determined

using DSC, TGA and SEM respectively. Flame test was also performed to determine the flame-retardant properties of sample on adding lignin.

1.2 Thesis outline

Chapter 2 of this thesis presents the literature review of different biomaterials used for 3D printing by FDM technique whereas detailed study of PLA-lignin, PLA-lignin-PEG and PLA-lignin-struktol composite filaments are discussed in Chapter 3. Summary of experimental details, results and discussion of HIPS-lignin composite are discussed in Chapter 4. Finally, the conclusion and recommendations of the overall study are presented in Chapter 5.

1.3 References

[1] Chiulan I, Frone A, Brandabur C, Panaitescu D. Recent advances in 3D printing of aliphatic polyesters. Bioengineering 2017;5:2. https://doi.org/10.3390/bioengineering5010002.

[2] Wimmer R, Steyrer B, Woess J, Koddenberg T, Mundigler N. 3D printing and wood. Wood Sci. Eng. Third Millenn., vol. 10, 2015, p. 145–50. https://doi.org/10.13140/RG.2.1.2483.6563.

[3] Meteyer S, Xu X, Perry N, Zhao YF. Energy and material flow analysis of binder-jetting additive manufacturing processes. Procedia CIRP 2014;15:19–25. https://doi.org/10.1016/j.procir.2014.06.030.

[4] Ou-Yang Q, Guo B, Xu J. Preparation and characterization of poly(butylene succinate)/polylactide blends for fused deposition modeling 3D printing. ACS Omega 2018;3:14309–17. https://doi.org/10.1021/acsomega.8b02549.

[5] Tran TN, Bayer IS, Heredia-Guerrero JA, Frugone M, Lagomarsino M, Maggio F, et al. Cocoa shell waste biofilaments for 3D printing applications. Macromol Mater Eng 2017;302:1–10. https://doi.org/10.1002/mame.201700219.

[6] Kim Y, Yoon C, Ham S, Park J, Kim S, Kwon O, et al. Emissions of nanoparticles and gaseous material from 3D printer operation. Environ Sci Technol 2015;49:12044–53. https://doi.org/10.1021/acs.est.5b02805.

[7] Tao Y, Wang H, Li Z, Li P, Shi SQ. Development and application of wood flour-filled polylactic acid composite filament for 3d printing. Materials (Basel) 2017;10:1–6. https://doi.org/10.3390/ma10040339.

[8] Osman MA, Atia MRA, Osman MA, Atia MRA. Investigation of ABS-rice straw composite feedstock filament for FDM. Rapid Prototyp J 2018;24:1067–75. https://doi.org/10.1108/RPJ-11-2017-0242.

[9] Nguyen NA, Bowland CC, Naskar AK. A general method to improve 3D-printability and inter-layer adhesion in lignin-based composites. Appl Mater Today 2018;12:138–52. https://doi.org/10.1016/j.apmt.2018.03.009.

[10] Nguyen NA, Barnes SH, Bowland CC, Meek KM, Littrell KC, Keum JK, et al. A path for lignin valorization via additive manufacturing of high-performance sustainable composites with enhanced 3D printability. Sci Adv 2018;4:eaat4967. https://doi.org/10.1126/sciadv.aat4967.

[11] Gkartzou E, Koumoulos EP, Charitidis CA. Production and 3D printing processing of bio-based thermoplastic filament. Manuf Rev 2017;4:1. https://doi.org/10.1051/mfreview/2016020.

[12] Mimini V, Sykacek E, Hashim SNA, Holzweber J, Hettegger H, Fackler K, et al. Compatibility of kraft lignin, organosolv lignin and lignosulfonate with PLA in 3D printing. J Wood Chem Technol 2019;39:14–30. https://doi.org/10.1080/02773813.2018.1488875.

[13] Tanase-Opedal M, Espinosa E, Rodríguez A, Chinga-Carrasco G. Lignin: A biopolymer from forestry biomass for biocomposites and 3D printing. Materials (Basel) 2019;12:1–15. https://doi.org/10.3390/ma12183006.

Chapter 2

Literature review

Three-dimensional (3D) printing is a revolutionary manufacturing technique that can fabricate a 3D object by depositing materials layer by layer. Among different 3D printing technologies, fused deposition modeling (FDM) is considered as the most commonly used 3D printing technique that uses thermoplastic filaments for printing purpose. Polylactic acid (PLA) is the commonly used biobased thermoplastic filaments for FDM printing. However, its high cost and some properties limits its application in several fields. This study is mainly focused in incorporating lignin, a second most abundant plant-based polymer, in PLA in order to reduce the usage of PLA and filament cost; and, to improve the properties of PLA-lignin composite filaments by adding plasticizers. 3D printing technology, FDM technology, PLA, PLA and PLA composites in 3D printing, lignin, polymer-lignin composites in 3D printing are discussed in detail in following sections.

2.1 Three-dimensional printing (3D printing)

Three-dimensional (3D) printing, also known as additive manufacturing, is transforming manufacturing technology at an amazing rate. It is an emerging technology implemented in different sectors such as research, automotive, aerospace, healthcare and medical, architecture and construction, fashion industries and food industries [1–11]. Interest in 3D printing has greatly increased since 2013, and is expected to grow from $6 billion in 2016 to $21 billion by 2021[4] due to its unique advantages such as freeform fabrication, sustainable, and efficient manufacturing, shorter time from design to production as compared to subtractive or traditional manufacturing technology [12–14]. In traditional manufacturing such as milling, grinding and machining; products are fabricated by removing materials from large stock or sheet that may not be able to

meet the requirement of small and highly complex products. This drawback of traditional manufacturing is overcome by 3D printing process as it fabricates highly complex parts by adding the materials layer by layer with minimum waste. Even after having many advantages over traditional manufacturing, poor mechanical properties, anisotropic nature of printed parts, and limited availability of materials limit its application in large scale and various industries [15]. Figure 2.1 shows the conceptual comparison between traditional and additive manufacturing processes.

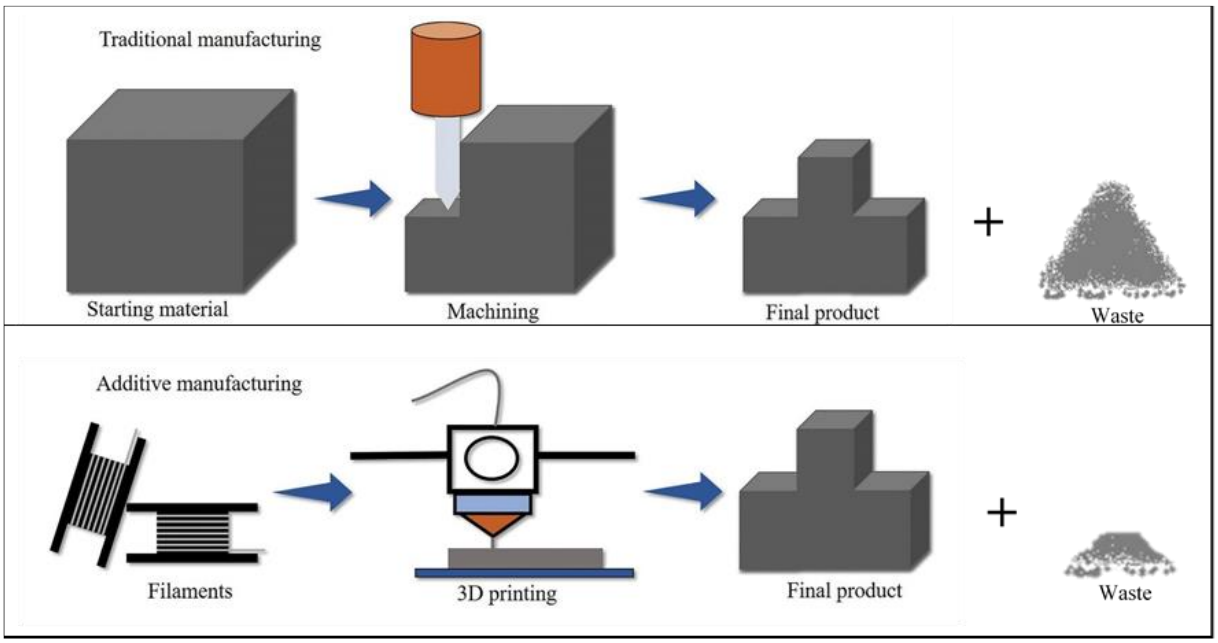

Figure 2.1 Conceptual comparison of traditional and additive manufacturing [16]

Figure 2.2 depicts steps during the 3D additive manufacturing process. The first step of 3D printing is creating a three-dimensional object in Computer Aided Design (CAD) software and converting it into the standard format of STL (Standard Tessellation Language). This file is then used in slicing software that slices the object in different layers. We can also change different printing parameters such as material deposition plane, number of envelopes of the parts and their thickness

and filling patterns. The file obtained from slicing software is then used in a printer to print a final object.

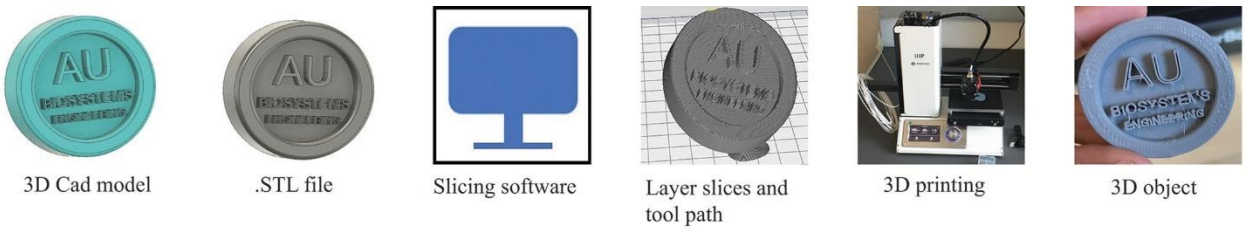

Figure 2.2 Process of 3D printing [12,17]

First 3D printing process developed was stereolithography (SLA) by Charles Hull in 1986 [15]. Till date, there are many 3D printing processes, which have been categorized into major seven groups by the American Society for Testing and Materials (ASTM) as shown in Table 2.1 [18,19].

Table 2.1 Additive manufacturing process category based on ASTM[18–21]

Process Category	**Description**	**Technologies**	**Materials**	**Pros**	**Cons**
Binder jetting	Inorganic or organic binders are used to bind powder materials	BJ, PBIH, PP	Polymers, metals, sand, bio-based materials	Variety of materials can be used, high precision, colored parts	Requires post curing, printed objects are less strong
Direct energy deposition	Materials are fused by melting them using thermal energy.	LMD, DALM, DMD, LDD	Metals	Used to produce high quality and functional parts	Limited material can be used, poor surface finish and accuracy
Materials extrusion	A certain size of filament is made to pass through feeding roller, heater and nozzle to print object layer by layer.	FDM	Polymer-based materials	Low machine cost, easy handling of materials, no post curing	Poor surface finish and accuracy, slow processing for large parts, anisotropic

					nature of printed parts
Material jetting	Droplets of build material are selectively deposited.	MJM	Polymers, waxes	Single part can be produced from multiple materials having different characteristics and properties, very precise and smooth surface finish	Requires support materials, expensive technology
Powder bed fusion	Thermal energy is used to fuse powder bed region.	EBM, SLS, SLM, DMLS, SHS	Metals, polymers	Does not require support structure, can produce complex parts	Poor surface finish
Sheet lamination	Sheets of material are bonded to form an object.	LOM, UC	Metals, paper	Low cost, ease of material handling, high speed	Limited material use, requires post processing
Vat photo-polymerization	Liquid photopolymer in a vat is selectively cured by light-activated or ultraviolet polymerization.	SLA, DLP	Photo-polymers	Good surface finish, can fabricate the very accurate and complex design	Support structure needed, requires post curing and post processing

BJ = binder jetting, PBIH = powder bed and inkjet head, PP= plaster based 3D printing, LMD = laser metal deposition, DALM = direct additive laser manufacturing, DMD = direct metal deposition, LDD = laser direct deposition, FDM = fused deposition modeling, MJM = multijet modeling, EBM = electron beam melting, SLS = selective laser sintering, SLM = selective laser melting, DMLS = direct metal laser sintering, SHS= selective heat sintering, LOM = laminated

object manufacturing, UC = ultrasonic consolidation, SLA = stereolithography (apparatus), DLP = digital light processing.

2.1.1 Fused Deposition Modeling

Among different types of additive manufacturing process, FDM or Fused Filament Fabrication (FFF) is rapid, versatile, low cost, and mostly used 3D printing technique which fabricates complex shaped part easily and promptly [22]. In FDM, a well-shaped thermoplastic filament is heated into the semi-liquid state, which is extruded through the nozzle and deposited layer by layer onto the build platform. The deposited layers fuse together and solidify to form the required final object [15,23].

Most commonly used thermoplastic materials are polylactic acid (PLA) [24,25], poly(ε-caprolactone) (PCL) [22,26,27], ethylene vinyl acetate (EVA) [28], polyamides [29], and acrylonitrile butadiene styrene (ABS) [30,31]. Chaunier et al.[32] mentioned that the polymers which have processing temperature higher than transition temperature and lower than degradation temperature with the rigidity of ≥ 1 GPa can be used for FDM application. The major drawbacks of FDM technique are poor parts and anisotropic mechanical properties, poor surface quality, high hygroscopic sensitivity, need for supports and limited thermoplastic material as feedstock. However, drawbacks like poor mechanical properties and surface finish can be improved by changing several processing parameters such as build direction, printing temperature, feed rate, layer thickness, raster angle, raster width, infill density and pattern [4,33–35]. Therefore, researchers are focusing on different printing parameters to minimize the shortcomings of this method.

Most of the materials used as filament for FDM are not environment-friendly since they are petroleum-based and could release toxic substances during printing process, which has an adverse effect on health and environment [36]. Hence, research regarding the development of biobased filament for FDM is gaining a lot of attention which not only helps to reduce the use of petroleum-derived plastic but also reduces the cost of filament.

2.2 Poly-Lactic Acid (PLA)

PLA is the most commonly used bioplastic [4], derived from the starch of agricultural plants such as corn, sugarcane, sugar beets, wheat [37,38]. PLA is one of the most studied thermoplastic aliphatic polyesters formed from ring-opening polymerization of lactide or polycondensation of lactic acid monomer [4,39]. Figure 2.3 represents the chemical structure of PLA. PLA can be found in semi crystalline or amorphous grade. Pure poly (l-lactic acid) (PLLA) or poly (D-lactic acid) are semi crystalline whereas PLA with 50–93% L-lactic acid is amorphous. Amorphous PLA exhibits better processability but poor mechanical properties as compared to crystalline [4]. PLA is ;, bio-compatible, user-friendly and can be easily processed with no toxic fumes [39,40]. It is found to be used for packaging and fabrication of several biomedical devices such as orthopedic implants, drug delivery systems, surgical sutures, and tissue engineering scaffolds [4,39]. Properties of PLA such as low glass transition temperature (Tg = 60 ℃-65 ℃), melting temperature (Tm= 173 ℃ - 178 ℃), lower coefficient of thermal expansion and property of non-adherence to the printing surface makes it a promising thermoplastic for 3D printing purpose [4,37]. However, low thermal stability, high degradation rate during processing, brittle in nature, low toughness, moisture sensitivity and high cost limit its application [4,38,40,41].

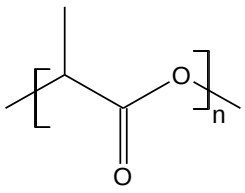

Figure 2.3 Chemical structure of PLA

2.2.1 3D printing of PLA

Jo et al.[42] used PLA filament to 3D print objects and investigate the effect of layer thickness, externally applied heat and pressure in FDM printed 3D object. The authors found that layer thickness directly affects mechanical properties of the printed object, and these properties could be improved on thermal heating. The authors also noticed that on heating printed object having small layer thickness, tensile strength, and elastic modulus were enhanced. This was due to the improvement in the bond between raster to raster and layer to layer. Applying higher external pressure had a similar improvement in tensile strength and modulus of the printed object. Further, Jo et al.[42] mentioned that controlling layer thickness, external heat and pressure helped in reducing the void in the internal structure of the printed object and creating an object of better finish and improved mechanical properties. Similarly, Rajpurohit et al.[43] studied the effect of raster angle, layer height and raster width on tensile properties of FDM printed PLA parts where they found highest tensile strength at 0^{o} raster angle. Those samples which had lower layer height exhibited higher tensile strength because of the larger bonding area. The authors also observed higher tensile strength of sample having higher raster width to a certain extent but after that, it decreased due to the void formation which helped in crack initiation and propagation. Other authors Yang et al.[44] used FDM PLA printed parts to investigate the effect of nozzle diameter, liquefier temperature, extrusion velocity, filling velocity and layer thickness on tensile strength, surface roughness and build time of printed parts. Results obtained indicated that nozzle diameter

and layer thickness are the most influencing factors on tensile strength, surface roughness and build time of printed parts. The authors also found that with larger nozzle diameter, high extrusion, filling velocity and larger layer thickness, tensile strength and surface roughness of printed parts increased noticeably, whereas there was less effect of liquefier temperature and extrusion velocity on surface roughness. Yang et al.[44] have further noted the reduction in build time with increment in nozzle diameter, filling velocity and layer thickness. Furthermore, Alafaghani et al.[45] looked at the effect of process parameters such as building direction, printing speed, extrusion temperature, layer height, infill percent and infill patterns on mechanical properties and dimensional accuracy of FDM printed PLA specimens. They concluded that building direction, extrusion temperature, layer height were more influencing parameters compared to infill percentage, infill pattern and printing speed on dimensional accuracy and mechanical properties. For the three-dimensional print parts of higher dimensional accuracy, the direction of the part should be parallel to layer orientation instead of building orientation, accompanied by lower layer height and extrusion temperature. Crystallinity, thermal resistance, modulus and strength of FDM printed PLA sample could also be increased by increasing bed temperature [46]. Benwood et al.[46] mentioned that in order to maximize the bond strength between deposited layers, bed temperature needs to be above the glass transition temperature.

Another group, Afrose et al.[47], studied the effect of build orientation on the fatigue behavior of PLA parts made by the FDM method. The parts which had X- build orientation exhibited higher tensile strength than Y and 45^{o}-build orientation under static loading. Under tensile loading, fatigue life was higher for PLA specimen with 45^{o}-build orientation and higher ability to store strain energy by part.

On comparing 3D printed PLA with injection molded PLA in terms of the mechanical response, Song et al.[48] found that 3D printed specimen had improved toughness because of their layered and filamentous nature. Additionally, the 3D printed specimen had increased crystallinity and reduced ductility.

From all these papers related to FDM printing of PLA, it was found that research with PLA was mostly done to investigate the effect of process parameters of FDM printing. Some parameters such as layer thickness, build direction, raster angle, raster width, infill density, extrusion temperature and bed temperature strongly affected the mechanical properties while extrusion speed, printing speed and infill pattern had no significant effect in mechanical properties. In all these research, different types of printers were used which were compatible with different slicing software and process condition. Therefore, it will be unfair to generalize and conclude based on their results. For generalization and comparison among different research scenario, standard set of conditions and parameters need to be developed for FDM printers and FDM printed test specimens.

2.2.2 3D printing of PLA composites

Production of PLA requires precise reaction conditions such as temperature and pressure which accounts for higher energy consumption. In addition to that, corn-based PLA has led to increasing concern over the food crisis. Adding fillers to PLA will not only decrease the amount of PLA usage and address the concern to the food crisis, but also reduce the cost as compared to the use of neat PLA. Poor thermal and mechanical properties of PLA limits it for many engineering application [49]. Chiulan et al.[4] also mentioned that PLA is not able to mimic nature (e.g. native bone architecture, cell colonization) properly. Therefore, to widen its applicability for both engineering and biomedical applications, it needs to be mixed with fillers.

Tao et al.[2] developed composite filament of PLA and 5 wt % of wood flour (WF) of particle size 14 μm for printing 3D object by FDM technique. Object printed from composite filament appeared like that of the wooden object as compared to that made from pure PLA filament. Due to the hydrophilic nature of WF and hydrophobic nature of PLA, there was a poor interfacial bond which resulted in clear gaps between PLA and WF interface. Moreover, the particle size of wood powder or any other material to be blended with PLA should be ultra-fine in order to prevent nozzle blocking during printing [12]. Also, wood particle properties and its compatibility with thermoplastic polymer should be taken into consideration as it affects properties of wood polymer composite filament [50]. Additionally, there will be variation in the properties of composite filament with variation in wood content. Kariz et al.[50] found that increasing wood concentration resulted in decreased filament density. There was a slight increase in tensile strength with a 10% increase in wood content, but the further increment of wood content led to decreased tensile strength. Guo et al.[51] got the similar result of poor mechanical properties with increase in poplar WF content in PLA. They explored different toughening agents for PLA/WF composite filament, namely thermoplastic polyurethane (TPU), polycaprolactone (PCL) and poly (ethylene-co-octene) (POE) and found that among all, TPU relatively showed better compatibility with PLA/WF composite. They also mentioned that impact strength, tensile strength, ductility, complex viscosity and storage modulus of the composite were increased. Ayrilmis[52] studied the effect of layer thickness on surface roughness and wettability of 3D printed object prepared from PLA/WF filament and found a direct impact of layer thickness on both properties. It was observed that with the increase in layer thickness, both surface roughness and wettability increased for the 3D printed object from PLA/WF filament.

Another group, Daver et al.[53], successfully developed a composite filament of PLA and 5 wt% cork for FDM application. It was found that the increase in cork content from 0 to 50 wt.%, the tensile strength, elastic modulus and elongation at break was decreased from 60 MPa to 10 MPa, 3.35 GPa to 1 GPa and 1.53% to 0.15%, respectively. On the other hand, impact strength decreased initially and increased on further addition of cork. Further addition of a biodegradable plasticizer named tributyl citrate (TBC), ductility of the composite was enhanced but their strength and modulus were decreased. On the comparison between 3D printed specimen and compression molded specimen made from cork-PLA composite, it was found that 3D printed specimen had a higher elongation at break than later. However, their elastic modulus and tensile strength were lower than compression molded.

Murphy et al.[54] worked on development of fully degradable biocomposite filaments for FDM application from microcrystalline cellulose (MCC) and PLA. They found that with the addition of MCC from 1-3 wt.%, the crystallinity of PLA and storage modulus of biocomposite was increased. Dong et al.[55] extruded composite filament for FDM application from neat PLA and poly(lactic acid) grafted cellulose nanofibers (PLA-g-CNFs) where PLA-g-CNFs was prepared by grafting L-lactide monomers on cellulose nanofibers (CNFs). The composite filament had improved storage modulus due to the incorporation of PLA-g-CNFs. Highest elastic modulus and tensile strength of 2.800 GPa and 39 MPa, respectively were obtained at 3 wt % of PLA-g-CNFs. The authors also revealed that on annealing the extruded composite filaments, the crystallinity of composite filament was increased, which led to enhancement in mechanical properties.

Xu et al.[39] applied solvent blending approach to uniformly blend galactoglucomannan (GGM), hemicellulose type found in softwood, and PLA. This blended composite was used for making filament for FDM application and showed higher storage modulus and decreased thermal stability

than neat PLA. PLA with up to 20 wt % GGM exhibited flexural modulus similar to PLA around 3.2 GPa.

Composite filament for 3D printing was developed using PLA and biocarbon, derived from pyrolysis of wheat stems, and processing and wear behavior of printed specimen was studied.[56]. It was found that specimen fabricated from PLA and 30 vol % biocarbon had less wear volume and a high coefficient of friction with fewer fluctuations. They also mentioned that with the increase in vol % of biocarbon in composite, there was an increase in voids in printed samples and difficulty in printing due to nozzle clogging.

Ou-Yang et al.[14] prepared the filament of PLA/poly(butylene succinate)(PBS) blend for 3D printing where they observed that all blends had excellent processing properties. The blends having PLA more than 40 wt % had smooth printing without any distortion or detachment from printing surface, higher tensile strength, modulus, melt viscosity and showed better suitability for FDM. Maximum tensile strength of printed sample was 21 MPa for blend composition PBS/PLA (40/60).

The study of effect of 3D printing direction in thermal and mechanical properties of specimen printed from PLA/polyhydroxyalkanoate (PHA) composite filament revealed that vertically printed specimen had better mechanical properties than horizontally printed specimen [34]. The horizontally printed specimen had longer disintegration time than vertical and degradation was more distinct at 50 ℃. Based on observation, the contact time of specimen with printing platform influenced their crystalline phase, however, additional study concluded that not only specimen's contact time on printing surface affected crystallinity, size of the specimen also played a vitalrole [35]. During the printing process, the specimen having a smaller surface area had increased crystalline phase.

Antoniac et al.[57] extruded the PLA + Mg + vitamin E (α-tocopherol) composed filament of 1.75 mm diameter for manufacturing test samples using the FDM process. They found good integration between Mg and PLA matrix due to the use of vitamin E during material preparation. However, according to the obtained results, authors were not able to guarantee the uniform distribution of Mg with the PLA matrix.

Prashantha et al.[58] studied the 3D printed specimen made up of PLA/graphene nanocomposites containing 10 wt % graphene in the PLA matrix. It was detected that specimen printed from these filaments by FDM technique had improved thermal and mechanical properties compared to object printed from neat PLA filaments. Addition of 10 wt % graphene in PLA increased the modulus and strength of PLA from 1827 to 2454 MPa and 31.6 to 40.2 MPa, respectively. Furthermore, uniform distribution of graphene in the PLA matrix was also found from scanning electron microscopy of the printed object.

Ferreira et al.[59] compared between 3D printed PLA and PLA with carbon fibers (CFs) (reinforced with 15 wt % short CFs of length about 60μm) found that reinforced material had increased stiffness in direction of printing due to the alignment of short carbon fibers in the printing direction. However, they found that on adding short CFs, printed samples turned out to be brittle. Poor adhesion between PLA and CFs was observed possibly due to the shorter length of CFs.

Rasselet et al.[60] found improved tensile properties and ductile behavior of 3D printed object of PLA/Polyamide 11 (PA11) blend, with 3 wt % incorporation of Joncryl, a multi-functionalized epoxide. From the results of SEM of the tensile fracture surface, they observed the improved interfacial adhesion which was due to Joncryl. They observed the maximum tensile strength and elongation at break of 58.8 MPa at 2 wt % Joncryl content and 9.8% at 3 wt % Joncryl content,

respectively. 3D printed samples from PLA/PA11 composite showed brittle nature than that of an injected sample. This was because of poor adhesion and porosity between the deposited layers whereas elastic modulus was higher for FDM printed specimen as compared to injection molded specimen.

To reduce the excess use of PLA and widen its applicability in diverse field, trend of using different fillers with PLA to develop biocomposite filaments have increased. Among all these fillers, WF is the extensively studied and used biomaterial to develop composite filaments. Beside WF, cellulose nanofiber and lignin are other two promising biobased materials which have abundant and sustainable source and needs further research and development. Investigation of several additives should be done to improve composite's properties so that they will be able to replace widely used petroleum-based composite filaments.

2.3 Lignin

Lignin is the second most abundant plant based polymer that acts as a supporting structure for plant cells [61,62]. Lignin has highly heterogenous complex structure. Lignin is basically composed of three types of phenyl propane units in different ratios based on plant species [63,64]. They are coniferyl alcohol, p-coumaryl alcohol, and sinapyl alcohol represented by Figures 2.4, 2.5 and 2.6, respectively.

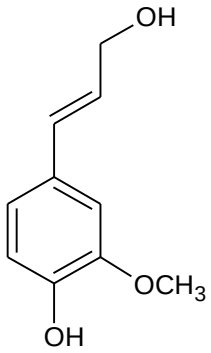

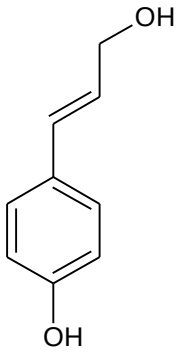

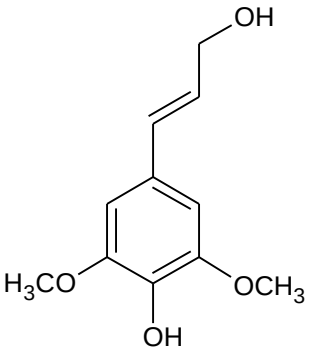

Figure 2.4 Coniferyl alcohol Figure 2.5 Coumaryl alcohol Figure 2.6 Sinapyl alcohol

Its structure and properties basically depends on the source from what it is obtained and how it is extracted [65]. Depending on the sources from where lignin is obtained, it can be classified into three types described below.

- Hardwood lignin – It is derived from deciduous trees like maple and contains both coniferyl alcohol and sinapyl alcohol in different ratios. It is also termed as guaiacyl- syringyl lignin.
- Softwood lignin – It is coniferous tree-based lignin, known as guaiacyl lignin. It is mainly composed of coniferyl alcohol and trace amounts of sinapyl alcohol.
- Grass lignin – It contains all three type of units, but major amount is derived from p-coumaryl alcohol. It is also known as guaiacyl-syringyl lignin.

2.3.1 Lignin extraction process

2.3.1.1 Sulfite process

It is the most commonly used process of extracting lignin. Annually approximately 1000 tons of lignin is produced by this method [63]. In this process, aqueous solution of sulphite or bisulfite salt with counter cations like sodium, ammonium, magnesium, calcium etc. are used and sulphonation reaction takes place between aqueous solution and lignin. The lignin thus formed can be isolated from aqueous solution using different techniques such as precipitation, ultrafiltration, chemical destruction of sugars. Lignin obtained from this process contains sulfur in it.

2.3.1.2 Soda process

Lignin from non-woody biomass is generally extracted using this process. Biomass is added in aqueous solution of sodium hydroxide and is heated to approximately 160 ℃ resulting in lignin depolymerization and formation of free phenolic groups [63]. The lignin obtained from this process does not contains sulfur and is pure than lignin obtained from sulfite process.

2.3.1.3 Kraft process

In this process, biomass is added to a mixture of sodium sulfide and sodium hydroxide and is heated between 150 ℃ and 180 ℃ [63]. Similar to soda process, lignin depolymerization occurs. The lignin, thus, obtained from this process contains sulfur in it. Kraft lignin is not active unless it is modified so it is generally burned to produce energy [66].

2.3.1.4 Organosolv process

In this method, organic solvents or organic acids are used in order to isolate lignin [63]. Besides lignin, cellulose and hemicellulose are also extracted along with. The lignin obtained from this process is highly pure and sulfur free and is also preferred for biomaterial production [66]. Additionally, organosolv process is considered as environmentally friendly process since it does not require condition of high temperature and pressure as other process [63].

Lignin is produced in large scale from pulp and paper industries and bioethanol industries [62,67,68]. Worldwide annual production of lignin is 50 million tons and among this 98% is burnt to generate energy [62,68]. However, the energy value is just 50 US dollars/ton because of low energy content of lignin [62]. Only remaining 2% of annually produced lignin is used for other purposes such as dispersant, carbon nanostructure, feedstock for resins, composites, aerogels, antioxidants [67]. Properties such as high abundancy, low cost, bio-degradability, ecologically

friendliness, high carbon content and reinforcing capacity makes lignin a potential filler for making biocomposites [62,67].

2.3.2 3D printing of polymer/lignin composites

Mimini et al.[41] compared the compatibility of kraft lignin (KL), organosolv lignin (OSL), and lignosulfonate (LS) with PLA in 3D printing by FDM. The mechanical behavior was poor for KL/PLA specimen, whereas OSL/PLA specimen showed higher compatibility as compared to others. KL/PLA and OSL/PLA composites exhibited better thermal resistance as compared to LS. There was no improvement in flexure strength of PLA with the addition of any of that lignin. In the research conducted by Gkartzou et al.[40] using PLA with low-cost kraft lignin, it was found that the addition of lignin content led the blend sample to become heterogeneous that resulted in increased surface roughness and affected thermal stability. In fact, there was an increase in PLA's brittleness because of lignin aggregates, while no adverse effect was seen on the modulus of elasticity. The authors also revealed that with addition of lignin from 0 to 15 wt %, tensile strength and elongation at break of PLA/lignin composite decreased from 56 MPa to 41 MPa and 4.57% to 1.88%, respectively.

Tanase-Opedal et al.[62] incorporated 40 wt% soda lignin in PLA matrix and developed bio-composite filaments for 3D printing. On performing thermogravimetry analysis, authors found that 42 wt% of lignin sample was still there at 800 ℃ which was due to the formation of highly condensed aromatic structure that has ability to form char. Also, with the increase in lignin concentration, degradation of composite started earlier. From the results of mechanical analysis, they found the decreased mechanical strength with increase in lignin. They explained the reason behind this might be due to poor layer adhesion between printing layers. However, the strength was improved on increasing extrusion temperature to 215 ℃ which was probably due to

improvement in layer adhesion. They also mentioned the decrease in strength with increase in extrusion temperature to 230 ℃ which was basically due to degradation of carbohydrates in lignin to volatile gases that led to formation of microstructures in polymer matrix.

Domínguez-Robles et al.[69] prepared 3D printable filaments having antioxidant properties using PLA and (3 wt %) lignin. Materials printed from these filaments could be used in different healthcare application like wound healing. Filaments were prepared by extruding PLA pellets coated with lignin and castor oil. Because of the incorporation of lignin, Domínguez-Robles et al.[69] found an increase in a maximum load before fracture and higher wettability.

Nguyen et al.[61] found that modulus of elasticity remained comparable with the addition of lignin (40 wt %) in ABS. The problem of increased brittleness due to addition of lignin in ABS was resolved by the addition of acrylonitrile butadiene rubber (NBR41, 41 mol% nitrile content). ABS/lignin composite displayed excellent plasticity and prominent increase in tensile strength with 10 wt % addition of NBR41. Mechanical properties were further enhanced with just 10 wt % addition of carbon fibers (CFs) in ABS/lignin/NBR41 composite. Akato et al.[70] revealed that the addition of 10 wt % PEO (polyethylene oxide) in ABS/lignin (30 wt %) composite showed similar properties to that of neat ABS. Nguyen et al.[49] performed research on nylon 12/hardwood lignin (6:4) composite, where they observed a significant increase in material's strength and stiffness with the addition of CFs.

Akota et al.[70] revealed that the use of kraft lignin simulates a strong olfactory response which could be detrimental for a commercial approach. They performed further experiments using organosolv (Alcell) lignin, instead of kraft lignin and found that unpleasant odor was eliminated because of the absence of sulfur. Finally, they concluded that all lignin-containing hydroxyl groups

such as organosolv lignin, soda pulped lignin and lignin from bio-refinery residues can be used for composite formation. Additionally, Nguyen et al.[49] mentioned that organosolv hardwood lignin offers good thermal processing and good printability characteristics in contradiction to kraft softwood lignin which has higher viscosity.

Table 2.2 represents the usage of different types of lignin obtained from various sources with different polymer to develop biocomposite filaments. It also presents the effect of varying concentration of lignin on the properties of polymer-lignin composites.

Table 2.2 Usage of different types of lignin to develop composite filaments

Polymer matrix	Type of lignin	Lignin content	Remarks	Reference
PLA (3D850)	Soda lignin (Norway spruce)	20, 40 wt%	• ↓ in mechanical strength with increase in lignin which was improved on increasing extrusion temperature to 215℃.	[62]
PLA (2003D)	Kraft lignin (Pine)	5,10,15, 20 wt%	• Elongation at break and TS of PLA/lignin composite ↓ on ↑ lignin. • No effect on E of PLA/lignin composite with addition of lignin. • On adding 20 wt % lignin, aggregation concentration ↑ due to coalescence of lignin particles.	[40]
PLA (4043D)	Kraft lignin (Pine) Organosolv lignin (Beech) Lignosulfonate (Beech)	5, 10, 15 wt%	• No improvement in flexural strength on incorporating any of that lignin.	[41]

			• ↓ in IS with ↑ in lignin content.	
PHB	Lignin (Pinus radiate wood chips)	10, 20, 50 wt %	• Storage modulus of PHB was ↓ with addition of 20 wt % of lignin. • Filament had polymer rich surface and lignin particles in central core.	[71]
ABS	Organosolv lignin (Hardwood)	20, 30, 40 wt%	• Incorporation 40 wt % lignin in ABS ↓ TS of composite. • Well dispersed phase separated lignin was seen.	[72]
Nylon	Organosolv lignin (Hardwood)	40, 50, 60 wt%	• Addition of 40 wt % lignin to nylon 12 matrix, led to ↑ in E while TS was nearly same as neat nylon 12. • Spherical aggregated lignin phases were seen in polymer matrix.	[49]

Note: ↑- increase, ↓- decrease

From all the above-mentioned research, it was found that with the addition of any type of unmodified lignin, there was degradation in tensile strength of composites. Various strategies were applied to increase the properties of polymer-lignin composites such as addition of plasticizer, carbon fibers and modification of lignin Plasticizers are the additives that are generally added to improve the processability, flexibility, impact toughness and reduce the Tg of the polymers [73]. For obtaining the high properties of polymer or polymer composites, it is very essential to select the appropriate plasticizer and its content. Two different plasticizers - one polyethylene glycol and

other commercial plasticizer Struktol TR451 were selected for our research and they are briefly described below.

2.4 Polyethylene glycol (PEG)

PEG is one of the efficient plasticizers that has broad range of molecular weight ranging from 200 - 20000 g/mole. This nature of broad range molecular weight makes its processability with different polymers easier [74,75]. It is also exhibits excellent water solubility, biodegradability, non-toxicity, lubrication, bondability and dispersibility [73,76]. These all properties make it (PEG) suitable for different field such as pharmaceutical and biomedical fields, cosmetics, chemical industries and food processing [73]. Figure 2.7 represents chemical structure of PEG.

Various researches [73,74,77,78] were carried out to investigate the effect of PEG in PLA matrix. Li et al. [73] found that properties of PLA/PEG blend depends on the molecular weight of PEG added. So, to obtain the optimal properties of PLA/PEG blend, proper selection of both the content and molecular weight of PEG should be done. Li et al. [74] found the similar effect molecular weight of PEG in mechanical properties of PLA/PEG composites. Terminal hydroxyl group of PEG reacts can react with carboxyl group of PLA making it miscible. Beside this optimal content of PEG improves the flexibility and elongation at break of PLA by increasing its chain mobility [74,75].

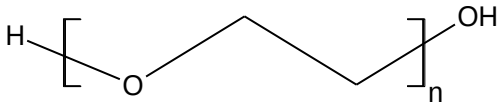

Figure 2.7 Chemical structure of PEG

2.5 Struktol TR451

Struktol TR451 is a commercial plasticizer composed up of special oleo chemicals. TR451 is generally used in order to increase the filler amount in the polymer without deteriorating processability and physical properties of the composites [79]. TR451 was found to improve the tensile strength and elongation at break of PLA-lignin composites by 20% and 90%, respectively [80]. It was mentioned that TR451 helped to improve the process ability and stress transfer ability of the PLA-lignin composites.

2.6 Conclusions

Very few researches [38,65,81,82] were done on improvement of PLA/lignin composites but none of them are applied for PLA/lignin composite filaments and 3D printed objected from those filaments. There is still a lack of study in the field to improve properties of PLA-lignin composite filaments. For our research, in order to improve the mechanical properties of PLA-lignin composite filaments, strategy of adding plasticizer was implemented. The result obtained from this study can help other researchers in appropriate selection of plasticizer and their effect in PLA-lignin composites.

Additionally, none of the research done with lignin in 3D printing were with HIPS. There is lack of study regarding HIPS-lignin composite filaments. The results obtained from this study of HIPS-lignin help other in developing HIPS-lignin composites that can be applied for several application.

2.7 References

[1] Shishkovsky I, editor. New trends in 3D printing. IntechOpen; 2016.

[2] Tao Y, Wang H, Li Z, Li P, Shi SQ. Development and application of wood flour-filled polylactic acid composite filament for 3D printing. Materials (Basel) 2017;10:1–6. https://doi.org/10.3390/ma10040339.

[3] Grimmelsmann N, Kreuziger M, Korger M, Meissner H, Ehrmann A. Adhesion of 3D printed material on textile substrates. Rapid Prototyp J 2018;24:166–70. https://doi.org/10.1108/RPJ-05-2016-0086.

[4] Chiulan I, Frone A, Brandabur C, Panaitescu D. Recent advances in 3D printing of aliphatic polyesters. Bioengineering 2017;5:2. https://doi.org/10.3390/bioengineering5010002.

[5] Liu J, Sun L, Xu W, Wang Q, Yu S, Sun J. Current advances and future perspectives of 3D printing natural-derived biopolymers. Carbohydr Polym 2019;207:297–316. https://doi.org/10.1016/j.carbpol.2018.11.077.

[6] Vanderploeg A, Lee SE, Mamp M. The application of 3D printing technology in the fashion industry. Int J Fash Des Technol Educ 2017;10:170–9. https://doi.org/10.1080/17543266.2016.1223355.

[7] Ozbolat IT, Peng W, Ozbolat V. Application areas of 3D bioprinting. Drug Discov Today 2016;21:1257–71. https://doi.org/10.1016/j.drudis.2016.04.006.

[8] Liu Z, Zhang M, Bhandari B, Wang Y. 3D printing: Printing precision and application in food sector. Trends Food Sci Technol 2017;69:83–94. https://doi.org/10.1016/j.tifs.2017.08.018.

[9] Wu P, Wang J, Wang X. A critical review of the use of 3-D printing in the construction industry. Autom Constr 2016;68:21–31. https://doi.org/10.1016/j.autcon.2016.04.005.

[10] Perkins I, Skitmore M. Three-dimensional printing in the construction industry: a review. Int J Constr Manag 2015;15:1–9. https://doi.org/10.1080/15623599.2015.1012136.

[11] Melnikova R, Ehrmann A, Finsterbusch K. 3D printing of textile-based structures by Fused Deposition Modelling (FDM) with different polymer materials. IOP Conf Ser Mater Sci Eng 2014;62. https://doi.org/10.1088/1757-899X/62/1/012018.

[12] Wimmer R, Steyrer B, Woess J, Koddenberg T, Mundigler N. 3D printing and wood. Wood Sci. Eng. Third Millenn., vol. 10, 2015, p. 145–50. https://doi.org/10.13140/RG.2.1.2483.6563.

[13] Meteyer S, Xu X, Perry N, Zhao YF. Energy and material flow analysis of binder-jetting additive manufacturing processes. Procedia CIRP 2014;15:19–25. https://doi.org/10.1016/j.procir.2014.06.030.

[14] Ou-Yang Q, Guo B, Xu J. Preparation and characterization of poly(butylene succinate)/polylactide blends for fused deposition modeling 3D printing. ACS Omega 2018;3:14309–17. https://doi.org/10.1021/acsomega.8b02549.

[15] Ngo TD, Kashani A, Imbalzano G, Nguyen KTQ, Hui D. Additive manufacturing (3D printing): a review of materials, methods, applications and challenges. Compos Part B Eng 2018;143:172–96. https://doi.org/10.1016/j.compositesb.2018.02.012.

[16] Persons T. 3D printing: opportunities, challenges, and policy implications of additive manufacturing. 2015.

[17] Campbell T, Williams C, Ivanova O, Garrett B. Could 3D printing change the world? Technologies, potential, and implications of additive manufacturing. Washington: 2011.

[18] ASTM International. F2792-12a - Standard terminology for additive manufacturing technologies.

[19] Lee JY, An J, Chua CK. Fundamentals and applications of 3D printing for novel materials. Appl Mater Today 2017;7:120–33. https://doi.org/10.1016/j.apmt.2017.02.004.

[20] Baumers M, Duflou JR, Flanagan W, Gutowski TG, Kellens K, Lifset R. Charting the environmental dimensions of additive manufacturing and 3D printing. J Ind Ecol 2017;21:S9–14. https://doi.org/10.1111/jiec.12668.

[21] Kellens K, Baumers M, Gutowski TG, Flanagan W, Lifset R, Duflou JR. Environmental dimensions of additive manufacturing: mapping application domains and their environmental implications. J Ind Ecol 2017;21:S49–68. https://doi.org/10.1111/jiec.12629.

[22] Tran TN, Bayer IS, Heredia-Guerrero JA, Frugone M, Lagomarsino M, Maggio F, et al. Cocoa shell waste biofilaments for 3D printing applications. Macromol Mater Eng 2017;302:1–10. https://doi.org/10.1002/mame.201700219.

[23] Xu W, Wang X, Sandler N, Willför S, Xu C. Three-dimensional printing of wood-derived biopolymers: a review focused on biomedical applications. ACS Sustain Chem Eng 2018;6:5663–80. https://doi.org/10.1021/acssuschemeng.7b03924.

[24] Valerga AP, Batista M, Salguero J, Girot F. Influence of PLA filament conditions on characteristics of FDM parts. Materials (Basel) 2018;11. https://doi.org/10.3390/ma11081322.

[25] Liu Z, Wang Y, Wu B, Cui C, Guo Y, Yan C. A critical review of fused deposition modeling 3D printing technology in manufacturing polylactic acid parts. Int J Adv Manuf Technol 2019;102:2877–89. https://doi.org/10.1007/s00170-019-03332-x.

[26] Goyanes A, Det-Amornrat U, Wang J, Basit AW, Gaisford S. 3D scanning and 3D printing as innovative technologies for fabricating personalized topical drug delivery systems. J Control Release 2016;234:41–8. https://doi.org/10.1016/j.jconrel.2016.05.034.

[27] Chim H, Hutmacher DW, Chou AM, Oliveira AL, Reis RL, Lim TC, et al. A comparative analysis of scaffold material modifications for load-bearing applications in bone tissue engineering. Int J Oral Maxillofac Surg 2006;35:928–34. https://doi.org/10.1016/j.ijom.2006.03.024.

[28] Kumar N, Jain PK, Tandon P, Pandey PM. 3D printing of flexible parts using eva material. Mater Phys Mech 2018;37:124–32. https://doi.org/10.18720/MPM.3722018-3.

[29] Terekhina S, Skornyakov I, Tarasova T, Egorov S. Effects of the infill density on the mechanical properties of nylon specimens made by filament fused fabrication. Technologies 2019;7:57. https://doi.org/10.3390/technologies7030057.

[30] McLouth TD, Severino J V., Adams PM, Patel DN, Zaldivar RJ. The impact of print orientation and raster pattern on fracture toughness in additively manufactured ABS. Addit Manuf 2017;18:103–9. https://doi.org/10.1016/j.addma.2017.09.003.

[31] Harris M, Potgieter J, Archer R, Arif KM. Effect of material and process specific factors on the strength of printed parts in fused filament fabrication: A review of recent developments. Materials (Basel) 2019;12. https://doi.org/10.3390/ma12101664.

[32] Chaunier L, Guessasma S, Belhabib S, Della Valle G, Lourdin D, Leroy E. Material extrusion of plant biopolymers: Opportunities & challenges for 3D printing. Addit Manuf 2018;21:220–33. https://doi.org/10.1016/j.addma.2018.03.016.

[33] Le Duigou A, Castro M, Bevan R, Martin N. 3D printing of wood fibre biocomposites: From mechanical to actuation functionality. Mater Des 2016;96:106–14. https://doi.org/10.1016/j.matdes.2016.02.018.

[34] Gonzalez Ausejo J, Rydz J, Musioł M, Sikorska W, Sobota M, Włodarczyk J, et al. A comparative study of three-dimensional printing directions: The degradation and toxicological profile of a PLA/PHA blend. Polym Degrad Stab 2018;152:191–207. https://doi.org/10.1016/j.polymdegradstab.2018.04.024.

[35] Gonzalez Ausejo J, Rydz J, Musioł M, Sikorska W, Janeczek H, Sobota M, et al. Three-dimensional printing of PLA and PLA/PHA dumbbell-shaped specimens of crisscross and

transverse patterns as promising materials in emerging application areas: Prediction study. Polym Degrad Stab 2018;156:100–10. https://doi.org/10.1016/j.polymdegradstab.2018.08.008.

[36] Wu C-S, Liao H-T. Fabrication, characterization, and application of polyester/wood flour composites. J Polym Eng 2017;37:689–98. https://doi.org/10.1515/polyeng-2016-0284.

[37] Cuiffo MA, Snyder J, Elliott AM, Romero N, Kannan S, Halada GP. Impact of the fused deposition (FDM) printing process on polylactic acid (PLA) chemistry and structure. Appl Sci 2017;7:579. https://doi.org/10.3390/app7060579.

[38] Gordobil O, Egüés I, Llano-Ponte R, Labidi J. Physicochemical properties of PLA lignin blends. Polym Degrad Stab 2014;108:330–8. https://doi.org/10.1016/j.polymdegradstab.2014.01.002.

[39] Xu W, Pranovich A, Uppstu P, Wang X, Kronlund D, Hemming J, et al. Novel biorenewable composite of wood polysaccharide and polylactic acid for three dimensional printing. Carbohydr Polym 2018;187:51–8. https://doi.org/10.1016/j.carbpol.2018.01.069.

[40] Gkartzou E, Koumoulos EP, Charitidis CA. Production and 3D printing processing of bio-based thermoplastic filament. Manuf Rev 2017;4:1. https://doi.org/10.1051/mfreview/2016020.

[41] Mimini V, Sykacek E, Hashim SNA, Holzweber J, Hettegger H, Fackler K, et al. Compatibility of kraft lignin, organosolv lignin and lignosulfonate with PLA in 3D printing. J Wood Chem Technol 2019;39:14–30. https://doi.org/10.1080/02773813.2018.1488875.

[42] Jo W, Kwon OC, Moon MW. Investigation of influence of heat treatment on mechanical strength of FDM printed 3D objects. Rapid Prototyp J 2018;24:637–44. https://doi.org/10.1108/RPJ-06-2017-0131.

[43] Rajpurohit SR, Dave HK. Effect of process parameters on tensile strength of FDM printed PLA part. Rapid Prototyp J 2018;24:1317–24. https://doi.org/10.1108/RPJ-06-2017-0134.

[44] Yang L, Li S, Li Y, Yang M, Yuan Q. Experimental investigations for optimizing the extrusion parameters on FDM PLA printed parts. J Mater Eng Perform 2019;28:169–82. https://doi.org/10.1007/s11665-018-3784-x.

[45] Alafaghani A, Qattawi A, Alrawi B, Guzman A. Experimental optimization of fused deposition modelling processing parameters: a design-for-manufacturing approach. Procedia Manuf 2017;10:791–803. https://doi.org/10.1016/j.promfg.2017.07.079.

[46] Benwood C, Anstey A, Andrzejewski J, Misra M, Mohanty AK. Improving the impact strength and heat resistance of 3D printed models: structure, property, and processing

correlationships during fused deposition modeling (FDM) of poly(lactic acid). ACS Omega 2018;3:4400–11. https://doi.org/10.1021/acsomega.8b00129.

[47] Afrose MF, Masood SH, Iovenitti P, Nikzad M, Sbarski I. Effects of part build orientations on fatigue behaviour of FDM-processed PLA material. Prog Addit Manuf 2016;1:21–8. https://doi.org/10.1007/s40964-015-0002-3.

[48] Song Y, Li Y, Song W, Yee K, Lee KY, Tagarielli VL. Measurements of the mechanical response of unidirectional 3D-printed PLA. Mater Des 2017;123:154–64. https://doi.org/10.1016/j.matdes.2017.03.051.

[49] Nguyen NA, Barnes SH, Bowland CC, Meek KM, Littrell KC, Keum JK, et al. A path for lignin valorization via additive manufacturing of high-performance sustainable composites with enhanced 3D printability. Sci Adv 2018;4:eaat4967. https://doi.org/10.1126/sciadv.aat4967.

[50] Kariz M, Sernek M, Obućina M, Kuzman MK. Effect of wood content in FDM filament on properties of 3D printed parts. Mater Today Commun 2018;14:135–40. https://doi.org/10.1016/j.mtcomm.2017.12.016.

[51] Guo R, Ren Z, Bi H, Song Y, Xu M. Effect of toughening agents on the properties of poplar wood flour/poly (lactic acid) composites fabricated with Fused Deposition Modeling. Eur Polym J 2018;107:34–45. https://doi.org/10.1016/j.eurpolymj.2018.07.035.

[52] Ayrilmis N. Effect of layer thickness on surface properties of 3D printed materials produced from wood flour/PLA filament. Polym Test 2018;71:163–6. https://doi.org/10.1016/j.polymertesting.2018.09.009.

[53] Daver F, Lee KPM, Brandt M, Shanks R. Cork–PLA composite filaments for fused deposition modelling. Compos Sci Technol 2018;168:230–7. https://doi.org/10.1016/j.compscitech.2018.10.008.

[54] Murphy CA, Collins MN. Microcrystalline cellulose reinforced polylactic acid biocomposite filaments for 3D printing. Polym Compos 2018;39:1311–20. https://doi.org/10.1002/pc.24069.

[55] Dong J, Li M, Zhou L, Lee S, Mei C, Xu X, et al. The influence of grafted cellulose nanofibers and postextrusion annealing treatment on selected properties of poly(lactic acid) filaments for 3D printing. J Polym Sci Part B Polym Phys 2017;55:847–55. https://doi.org/10.1002/polb.24333.

[56] Welzel T, Ertane EG, Dorner-Reisel A, Matner V, Baran O, Svoboda S. Processing and wear behaviour of 3D printed PLA reinforced with biogenic carbon. Adv Tribol 2018;2018:1–11. https://doi.org/10.1155/2018/1763182.

[57] Antoniac I, Popescu D, Zapciu A, Antoniac A, Miculescu F, Moldovan H. Magnesium filled polylactic acid (PLA) material for filament based 3D printing. Materials (Basel) 2019;12:719. https://doi.org/10.3390/ma12050719.

[58] Prashantha K, Roger F. Multifunctional properties of 3D printed poly(lactic acid)/graphene nanocomposites by fused deposition modeling. J Macromol Sci Part A Pure Appl Chem 2017;54:24–9. https://doi.org/10.1080/10601325.2017.1250311.

[59] Ferreira RTL, Amatte IC, Dutra TA, Bürger D. Experimental characterization and micrography of 3D printed PLA and PLA reinforced with short carbon fibers. Compos Part B Eng 2017;124:88–100. https://doi.org/10.1016/j.compositesb.2017.05.013.

[60] Rasselet D, Caro-Bretelle A-S, Taguet A, Lopez-Cuesta J-M. Reactive compatibilization of PLA/PA11 blends and their application in additive manufacturing. Materials (Basel) 2019;12:485. https://doi.org/10.3390/ma12030485.

[61] Nguyen NA, Bowland CC, Naskar AK. A general method to improve 3D-printability and inter-layer adhesion in lignin-based composites. Appl Mater Today 2018;12:138–52. https://doi.org/10.1016/j.apmt.2018.03.009.

[62] Tanase-Opedal M, Espinosa E, Rodríguez A, Chinga-Carrasco G. Lignin: A biopolymer from forestry biomass for biocomposites and 3D printing. Materials (Basel) 2019;12:1–15. https://doi.org/10.3390/ma12183006.

[63] Upton BM, Kasko AM. Strategies for the conversion of lignin to high-value polymeric materials: review and perspective. Chem Rev 2016;116:2275–306. https://doi.org/10.1021/acs.chemrev.5b00345.

[64] Naseem A, Tabasum S, Zia KM, Zuber M, Ali M, Noreen A. Lignin-derivatives based polymers, blends and composites: a review. Int J Biol Macromol 2016;93:296–313. https://doi.org/10.1016/j.ijbiomac.2016.08.030.

[65] Gordobil O, Delucis R, Egüés I, Labidi J. Kraft lignin as filler in PLA to improve ductility and thermal properties. Ind Crops Prod 2015;72:46–53. https://doi.org/10.1016/j.indcrop.2015.01.055.

[66] Chio C, Sain M, Qin W. Lignin utilization : A review of lignin depolymerization from various aspects. Renew Sustain Energy Rev 2019;107:232–49. https://doi.org/10.1016/j.rser.2019.03.008.

[67] Leão AL, Cesarino I, Dias OAT, Negrão DR, Gonçalves DFC. Recent approaches and future trends for lignin-based materials. Mol Cryst Liq Cryst 2017;655:204–23. https://doi.org/10.1080/15421406.2017.1360713.

[68] Kun D, Pukánszky B. Polymer/lignin blends: interactions, properties, applications. Eur Polym J 2017;93:618–41. https://doi.org/10.1016/j.eurpolymj.2017.04.035.

[69] Domínguez-Robles J, Martin N, Fong M, Stewart S, Irwin N, Rial-Hermida M, et al. Antioxidant PLA composites containing lignin for 3D printing applications: a potential material for healthcare applications. Pharmaceutics 2019;11:165. https://doi.org/10.3390/pharmaceutics11040165.

[70] Akato K, Tran CD, Chen J, Naskar AK. Poly(ethylene oxide)-assisted macromolecular self-assembly of lignin in ABS matrix for sustainable composite applications. ACS Sustain Chem Eng 2015;3:3070–6. https://doi.org/10.1021/acssuschemeng.5b00509.

[71] Vaidya AA, Collet C, Gaugler M, Lloyd-Jones G. Integrating softwood biorefinery lignin into polyhydroxybutyrate composites and application in 3D printing. Mater Today Commun 2019;19:286–96. https://doi.org/10.1016/j.mtcomm.2019.02.008.

[72] Nguyen NA, Bowland CC, Naskar AK. Mechanical, thermal, morphological, and rheological characteristics of high performance 3D-printing lignin-based composites for additive manufacturing applications. Data Br 2018;19:936–50. https://doi.org/10.1016/j.dib.2018.05.130.

[73] Li FJ, Zhang SD, Liang JZ, Wang JZ. Effect of polyethylene glycol on the crystallization and impact properties of polylactide-based blends. Polym Adv Technol 2015;26:465–75. https://doi.org/10.1002/pat.3475.

[74] Li D, Jiang Y, Lv S, Liu X, Gu J, Chen Q, et al. Preparation of plasticized poly (lactic acid) and its influence on the properties of composite materials. PLoS One 2018;13:1–15. https://doi.org/10.1371/journal.pone.0193520.

[75] Chieng BW, Ibrahim NA, Yunus WMZW, Hussein MZ. Poly(lactic acid)/poly(ethylene glycol) polymer nanocomposites: effects of graphene nanoplatelets. Polymers (Basel) 2014;6:93–104. https://doi.org/10.3390/polym6010093.

[76] Arrieta MP, López J, Rayón E, Jiménez A. Disintegrability under composting conditions of plasticized PLA–PHB blends. Polym Degrad Stab 2014;108:307–18. https://doi.org/10.1016/j.polymdegradstab.2014.01.034.

[77] Sungsanit K, Kao N, Bhattacharya SN. Properties of linear poly(lactic Acid)/polyethylene glycol blends. Polym Eng Sci 2012:108–16. https://doi.org/10.1002/pen.

[78] Chieng BW, Ibrahim NA, Yunus WMZW, Hussein MZ. Plasticized poly(lactic acid) with low molecular weight poly(ethylene glycol): Mechanical, thermal, and morphology properties. J Appl Polym Sci 2013;130:4576–80. https://doi.org/10.1002/app.39742.

[79] Technical data n.d. https://doi.org/10.1515/9783034615877.164.

[80] Faruk O, Sain M. Lignin in polymer composites. 1st ed. 2015.

[81] Gordobil O, Egüés I, Labidi J. Modification of eucalyptus and spruce organosolv lignins with fatty acids to use as filler in PLA. React Funct Polym 2016;104:45–52. https://doi.org/10.1016/j.reactfunctpolym.2016.05.002.

[82] Sun Y, Yang L, Lu X, He C. Biodegradable and renewable poly(lactide)-lignin composites: synthesis, interface and toughening mechanism. J Mater Chem A 2015;3:3699–709. https://doi.org/10.1039/c4ta05991c.

Chapter 3

Lignin-PLA filament for 3D printing

3.1 Abstract

The growing concern towards environmental pollution due to the excessive use of petroleum-based plastic has led to increase in interest towards the biobased sustainable alternative. The objective of this work was to develop polylactic acid (PLA)-lignin biocomposite filaments with improved properties. PLA and organosolv lignin were mixed in different ratios, and extruded to obtain composite filaments. The mechanical, thermal, and morphological properties of filaments were examined. This study found that the tensile strength and elongation decreased with increase in lignin content. We were able to incorporate till 20 wt% lignin; however, its tensile strength and elongation was significantly decreased. Two plasticizers (polyethylene glycol-PEG 2000) and struktol® TR451) were added separately in varying concentration to enhance the properties of PLA_L20 (20% lignin) composite filaments. Investigation on the effect of lignin in PLA, and PEG and struktol in PLA_L20 was performed using tensile test, differential scanning calorimeter, thermogravimetric analysis, scanning electron microscopy, Fourier transform infrared spectroscopy of the filaments and dynamic mechanical analysis of 3D printed samples. Adding 2 wt% of PEG in PLA_L20 showed significant improvement in mechanical properties. PEG in PLA_L20 composite resulted in decreasing the size of lignin particles and improvement in dispersion of lignin in PLA matrix. On the other hand, struktol did not show significant enhancement in tensile stress at max. load of PLA_L20 composite.

Keywords: PLA, lignin, filaments, 3D printing, PEG 2000, Struktol® TR451.

3.2 Introduction

Additive manufacturing or 3D printing is a rapidly growing manufacturing technology that allows freeform fabrication of complex geometrical structure in an efficient way. Among different additive manufacturing technologies, fused deposition modeling (FDM) is the most popular and versatile technique in which a solid thermoplastic-filament is used as a feedstock [1]. The filament is passed through an extruder where it is melted and material is deposited layer by layer in the build platform which then solidifies to form a final object [2,3]. Various thermoplastic polymers such as polylactic acid (PLA) [4,5], poly(ε-caprolactone) (PCL) [6–8], ethylene vinyl acetate (EVA) [9], polyamides [10], and acrylonitrile butadiene styrene (ABS)[11,12] are generally used for FDM printing, and most of them are petroleum-based.

Petroleum-based plastics are extensively used in packaging, automobiles industries, construction [13]. Their excessive use has created environment problems such as “plastic plague” and increase in greenhouse gas emissions. To address environmental issues as a result of excessive use of petroleum-based plastic, and the society transitioning for single-use economy to circular-economy, researchers are working on the development of bio-based sustainable materials that can be alternative of petroleum-based plastics.

PLA is the most commonly used thermoplastic biopolymer produced from glucose derived from corn-starch, sugarcane, and sugar beets [13–16]. It is biodegradable and biocompatible polymer widely used for 3D printing application [17,18]. Lower glass transition temperature, lower melting point and non-adherence to printing surface makes it suitable for 3D printing application [14,18,19]. Despite of its promising properties, brittle nature, low toughness, moisture sensitivity and comparatively higher cost limit its wider applications [13,18].

On the other hand, lignin is the second most abundant biomaterial after cellulose. It is available relatively in large amount as a byproduct from pulp and paper, and potentially from the 2nd generation bioethanol industries [20–22]. The large portion of annually produced lignin is burnt to generate energy [20]. Due to lignin's properties such as heterogeneous-complex structure, low-purity standard, smell and color problem, and the need of some form of physical and chemical modifications before its use, only 2% of annually produced lignin is used for preparing carbon fibers, chemicals, adhesives, plastics and composites. However, all those applications still lack successful commercialization [18,20,23].

Blending lignin with PLA to produce composite filaments for 3D printing is a promising bio-based option that could increase the utilization of lignin other than burning for energy. In other words, using lignin as a feedstock in this rapidly growing manufacturing technology helps in valorization of lignin. Additionally, incorporating lignin in PLA decreases the amount of PLA being used and thus, decreases the overall cost of filaments. Several studies were carried out regarding the incorporation of lignin in PLA matrix to form composite filaments for 3D printing [13,18,20]. From all the previous studies, it was evident that the addition of lignin led to decrease in tensile strength and elongation. Filaments with poor properties will dearth successful commercialization. There is still a lack of studies done regarding enhancement in properties of PLA-lignin composite filaments. From literature, various strategies were found to be applied for enhancing the properties of polymer-lignin composite filaments such as modifying lignin, adding plasticizers and carbon fibers [1,23,24].

In this study, organosolv lignin was blended with the PLA in varying amount to obtain composite filaments. We were successfully able to incorporate 20 wt% lignin in composite filament and beyond 20 wt%, filaments were too brittle that could not be coiled around the spooler. The thermal,

mechanical, and morphological properties of produced composite filaments were studied. On observing the results, adding 20 wt% lignin in PLA showed poor mechanical properties. Only getting the filaments out of lignin will be of no use if its properties are degraded. Therefore, two different plasticizers (polyethylene glycol-PEG 2000 and struktol® TR451) were added in varying concentration in PLA-20 wt% lignin mixture. Furthermore, the thermal, mechanical, and morphological properties of the composites were examined to determine the effect of plasticizers. The main hypothesis of this study is that plasticizer can improve the mechanical properties of PLA-lignin composite filaments.

3.3 Materials and methods

3.3.1 Materials

PLA pellets (commercial grade: Ingeo 2003D) were purchased from Jamplast Inc. (Ellisville, MO, USA). Organosolv lignin (hardwood) was supplied by Attis Innovations, LLC (Milton, GA, USA). PEG 2000 was obtained from ThermoFisher Scientific Chemicals, Inc. (Waltham, MA, USA) whereas struktol® TR451 was supplied by Struktol Company of America, LLC (Stow, OH, USA).

3.3.2 Sample preparation

PLA pellets and lignin were oven dried at 50 ℃ for more than 24 hours prior to processing for filaments. Composition of the filaments that were prepared in this study is presented in Table 3.1, and the samples were coded. For example, PLA_L20_S0.25 means that the filaments were made from 20% lignin, 0.25% struktol and the balance is PLA (79.75%).

PLA pellets and lignin were first manually mixed (more like PLA pellets were coated with lignin) before feeding to the twin extruder (Leistritz Mic 18/GL 40D, Nuremberg, Germany). The twin extruder has seven temperature zones, and they were set as follows from zone 1 to 7: 154 ℃, 157

℃, 165 ℃, 170 ℃, 175 ℃, 178 ℃, and 178 ℃, respectively. Temperature selection was done based on the different literatures that were focused on extrusion of PLA, and trial and error based on those temperature ranges in order to produce successful filaments [13,18]. The screw speed was set at 50 rpm. Filaments obtained were of varying diameter from the range of 1.30 mm to 2.10 mm, which were coiled around the filament spooler and later was stored in zip-lock bags. Figure 3.1 represents the extrusion process of filaments, and Figure 3.2 is the twin extruder used for extrusion.

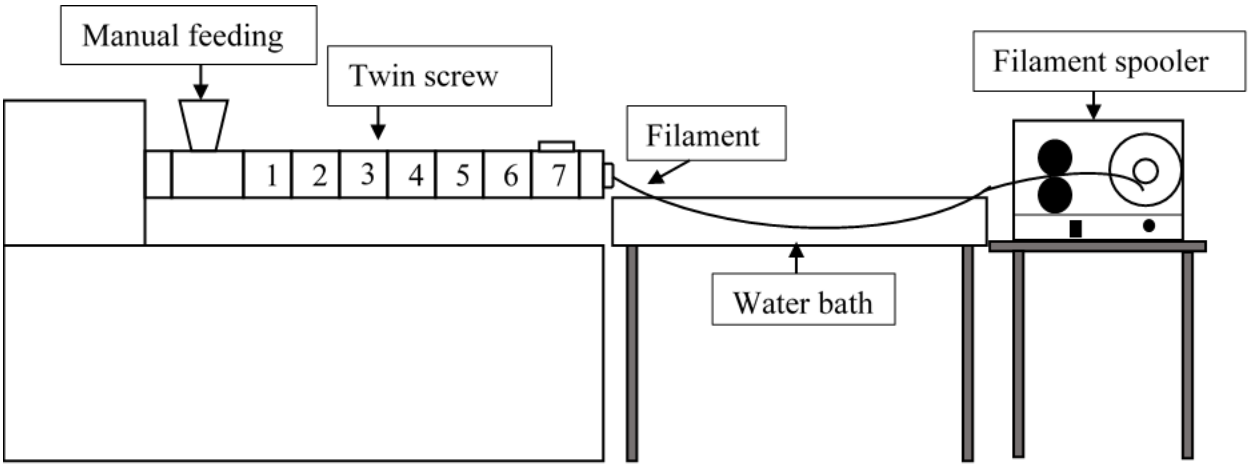

Figure 3.1 Schematic representation of filament extrusion

Figure 3.2 Twin extruder used for filament extrusion

Table 3.1 Total samples prepared along with their sample codes

Sample code	PLA (wt%)	Lignin (wt%)	PEG (wt%)	Struktol (wt%)
PLA	100	-	-	-
PLA_L5	95	5	-	-
PLA_L10	90	10	-	-
PLA_L15	85	15	-	-
PLA_L20	80	20	-	-
PLA_L20_P0.25	79.75	20	0.25	-
PLA_L20_P0.5	79.5	20	0.5	-
PLA_L20_P0.75	79.25	20	0.75	-
PLA_L20_P1	79	20	1	-
PLA_L20_P2	78	20	2	-
PLA_L20_P3	77	20	3	-
PLA_L20_P4	76	20	4	-
PLA_L20_P5	75	20	5	-
PLA_L20_S0.25	79.75	20	-	0.25
PLA_L20_S0.5	79.5	20	-	0.5
PLA_L20_S0.75	79.25	20	-	0.75
PLA_L20_S1	79	20	-	1

3.3.3 3D printing of filaments

3D cad model of dynamic mechanical analysis (DMA) samples of dimension 40mm × 10mm × 2mm, and dog bone sample according to ASTM D638 type V were prepared first using Autodesk Fusion 360, and the files were converted into .STL format. Figures 3.3 and 3.4 represent the drawing of dog bone and DMA samples, respectively. Ultimaker Cura 4.2.1 slicing software was used to slice the 3D model, and the gcode files were prepared. Filaments with the diameter in the range of 1.6 to 1.9 mm were selected and used for 3D printing using Monoprice MP Select Mini 3D Printer V2 (Monoprice Inc., Rancho Cucamonga, CA, USA). Printing parameters used for 3D printing are represented in Table 3.2 below.

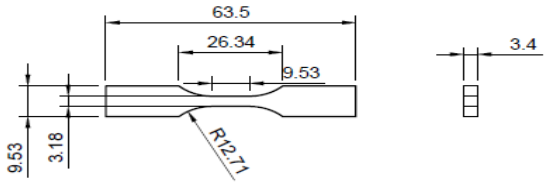

Figure 3.3 CAD drawing of dog bone sample

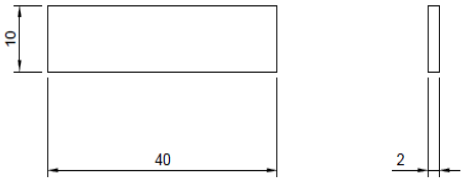

Figure 3.4 CAD drawing of DMA sample

Table 3.2 3D printing parameters

Nozzle temperature	210 ℃
Bed temperature	60 ℃

Nozzle diameter	0.4 mm
Layer height	0.1 mm
Infill density	100%
Infill pattern	Rectilinear
Infill angle	45^{o}
Printing speed	30 mm/s
Fan speed	100%

3.3.4 Lignin characterization

3.3.4.1 Proximate analysis

Proximate analysis includes determination of moisture, volatile matter, ash, and fixed carbon content. Moisture content of lignin was determined according to the ASTM E871 using Mettler Toledo moisture analyzer (Columbus, OH, USA). Volatile matter and ash content were determined according to the ASTM E872 and E1755, respectively. Finally, the fixed carbon was calculated by subtracting moisture, volatile matter, and ash content from 100.

3.3.4.2 Particle size distribution

From the ground lignin sample, 50 grams was used to determine the particle size distribution using Camsizer (Retsch Technology, Jenoptik, Germany).

3.3.4.3 Ultimate analysis

The total C, H, N and S content of lignin was determined using Vario micro elemental analyzer (Elementar Americas Inc, Ronkonkoma, NY, USA). Three replicates of lignin samples were prepared, and average values of C, H, N and S content were reported.

3.3.5 TGA

Thermogravimetric analysis of all the samples were carried out by Q500 (TA instruments, New Castle, DE, USA) under nitrogen atmosphere at the flow rate of 60 mL/min. Samples of mass ranged from 7 to 13 mg were placed on platinum pan and was heated from room temperature to 600 °C at the heating rate of 10 °C/min.

3.3.6 DSC

Differential scanning calorimetry (DSC) was carried out in order to determine glass transition temperature (Tg), cold crystallization temperature (Tcc), cold crystallization enthalpy (Hcc), melting temperature (Tm) and melting enthalpy (Hm) for PLA, PLA-lignin and PLA-lignin-plasticizer composites. DSC was performed using Q 2000 (TA instruments, New Castle, DE, USA) which was operated under nitrogen environment. Nitrogen flow rate was maintained at 50 mL/min. Tzero aluminum pan was used for samples and empty tzero aluminum pan was used for reference. Samples of weight ranged 4 to 6 mg were prepared, and they were first heated to 200 °C from room temperature at a heating rate of 10 °C/min and then was cooled from 200 °C to 40°C at a cooling rate of 10 °C/min.

3.3.7 Mechanical testing

Mechanical properties of filaments were measured using Instron 5565 (Norwood, MA, USA) with load cell 1 kN. The gauge length was fixed at 50 mm and cross-head speed was set at 5 mm/min. The tensile test was carried out on 15 specimens for each case, and average values were reported.

3.3.8 DMA

Dynamic mechanical analysis was carried out to determine the viscoelastic behavior of the composites over the temperature range. Viscoelastic behavior is represented by storage modulus

(E'), loss modulus (E") and tan δ. Viscoelastic properties of the 3D printed composites were studied using RSA 3 (TA instruments, New Castle, DE, USA) under three-point bending mode. Dynamic temperature ramp test was performed over a temperature range from 25 ℃ to 100 ℃ at a ramp rate of 5 ℃/min, frequency of 1 Hz and strain of 0.3%. Three specimens for each case were tested and average values were reported.

3.3.9 SEM

Scanning Electron Microscopy (SEM) was used to study surface of mechanically tested filaments and 3D printed samples using Zeiss EVO50 (Carl Zeiss Microscopy, NY, USA). Liquid nitrogen was used to fracture filaments. As the specimens were non-conductive, they were gold-sputtered using EMS 150R ES (Electron Microscopy Sciences, PA, USA) sputtering system. Surface was studied at different magnification at an accelerating voltage of 15 kV, and a working distance of 8 mm to 10.5 mm approximately.

3.3.10 FTIR

Fourier transform infrared spectroscopy (FTIR) analysis of the samples was carried out using Nicolet 6700 FTIR (ThermoFisher Scientific, Madison, WI, USA). Two spectra were collected in the wavelength range from 400-4000 cm^{-1} for each sample, and average spectrum was reported. Each spectrum was recorded for total of 64 scans with a resolution of 4 cm^{-1}.

3.3.11 Statistical analysis

Statistical analyses were performed using SAS 9.4 (Cary, NC). Analysis of variance (ANOVA) was carried out to evaluate the effect on mechanical properties upon addition of lignin and plasticizers in PLA. All analyses were performed at 0.05 significance level (i.e. $\alpha = 0.05$).

3.4 Results

3.4.1 Lignin characterization

3.4.1.1 Proximate analysis

The value of moisture, volatile matter, ash, and fixed carbon content depends in the type of lignin used as well as their extraction process. The moisture, volatile matter, ash, and fixed carbon content of the lignin sample used for experiment were found to be 1.39 ± 0.07 %, 78.25 ± 0.51%, 2.88 ± 0.27% and 17.49 ± 0.61% (all on mass basis), respectively. On comparing the moisture content among different lignin, Gordobil et al. [25] mentioned that the average moisture content of all types of lignin are in the range of 2-5% which is nearly similar to the values obtained in our analysis. However, the values of volatile matter and fixed carbon content of the lignin used in this study had huge variation than that mentioned by Gordobil et al. [25]. Gordobil et al. [25] found 63% of volatile matter and 33% of fixed carbon content in organosolv eucalyptus lignin. Furthermore, ash content of the lignin used for this study was slightly less than that mentioned by Gordobil et al. [25]. They found the ash content of organosolv eucalyptus lignin to be 3.6%, which was relatively less that kraft eucalyptus lignin (ash content of 49.8%).

3.4.1.2 Particle size

From the Camsizer, average particle size of the lignin sample was found to be 911μm. Figure 3.5 represents the particle size distribution of lignin. It was found that particle size of filler affects the mechanical properties of the composites [26]. However, none of the research done on bio-composite filaments using lignin has mentioned the exact values or range of particle size of lignin for better filament processing.

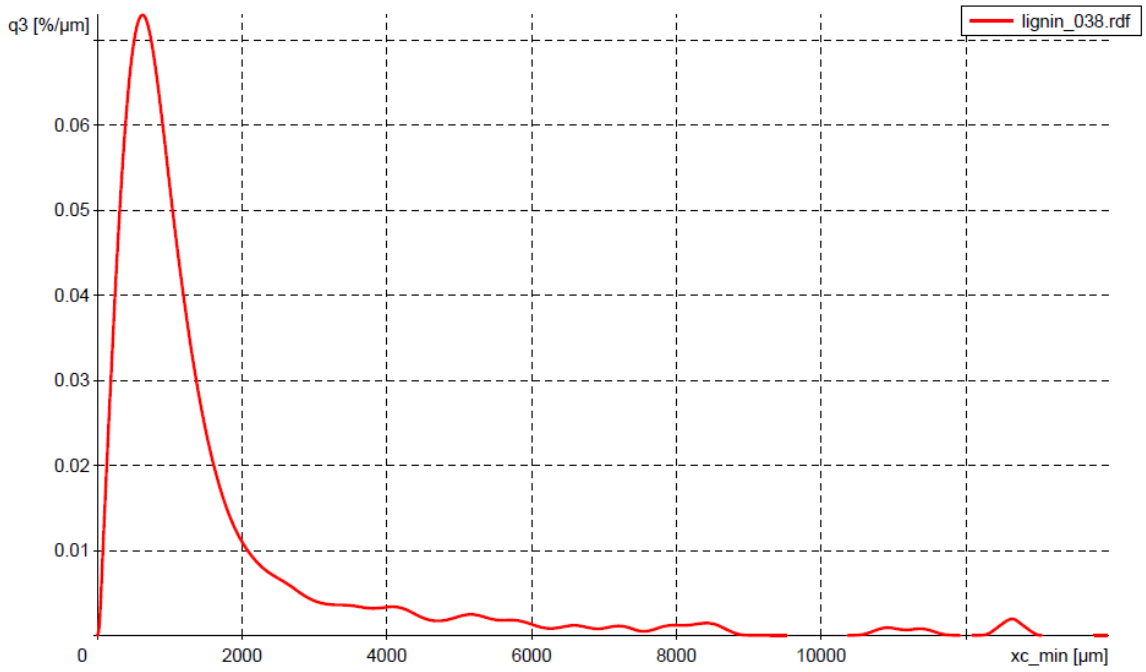

Figure 3.5 Particle size distribution of lignin

3.4.1.3 Ultimate analysis

With regards to ultimate analysis of the lignin sample, average carbon, hydrogen, nitrogen, and sulfur content was found to be 65.70 ± 0.70%, 6.10 ± 0.05%, 0.15 ± 0.01% and 0.30 ± 0.10%, respectively. Mimini et al. [13] have also reported the CHNS analysis of kraft, organosolv and lignosulphate lignin used for blending with PLA. They found that among three types of lignin, organoslov lignin had the highest carbon content and lowest sulfur content. The values of C, H, N and S reported by Mimini et al. [13] were 62.3%, 6.28%, 0.29% and <0.02%, respectively, and is similar to our result of ultimate analysis.

3.4.2 TGA

TG curve gives the weight loss of the substance with respect to temperature whereas first derivative (DTG) reveals the corresponding rate of weight loss. The peak of the DTG can be used to compare the thermal stability among different materials.

From the TG curve of lignin (Figure 3.6), it was found that 36.62% of lignin sample still was remaining at 600 ℃ which was due to the formation of highly condensed aromatic structure having ability to form char [20,27]. The TG graph of lignin reveals that weight loss of lignin has different stages. Lignin structure contains different functional group and structural elements. All these functional group and structural elements have different decomposition temperature. This leads to the multistage degradation of lignin. From the DTG curve of Figure 3.6, two different degradation peaks were observed, one with maximum degradation peak at 215 ℃ and other with the maximum degradation peak at 340 ℃. First weight loss is due to evaporation of water which starts nearly at 80 ℃. Second weight loss starts from nearly 175 ℃ to 240 ℃ which is due to degradation of components of carbohydrate in lignin sample to gases such as CO, CO_2 and CH_4 [27]. Further, the other weight loss occurs in the range of 275 ℃ and 460 ℃. This stage takes place at the slower rate and removal of gaseous products, phenolics, alcohols and aldehyde acids take place [27].

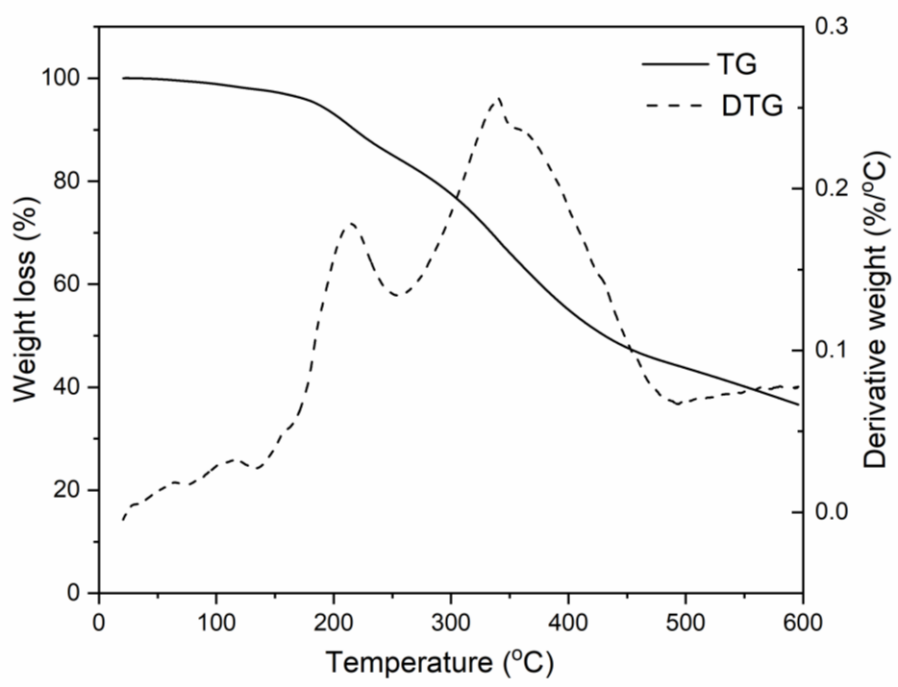

Figure 3.6 TG and DTG curve of lignin

Figure 3.7 shows the TG curve of PLA and PLA-lignin composites (5%, 10%, 15% and 20% lignin concentration). It was found that with the addition of lignin, there was a gradual decrease in onset decomposition temperature of PLA. The result shows that onset temperature of decomposition of PLA decreases from 349 ℃ to 342 ℃ on adding 20 wt% lignin in PLA. This decrease in onset decomposition temperature of PLA_L20 might be earlier decomposition of lignin present in PLA matrix. It was also found that at 600 ℃, there was increase in residue to 7% with the addition of 20 wt% lignin.

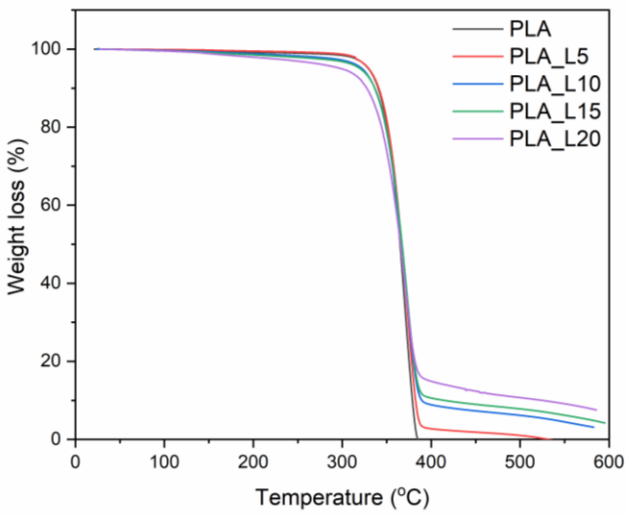

Figure 3.7 TG curve of PLA-lignin composites

On adding different concentration of PEG (0.25%, 0.5%, 0.75% and 1%) in PLA_L20 composite, there was no change in TG curves (Figure 3.8). However, there was a decrease in maximum decomposition temperature from 371 ℃ to 345℃ with the increase in PEG to 2 wt% which can be observed in DTG curve presented in Figure 3.9. On further increasing the PEG content to 5wt% there was no notable change in TG and DTG curves (Figure 3.8 and 3.9). Li et al. [28] observed similar decrease in maximum degradation temperature of PLA with the addition of PEG.

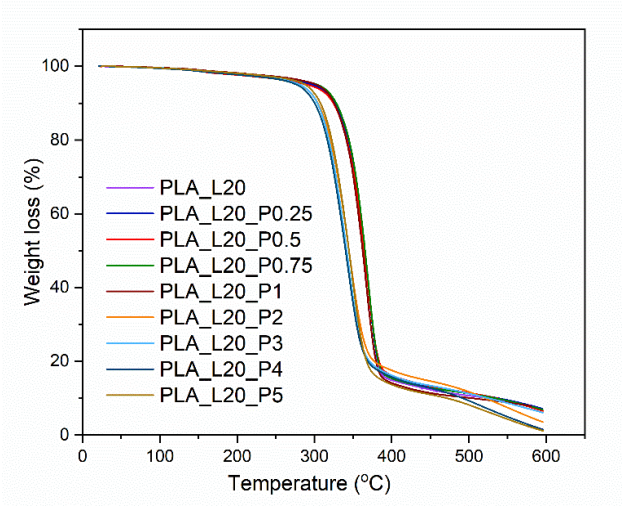

Figure 3.8 TG curve of PLA-lignin-PEG composites

However, with the addition of up to 1wt% struktol® TR451 in PLA_L20, there was no notable change in TG curve (Appendix, Figure A.1).

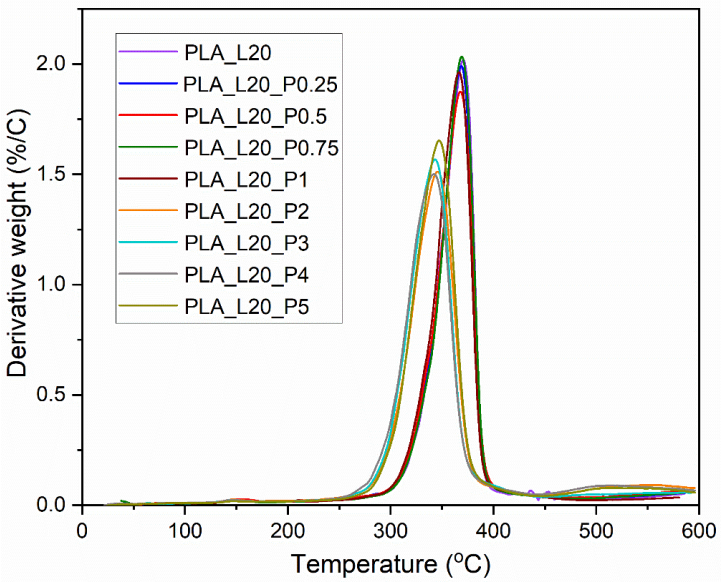

Figure 3.9 DTG curve of PLA-lignin-PEG composites

3.4.3 DSC

The results of DSC using PLA, PLA-lignin and PLA-lignin plasticizer composites are presented in Figure 3.10. Heating cycle gives the three characteristics features namely glass transition, cold

crystallization and melting while cooling cycle gives the crystallization peak that determines the crystalline nature of materials. At 10 ℃/min cooling rate, no significant crystallization peaks were found in case of PLA as well as PLA composites.

From the obtained results, neat PLA showed the Tg of 59 ℃ which decreased to 53 ℃ on incorporating 20 wt% of lignin. This implies that on adding 20 wt% lignin in PLA, PLA shows soft and rubbery properties at lower temperature than neat PLA. On performing DSC of same grade PLA, Gkartzou et al. [18] reported the value of Tg to be 59 ℃ which is same as the value obtained in our study. The decrease in Tg with addition of lignin was due to the modification of molecular mobility of the PLA matrix on adding lignin[29]. However, there was no noticeable change in Tg of PLA-lignin composites on adding PEG and struktol. This might be because of low concentration of incorporated PEG and struktol.

There are several factors such as spatial confinement, nucleation on sample boundaries, temperature gradient and melt flow which affects crystallization [13]. Crystallization rate is also affected on adding filler like lignin in PLA matrix. These additional phase (i.e. lignin) either assist or hinders the chain mobility and thus affects the crystallization [13]. From the DSC thermographs (Figure 3.10 a) and a table (Table A.1 in appendix), change in cold crystallization temperature (Tcc) of PLA can be seen with the addition of lignin particles. With the addition of 20wt% lignin, Tcc of PLA decreases from 121 ℃ to 113 ℃ which means that crystallization occurs at lower temperature than neat PLA. Mimini et al. [13] observed the decrease in Tcc from 130 ℃ to 120 ℃ and to 115 ℃ upon adding kraft lignin and lignosulphate in PLA matrix, respectively. Tcc of PLA_L20 further decreased to 107 ℃ and 109 ℃ on adding 5 wt% PEG and 1 wt% struktol, respectively. This decrease in Tcc was basically due to increase in chain mobility [28]. Similarly, on adding 20 wt% lignin, melting temperature of PLA-lignin composite decreased from 150℃ to

146 ℃. However, there was no change in melting temperature of PLA_L20 composite with the addition of PEG and struktol (Figure 3.10 b and c).

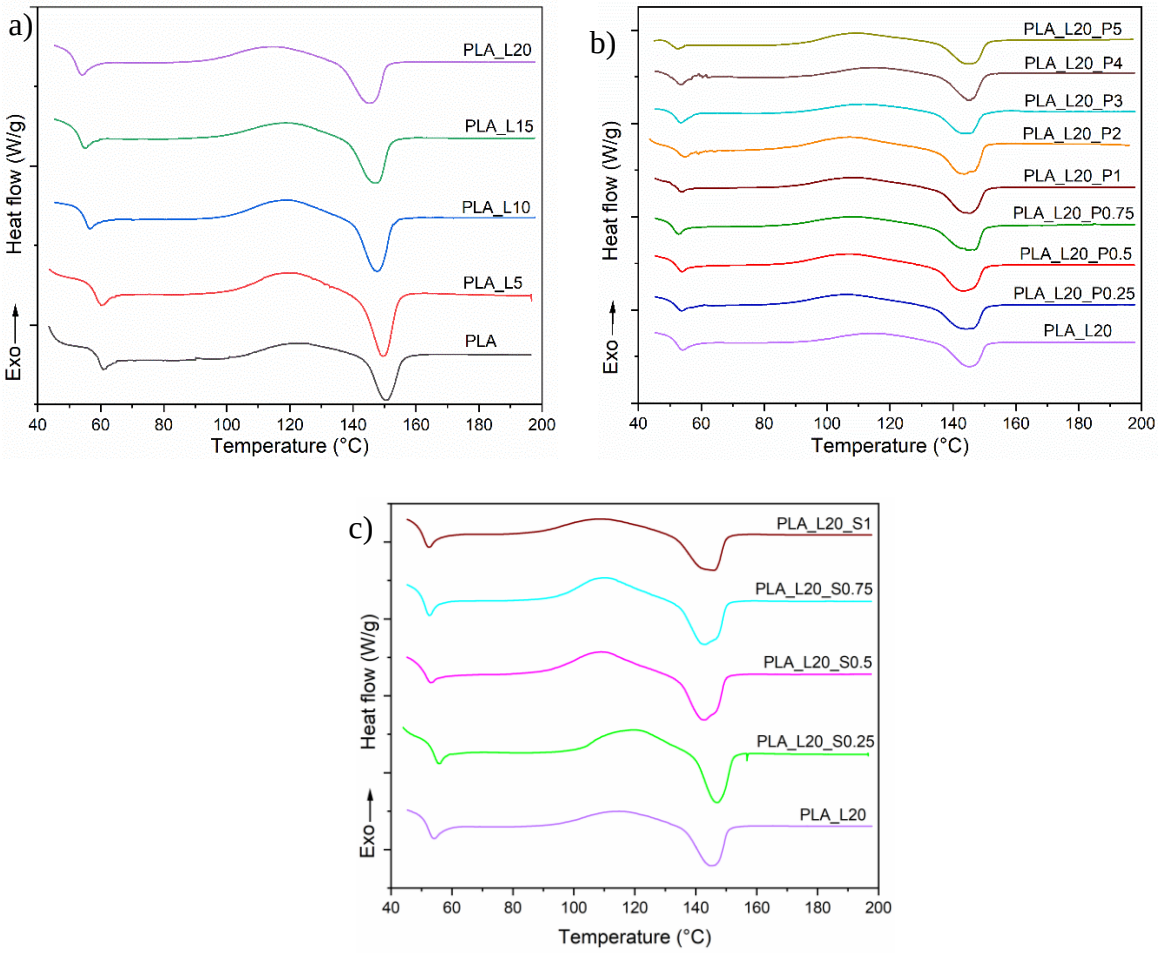

Figure 3.10 DSC graphs (1st heating cycle) of a) PLA-lignin composites b) PLA-lignin-PEG composites and c) PLA-lignin-struktol composites

3.4.4 Mechanical testing

3.4.4.1 PLA-lignin composites

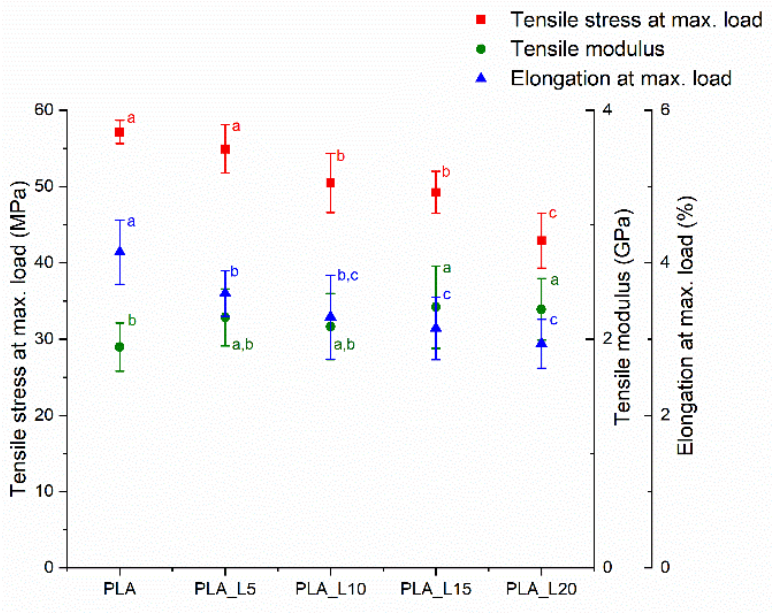

Figure 3.11 Mechanical properties of PLA-lignin composite filaments

(Data presented as average ± standard deviation. Different letter denotes statistically different at $p<0.05$.)

Results of mechanical testing of PLA and PLA-lignin composite filaments are presented in Figure 3.11. Result shows that with the addition of lignin in PLA, tensile strength of the composite decreases. There is a 25% decrease in tensile strength with a 20 wt% addition of lignin. From the statistical analysis, it was found that tensile stress at maximum load of PLA decreased significantly upon adding 10, 15 and 20 wt% of lignin. This was due to decrease in effective load bearing cross-section of PLA in presence of lignin [30]. With the increase in lignin amount, the size of lignin particle gets larger (can be seen in SEM images, Figure 3.17 b to e). Larger the filler size, smaller is the surface area to volume ratio that results in smaller interfacial area and stress transfer to the matrix-filler interface. Anwer et al. [29] also found the decrease in tensile strength with the increase filler size and filler content in the polymer matrix. Similarly, there was significant decrease in elongation at maximum load on adding lignin to PLA matrix. Spiridon et al.[31] also

mentioned 50% decrease in elongation of PLA on adding 15 wt% lignin and explained the reason of decrease might be due to H-bonding and polar interaction between PLA and lignin particles, which restricted the ductile flow. On contrary, tensile modulus increased on adding lignin to PLA matrix which was possibly due to the constraint exerted by the lignin on the PLA matrix [31].

3.4.4.2 PLA-lignin-PEG composites

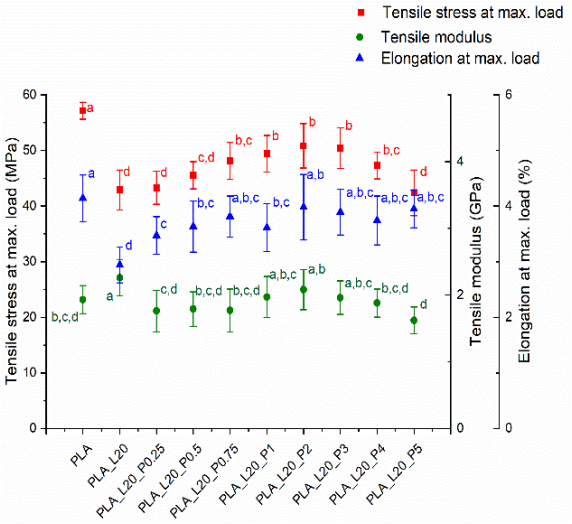

Figure 3.12 Mechanical properties of PLA-lignin-PEG composite filaments

(Data presented as average ± standard deviation. Different letter denotes statistically different at $p<0.05$.)

Tensile stress at maximum load of PLA_L20 increased on adding PEG till 2 wt%. Tensile stress at maximum load of PLA_L20 was increased by nearly 19% on adding 2 wt% PEG. Tensile stress at maximum load decreased on further adding PEG. PLA_L20_P5 had similar tensile strength as that of PLA_L20. On applying Tukey's HSD test for multiple comparison, it was found that concentration of PEG from 0.75-4 wt% in PLA_L20 composite had significant improvement in tensile stress at maximum load when compared with PLA_L20 ($p<0.05$) however the improvement

was not in the range of tensile stress of neat PLA. There still was a significant difference of 11% in tensile stress at max. load between PLA and PLA_L20_P2.

Elongation at maximum load of PLA_L20 on other hand was significantly increased by 35% on adding 2 wt% PEG. There was no significant change in elongation at max. load on further adding PEG till 5 wt%. Also, adding 2-5 wt% PEG in PLA_L20 composite had similar elongation at max. load as that of neat PLA. There was decrease in tensile modulus of PLA_L20 on addition of PEG, and the value was similar to that of neat PLA. Gordobil et al.[32] found the similar decrease in modulus with the addition of plasticizer.

3.4.4.3 PLA-lignin-struktol composites

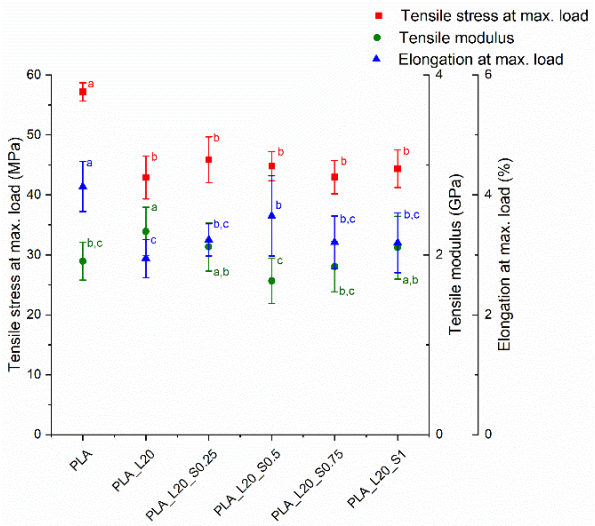

Figure 3.13 Mechanical properties of PLA-lignin-struktol composite filaments

(Data presented as average ± standard deviation. Different letter denotes statistically different at $p<0.05$.)

On adding struktol, a commercial plasticizer, there was slight increase in tensile stress at max load. PLA_L20_S0.25 showed maximum increase in tensile stress at maximum load. Tensile stress at maximum load of PLA_L20 was increased by 7% on adding 0.25 wt% struktol. On performing

Tukey's HSD test for multiple comparison on obtained results of tensile stress of PLA-lignin-struktol composites, it was found that there was no significant improvement in tensile stress at max. load of PLA_L20 composite upon adding struktol till 1 wt% ($p>0.05$).

However, it was found that elongation at maximum load was increased significantly by 24% on adding 0.5 wt% struktol in PLA_L20 composite. On adding struktol above that there was a decrease in elongation at max. load of PLA_L20. On the other hand, as expected, tensile modulus of PLA_L20 decreased on adding struktol plasticizer. And the tensile modulus of PLA_L20 with varying concentration of struktol had no significant difference than that of neat PLA.

3.4.5 DMA

Storage or dynamic modulus (E') indicates the stiffness of the material and is related to Young's modulus [33]. It represents the ability of material to store the applied energy. With the increase in temperature, E' decreases and the decrease is sharp once it reaches the glass transition temperature. This decrease in E' is due to increment in molecular mobility of polymer chain [34,35]. The variation in E' as a function of temperature for PLA-lignin composites, PLA-lignin-PEG composites and PLA-lignin-struktol composites are shown in Figure 3.14a, 3.14b and 3.14c, respectively. E' of PLA-lignin composite was higher than that of PLA implying that stiffness of PLA increases on adding lignin. It was found that even with the lower concentration of lignin, PLA_L5 exhibited similar E' as that of PLA_L15 and PLA_L20 which might be due to the better dispersion of lignin at lower concentration (which can be seen from SEM image, Figure 3.17b). Better dispersion is expected to have stronger interfacial bonding which results in higher storage modulus. Dahal et al.[35] also found the improvement in E' of the composite with the improvement in filler dispersion in polymer matrix.

It was found that with the addition of PEG in PLA_L20 composite, there was decrease in E'. The rigidity and stiffness of PLA_L20 composite declines due to plasticizing effect of PEG and flexibility of molecular chain. Guo et al. [36] found similar decrease in storage modulus upon adding epoxidized soybean oil in PLA-succinylated lignin-epoxidized soybean oil composites. There was also a decrease in E' upon addition of struktol to 1 wt% in PLA_L20 composite which might also be due to plasticization effect of struktol.

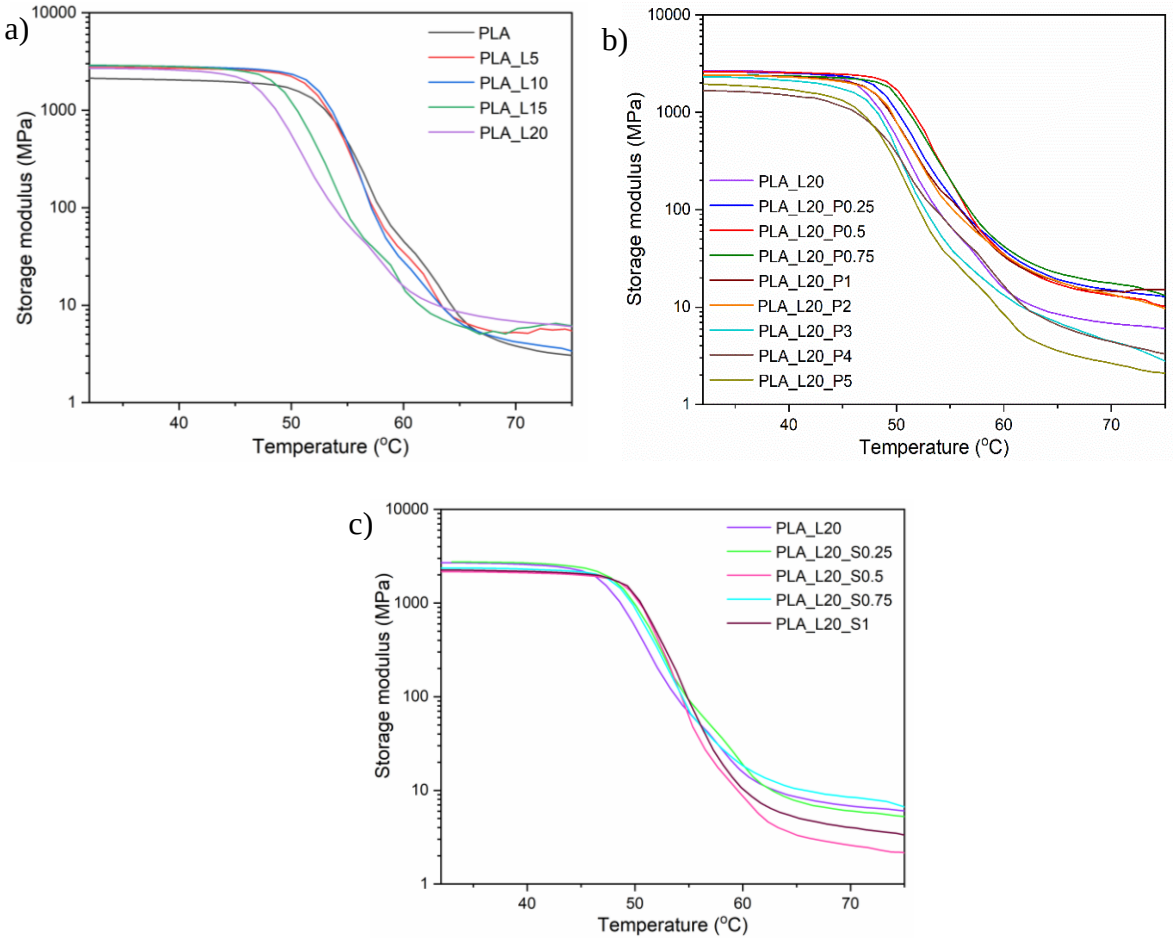

Figure 3.14 Storage modulus of a) PLA-lignin composites b) PLA-lignin-PEG composites and c) PLA-lignin-struktol composites

Tan δ is the mechanical damping factor or loss factor and is represented as ratio of loss modulus to storage modulus. From the Figure 3.15, it can be noted that with the increase in temperature,

tan δ value increases till it reaches Tg and then decreases. Temperature at which gives maximum tan δ value is Tg. High value of tan δ represents the non-elastic nature of material whereas lower value represents the elasticity [33]. From Figure 3.15a, it was found that there was no notable change in Tg on adding 5 and 10 wt% lignin. However, Tg shifts slightly to the lower temperature with addition of 15 and 20 wt% of lignin which is due to poor dispersion of lignin particles in PLA matrix (can be seen in SEM images, Figure 3.17d and e)

Figure 3.15b represents the loss factor with respect to temperature of PLA_L20 and PLA_L20 with varying concentration of PEG. It was found that the value of tan δ decreased with the addition of PEG. Decrease in value of tan δ with addition of PEG (till 3 wt%) represents elastic nature of composite which is due to plasticizing effect of PEG and improvement in dispersion of lignin particles in PLA matrix. However, there was increase in the value of tan δ on further increasing PEG to 5 wt% which is probably due to presence of void as seen in SEM images (Figure 3.17h). Furthermore, there was no notable shift in glass transition temperature with the addition of PEG.

Loss factor with respect to temperature of PLA_L20 and PLA_L20 with varying concentration of struktol is represented in Figure 3.15c. It was found that there was slight decrease in the value of tan δ on adding struktol on varying concentration. This was probably due to less improvement in lignin dispersion on adding struktol.

On comparing the value of Tg between the one obtained from DSC and DMA, value of Tg obtained from DMA are comparatively higher than that obtained from DSC. Since Tg represents thermo dynamic transition, its value for same material depends on several factors such as measurement technique, sample geometry, and anisotropy [37]. And the anisotropic nature of 3D printed samples is the reason behind the difference in values obtained among DMA and DSC [37].

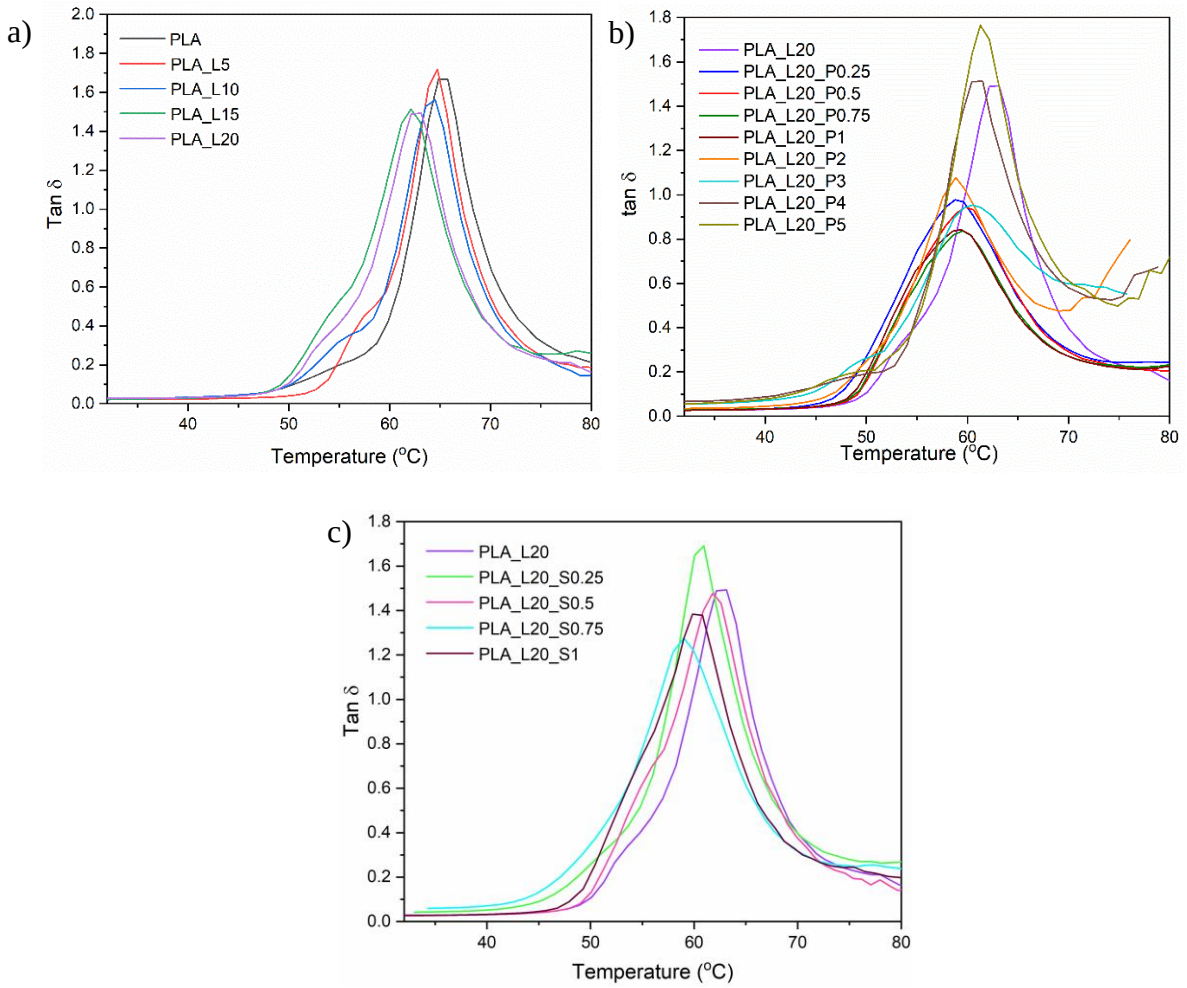

Figure 3.15 Loss factor of a) PLA-lignin composites b) PLA-lignin-PEG composites and c) PLA-lignin-struktol composites

Loss modulus is the material's ability to dissipate applied energy. It represents the viscous response of the material. E" is sensitive to different molecular motions, transition, morphology and structural heterogeneities [33]. The curves of PLA and PLA-lignin composites are presented in Figure 3.16a. At room temperature, it was found that neat PLA had low E'' than other composites. This represented that there was change in polymer motion [36]. Increase in lignin content resulted to increase in the molecular friction and this might be the reason of higher E" of PLA-lignin composites. From Figure 3.16b and Figure 3.16c, it was found that there was slight decrease in E" with addition of 1 wt% of both PEG and struktol.

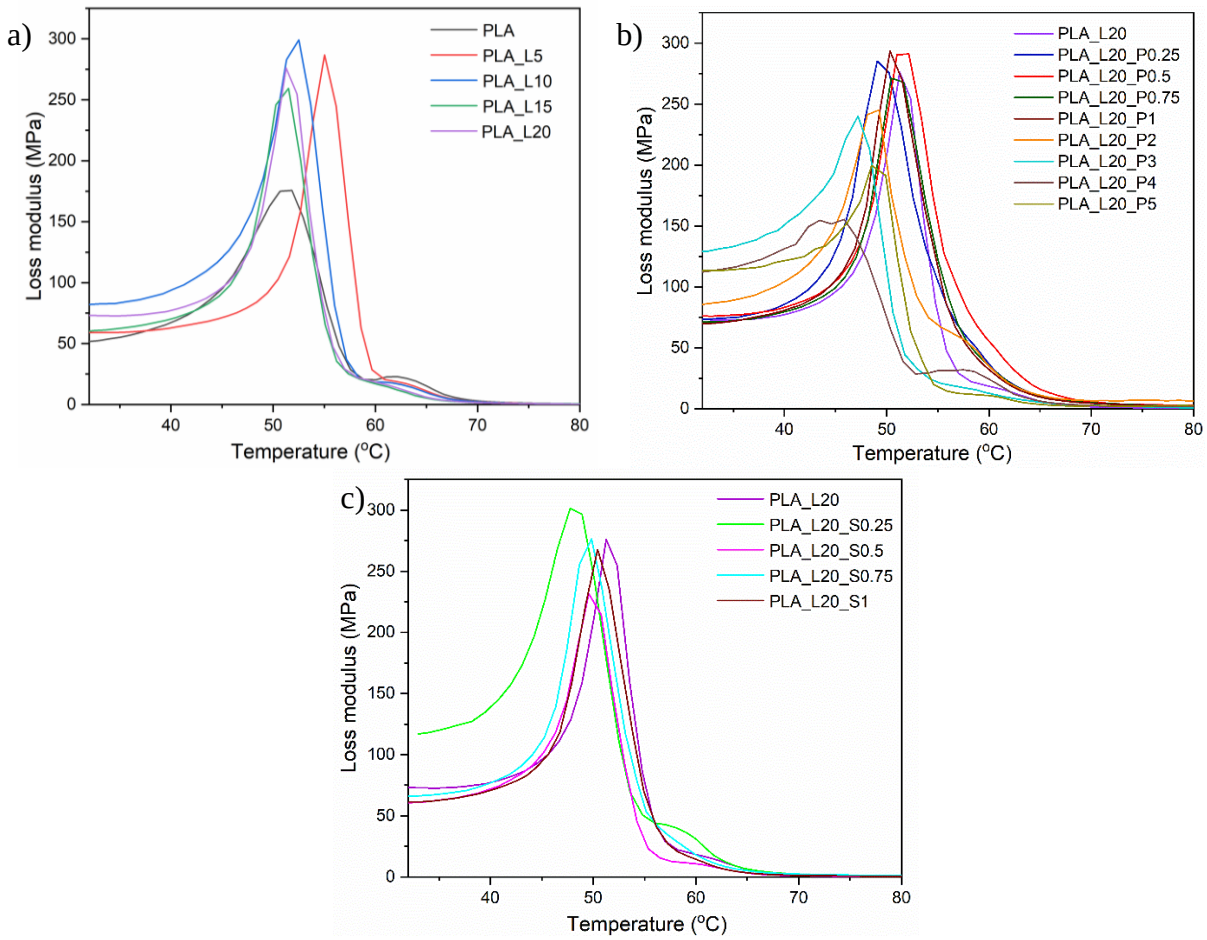

Figure 3.16 Loss modulus of a) PLA-lignin composites b) PLA-lignin-PEG composites and c) PLA-lignin-struktol composites

3.4.6 SEM

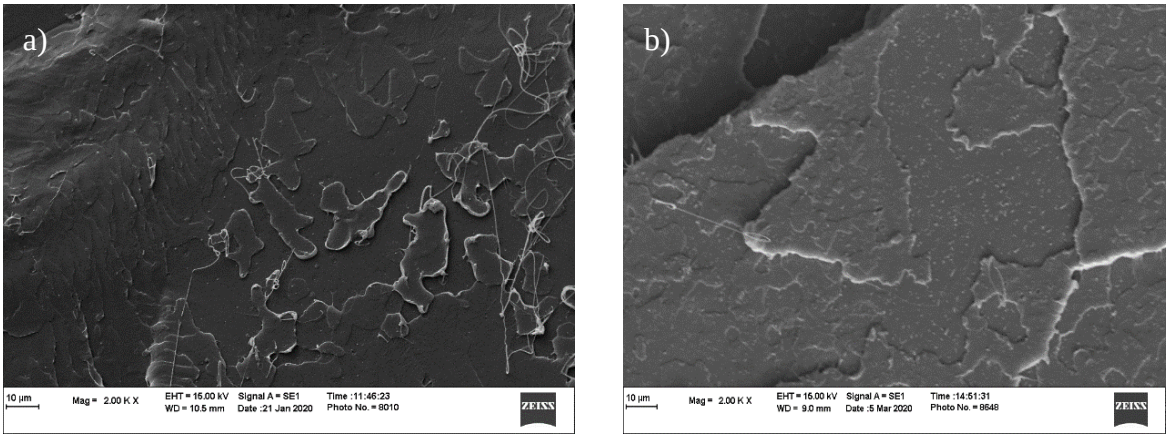

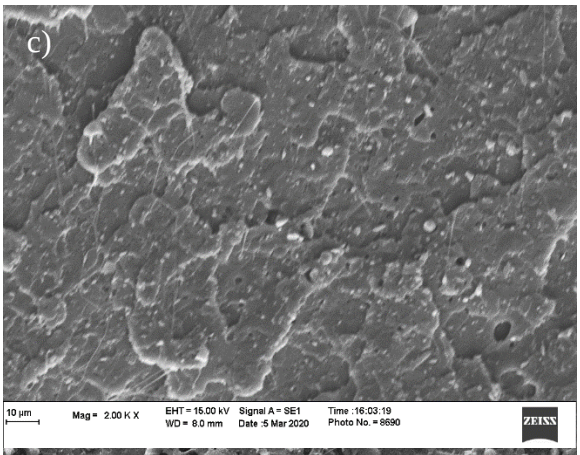
c)
10 µm
Mag = 2.00 K X
EHT = 15.00 kV
WD = 8.0 mm
Signal A = SE1
Date :5 Mar 2020
Time :16:03:19
Photo No. = 8690
ZEISS

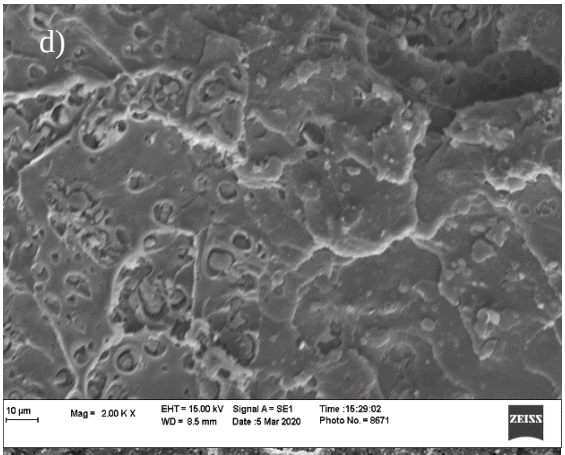
d)
10 µm
Mag = 2.00 K X
EHT = 15.00 kV
WD = 8.5 mm
Signal A = SE1
Date :5 Mar 2020
Time :15:29:02
Photo No. = 8671
ZEISS

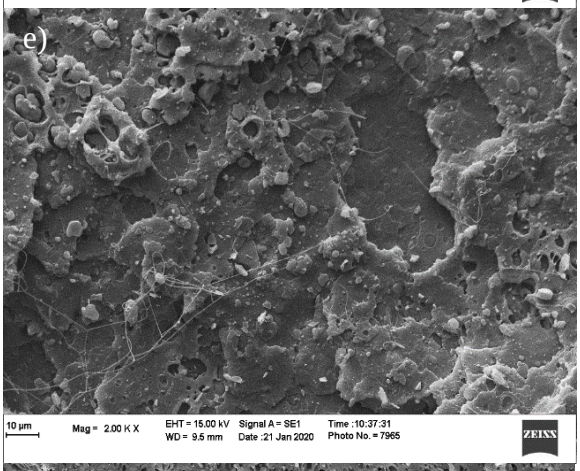
e)
10 µm
Mag = 2.00 K X
EHT = 15.00 kV
WD = 9.5 mm
Signal A = SE1
Date :21 Jan 2020
Time :10:37:31
Photo No. = 7965
ZEISS

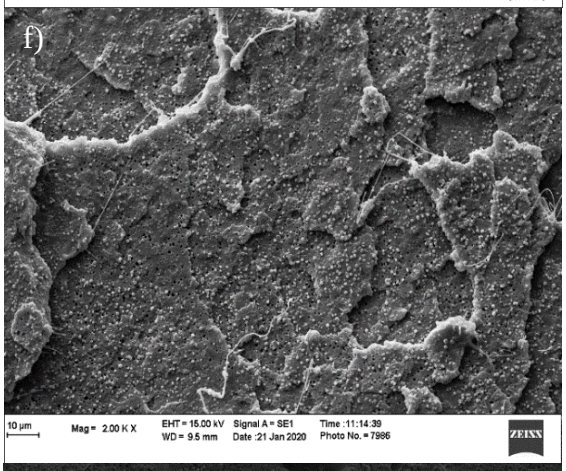
f)
10 µm
Mag = 2.00 K X
EHT = 15.00 kV
WD = 9.5 mm
Signal A = SE1
Date :21 Jan 2020
Time :11:14:39
Photo No. = 7986
ZEISS

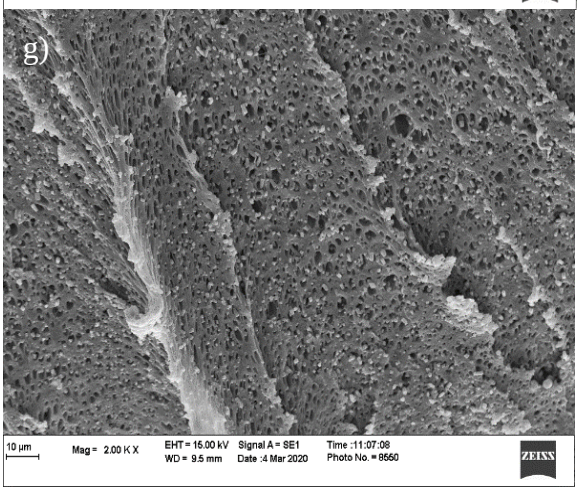
g)
10 µm
Mag = 2.00 K X
EHT = 15.00 kV
WD = 9.5 mm
Signal A = SE1
Date :4 Mar 2020
Time :11:07:08
Photo No. = 8550
ZEISS

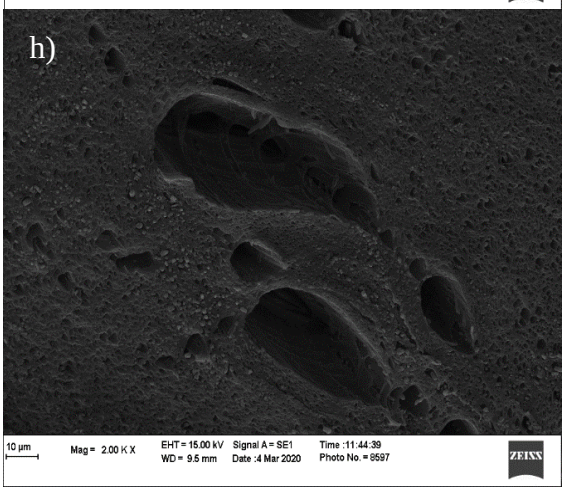
h)
10 µm
Mag = 2.00 K X
EHT = 15.00 kV
WD = 9.5 mm
Signal A = SE1
Date :4 Mar 2020
Time :11:44:39
Photo No. = 8597
ZEISS

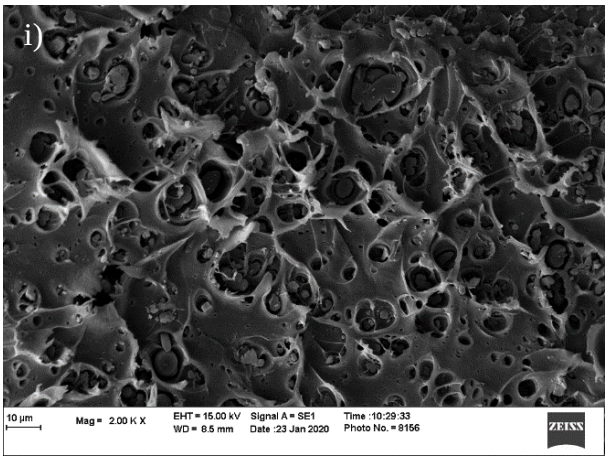

Figure 3.17 SEM images of cryogenically fractured a) PLA b) PLA_L5 c) PLA_L10 d) PLA_L15 e) PLA_L20 f) PLA_L20_P1 g) PLA_L20_P2 h) PLA_L20_P5 and i) PLA_L20_S1 composite filament

SEM of neat PLA (Figure 3.17a) seems smooth with little plastic deformation representing a brittle failure. With the increase of lignin content, size of lignin particle enlarges. Similar enlargement in particle size of lignin with increase in lignin content was observed by Nguyen et al.[1] too. On adding PEG in PLA_L20 composite, particle size of lignin was greately reduced and lignin paticles were well dispersed in PLA matrix as well. The mechanical properties of PLA-lignin composites were highly influenced by the dispersion of lignin. Smaller the particle size, larger is the interfacial area and larger is the stress transfer to matrix-filler inteface. This was the reason of increase in tensile strength of PLA_L20 composite with addition of PEG to 1-2 wt%. There was increase in ductile fibrils with the increase in PEG content till 2 wt% (in Figure 3.17g) which represented equal dispersion of PEG particles in PLA matrix and resulted in increase in elongation at maximum load [38]. However on further increase in PEG content to 5 wt%, there was observable voids in fractured surface, which was probably due to accumulation of PEG during phase separation (Figure 3.17h). These observable voids and cavities were probably the reason for decrease in tensile strength of the composite. Similar ductile fibrils as well as voids were observed by Sungsanit et al.[38] on varying PEG content in PLA matrix.

On observing the SEM image of PLA_L20_S1 composite (Figure 3.17i), it was found that there was not significant decrease in lignin particle size. Also the distribution of lignin particle in PLA matrix was not improved on adding struktol. Cryogenically fractured surface had short fibrially structure which represents the ductile failure nature. This was the reason behind slight improvement in elongation at maximum load on adding 1 wt% struktol in PLA_L20.

PLA_L20_P2 composite filaments showed better mechanical properties among PLA_L20 and PLA_L20_plasticizer composites so the PLA_L20_P2 filaments were used for 3D printing of dog bone sample to investigate the 3D printing behavior and print quality. It was found that nature of filament diameter and its consistency played the crucial role in the final print obtained, sample's mechanical properties and shape accuracy. It was found that region printed with lower filament diameter had observable voids, pores and missing layers whereas the one printed with diameter above 1.9 mm had problem of over-extrusion. Over- extrusion was major reason behind the poor shape and dimension accuracy. On observing the SEM images of fractured dog bone sample (Figure 3.18), it was found that there was good layer adhesion between two printed layers and no voids.

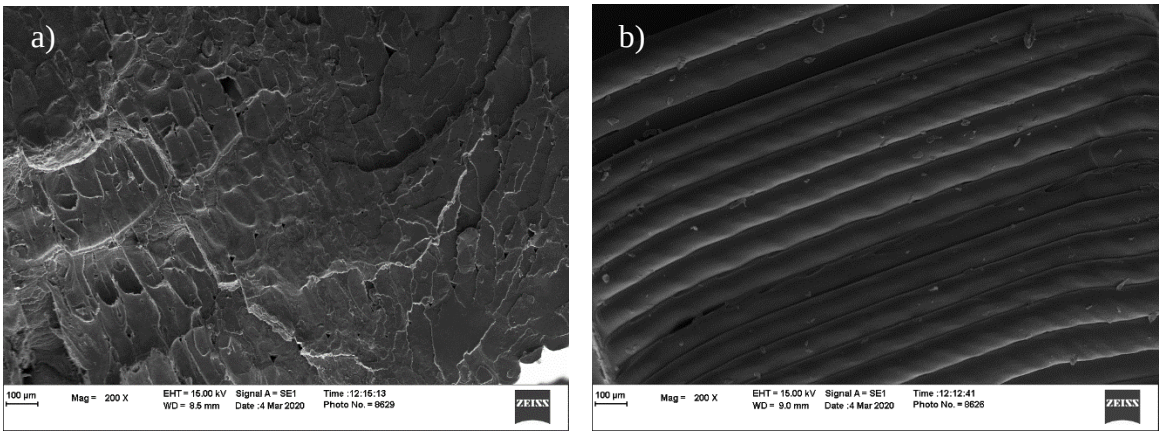

Figure 3.18 SEM images of a) fracture surface and b) side view of dog bone sample prepared from PLA_L20_P2 filaments

3.4.7 FTIR

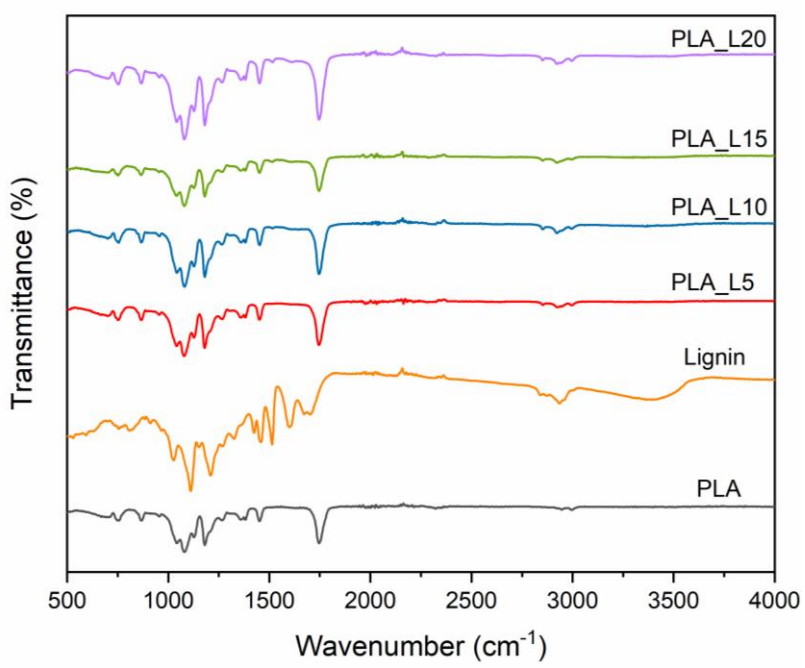

Figure 3.19 FTIR spectra of PLA and PLA-lignin composites

FTIR spectra of PLA and PLA-lignin composites are presented in the Figure 3.19. From the FTIR spectrum of neat PLA, strong absorption band near 1746 cm^{-1} is seen which was attributed by C=O stretching of carbonyl group. Lignin spectrum had similar IR absorption near this region, but the peak intensity is weaker as compared to that of PLA. In the spectrum of PLA, peak at 1450 cm^{-1}, 1380 cm^{-1} and 1360 cm^{-1} were induced by CH_3 anti-symmetric bending vibration, Deformation and symmetric mode of CH group respectively whereas the one nearly at 2996 cm^{-1} was due to stretching of CH_3 group.

O-H stretching of hydroxyl group of lignin, yielded a strong absorption band near 3400 cm^{-1} [30]. On adding lignin in PLA matrix, there was slight increase in peak intensity at 3450 cm^{-1}. This might be because of formation of hydrogen bond between phenolic hydroxyl group of lignin and

carbonyl groups of PLA [30,39]. Small peak at 1515 cm^{-1} can be seen in PLA_L20 composite which might have attributed by C=C groups of aromatic rings of lignin[20].

Table 3.3 represents the different peaks for PLA and lignin along with the representation of vibration for respective peaks. Since the amount of PEG and struktol added was in small, there was not any notable changes in spectra.

Table 3.3 Data of FTIR spectra of PLA and lignin [30,40]

Material	Wavenumber (cm^{-1})	Vibration
PLA	2996 and 2940	Asymmetric and symmetric stretching vibration of CH_3
	1746	C=O stretching vibration
	1450	CH_3 antisymmetric bending vibration
	1380 and 1360	Deformation and symmetric mode of CH group
	1180, 1080 and 1038	C-O-C stretching vibration
Lignin	3380	OH stretching vibration in aromatic and aliphatic OH group
	2935 and 2865	CH asymmetric and symmetric vibration in methyl and methylene group
	1600 and 1513	C-C of aromatic skeletal vibration
	1459	CH deformation in CH_2 and CH_3
	1424	CH aromatic ring vibration

3.5 Conclusions

Biocomposite filaments using PLA and lignin were developed, and their thermal, mechanical, and morphological properties were studied. On adding lignin, there was gradual decrease in tensile strength and elongation whereas increase in tensile modulus and storage modulus. Even upon 5 wt% addition of lignin, there was significant drop in elongation at maximum load; however, tensile strength was comparable to that of PLA. We demonstrated that 20 wt% PLA can be replaced by lignin while making filaments but with the significant decrease in tensile strength and elongation. However, the modulus increased with the increase in lignin percentage. On increasing the lignin

content above that, filament obtained were brittle and did not have enough flexibility to be rolled in the filament spooler.

It was found that addition of 2 wt% of PEG in PLA_L20 composite, tensile strength, and elongation of PLA_L20 significantly increased by 19% and 35%, respectively. On the other hand, adding 0.5 wt% struktol in PLA_L20 significantly increased elongation by 24%. However, there was no significant improvement in tensile strength. Prepared bio-composites showed good extrudability and printability. SEM images of the 3D printed specimen suggested the better adhesion between the layers with no observable voids. Even after adding the plasticizer in PLA_L20 composites, tensile strength was still significantly lower by 11% than neat PLA.

3.6 References

[1] Nguyen NA, Barnes SH, Bowland CC, Meek KM, Littrell KC, Keum JK, et al. A path for lignin valorization via additive manufacturing of high-performance sustainable composites with enhanced 3D printability. Sci Adv 2018;4:eaat4967. https://doi.org/10.1126/sciadv.aat4967.

[2] Ngo TD, Kashani A, Imbalzano G, Nguyen KTQ, Hui D. Additive manufacturing (3D printing): a review of materials, methods, applications and challenges. Compos Part B Eng 2018;143:172–96. https://doi.org/10.1016/j.compositesb.2018.02.012.

[3] Xu W, Wang X, Sandler N, Willför S, Xu C. Three-dimensional printing of wood-derived biopolymers: a review focused on biomedical applications. ACS Sustain Chem Eng 2018;6:5663–80. https://doi.org/10.1021/acssuschemeng.7b03924.

[4] Valerga AP, Batista M, Salguero J, Girot F. Influence of PLA filament conditions on characteristics of FDM parts. Materials (Basel) 2018;11. https://doi.org/10.3390/ma11081322.

[5] Liu Z, Wang Y, Wu B, Cui C, Guo Y, Yan C. A critical review of fused deposition modeling 3D printing technology in manufacturing polylactic acid parts. Int J Adv Manuf Technol 2019;102:2877–89. https://doi.org/10.1007/s00170-019-03332-x.

[6] Tran TN, Bayer IS, Heredia-Guerrero JA, Frugone M, Lagomarsino M, Maggio F, et al. Cocoa shell waste biofilaments for 3D printing applications. Macromol Mater Eng 2017;302:1–10. https://doi.org/10.1002/mame.201700219.

[7] Goyanes A, Det-Amornrat U, Wang J, Basit AW, Gaisford S. 3D scanning and 3D printing as innovative technologies for fabricating personalized topical drug delivery systems. J Control Release 2016;234:41–8. https://doi.org/10.1016/j.jconrel.2016.05.034.

[8] Chim H, Hutmacher DW, Chou AM, Oliveira AL, Reis RL, Lim TC, et al. A comparative analysis of scaffold material modifications for load-bearing applications in bone tissue engineering. Int J Oral Maxillofac Surg 2006;35:928–34. https://doi.org/10.1016/j.ijom.2006.03.024.

[9] Kumar N, Jain PK, Tandon P, Pandey PM. 3D printing of flexible parts using eva material. Mater Phys Mech 2018;37:124–32. https://doi.org/10.18720/MPM.3722018-3.

[10] Terekhina S, Skornyakov I, Tarasova T, Egorov S. Effects of the infill density on the mechanical properties of nylon specimens made by filament fused fabrication. Technologies 2019;7:57. https://doi.org/10.3390/technologies7030057.

[11] McLouth TD, Severino J V., Adams PM, Patel DN, Zaldivar RJ. The impact of print orientation and raster pattern on fracture toughness in additively manufactured ABS. Addit Manuf 2017;18:103–9. https://doi.org/10.1016/j.addma.2017.09.003.

[12] Harris M, Potgieter J, Archer R, Arif KM. Effect of material and process specific factors on the strength of printed parts in fused filament fabrication: a review of recent developments. Materials (Basel) 2019;12. https://doi.org/10.3390/ma12101664.

[13] Mimini V, Sykacek E, Hashim SNA, Holzweber J, Hettegger H, Fackler K, et al. Compatibility of kraft lignin, organosolv lignin and lignosulfonate with PLA in 3D printing. J Wood Chem Technol 2019;39:14–30. https://doi.org/10.1080/02773813.2018.1488875.

[14] Cuiffo MA, Snyder J, Elliott AM, Romero N, Kannan S, Halada GP. Impact of the fused deposition (FDM) printing process on polylactic acid (PLA) chemistry and structure. Appl Sci 2017;7:579. https://doi.org/10.3390/app7060579.

[15] Gordobil O, Egüés I, Llano-Ponte R, Labidi J. Physicochemical properties of PLA lignin blends. Polym Degrad Stab 2014;108:330–8. https://doi.org/10.1016/j.polymdegradstab.2014.01.002.

[16] Wasti S, Adhikari S. Use of biomaterials for 3D printing by fused deposition modeling technique: a review. Front Chem 2020;8:1–14. https://doi.org/10.3389/fchem.2020.00315.

[17] Xu W, Pranovich A, Uppstu P, Wang X, Kronlund D, Hemming J, et al. Novel biorenewable composite of wood polysaccharide and polylactic acid for three dimensional printing. Carbohydr Polym 2018;187:51–8. https://doi.org/10.1016/j.carbpol.2018.01.069.

[18] Gkartzou E, Koumoulos EP, Charitidis CA. Production and 3D printing processing of bio-based thermoplastic filament. Manuf Rev 2017;4:1. https://doi.org/10.1051/mfreview/2016020.

[19] Chiulan I, Frone A, Brandabur C, Panaitescu D. Recent advances in 3D printing of aliphatic polyesters. Bioengineering 2017;5:2. https://doi.org/10.3390/bioengineering5010002.

[20] Tanase-Opedal M, Espinosa E, Rodríguez A, Chinga-Carrasco G. Lignin: a biopolymer from forestry biomass for biocomposites and 3D printing. Materials (Basel) 2019;12:1–15. https://doi.org/10.3390/ma12183006.

[21] Leão AL, Cesarino I, Dias OAT, Negrão DR, Gonçalves DFC. Recent approaches and future trends for lignin-based materials. Mol Cryst Liq Cryst 2017;655:204–23. https://doi.org/10.1080/15421406.2017.1360713.

[22] Kun D, Pukánszky B. Polymer/lignin blends: Interactions, properties, applications. Eur Polym J 2017;93:618–41. https://doi.org/10.1016/j.eurpolymj.2017.04.035.

[23] Nguyen NA, Bowland CC, Naskar AK. A general method to improve 3D-printability and inter-layer adhesion in lignin-based composites. Appl Mater Today 2018;12:138–52. https://doi.org/10.1016/j.apmt.2018.03.009.

[24] Akato K, Tran CD, Chen J, Naskar AK. Poly(ethylene oxide)-assisted macromolecular self-assembly of lignin in ABS matrix for sustainable composite applications. ACS Sustain Chem Eng 2015;3:3070–6. https://doi.org/10.1021/acssuschemeng.5b00509.

[25] Gordobil O, Moriana R, Zhang L, Labidi J, Sevastyanova O. Assesment of technical lignins for uses in biofuels and biomaterials: structure-related properties, proximate analysis and chemical modification. Ind Crops Prod 2016;83:155–65. https://doi.org/10.1016/j.indcrop.2015.12.048.

[26] Migneault S, Koubaa A, Erchiqui F, Chaala A, Englund K, Wolcott MP. Effects of processing method and fiber size on the structure and properties of wood-plastic composites. Compos Part A Appl Sci Manuf 2009;40:80–5. https://doi.org/10.1016/j.compositesa.2008.10.004.

[27] Watkins D, Nuruddin M, Hosur M, Tcherbi-Narteh A, Jeelani S. Extraction and characterization of lignin from different biomass resources. J Mater Res Technol 2015;4:26–32. https://doi.org/10.1016/j.jmrt.2014.10.009.

[28] Li D, Jiang Y, Lv S, Liu X, Gu J, Chen Q, et al. Preparation of plasticized poly (lactic acid) and its influence on the properties of composite materials. PLoS One 2018;13:1–15. https://doi.org/10.1371/journal.pone.0193520.

[29] Anwer MAS, Naguib HE, Celzard A, Fierro V. Comparison of the thermal, dynamic mechanical and morphological properties of PLA-Lignin & PLA-Tannin particulate green composites. Compos Part B Eng 2015;82:92–9. https://doi.org/10.1016/j.compositesb.2015.08.028.

[30] Kumar Singla R, Maiti SN, Ghosh AK. Crystallization, morphological, and mechanical response of poly(lactic Acid)/lignin-based biodegradable composites. Polym - Plast Technol Eng 2016;55:475–85. https://doi.org/10.1080/03602559.2015.1098688.

[31] Spiridon I, Tanase CE. Design, characterization and preliminary biological evaluation of new lignin-PLA biocomposites. Int J Biol Macromol 2018;114:855–63. https://doi.org/10.1016/j.ijbiomac.2018.03.140.

[32] Gordobil O, Egüés I, Labidi J. Modification of Eucalyptus and Spruce organosolv lignins with fatty acids to use as filler in PLA. React Funct Polym 2016;104:45–52. https://doi.org/10.1016/j.reactfunctpolym.2016.05.002.

[33] Saba N, Jawaid M, Alothman OY, Paridah MT. A review on dynamic mechanical properties of natural fibre reinforced polymer composites. Constr Build Mater 2016;106:149–59. https://doi.org/10.1016/j.conbuildmat.2015.12.075.

[34] Jyoti J, Singh BP, Arya AK, Dhakate SR. Dynamic mechanical properties of multiwall carbon nanotube reinforced ABS composites and their correlation with entanglement density, adhesion, reinforcement and C factor. RSC Adv 2016;6:3997–4006. https://doi.org/10.1039/c5ra25561a.

[35] Dahal RK, Acharya B, Saha G, Bissessur R, Dutta A, Farooque A. Biochar as a filler in glassfiber reinforced composites: experimental study of thermal and mechanical properties. Compos Part B Eng 2019;175:107169. https://doi.org/10.1016/j.compositesb.2019.107169.

[36] Guo J, Wang J, He Y, Sun H, Chen X, Zheng Q, et al. Triply biobased thermoplastic composites of polylactide/succinylated lignin/epoxidized soybean oil. Polymers (Basel) 2020;12.

[37] Idrees M, Jeelani S, Rangari V. Three-dimensional-printed sustainable biochar-recycled PET composites. ACS Sustain Chem Eng 2018;6:13940–8. https://doi.org/10.1021/acssuschemeng.8b02283.

[38] Sungsanit K, Kao N, Bhattacharya SN. Properties of linear poly(lactic Acid)/polyethylene glycol blends. Polym Eng Sci 2012:108–16. https://doi.org/10.1002/pen.

[39] Li J, He Y, Inoue Y. Thermal and mechanical properties of biodegradable blends of poly(L-lactic acid) and lignin. Polym Int 2003:949–52. https://doi.org/10.1002/pi.1137.

[40] Guo J, Chen X, Wang J, He Y, Xie H, Zheng Q. The influence of compatibility on the structure and properties of PLA/lignin biocomposites by chemical modification. Polymers (Basel) 2020;12. https://doi.org/10.3390/polym12010056.

Chapter 4

Development of biocomposite filaments using high impact polystyrene (HIPS) and lignin for 3D printing

4.1 Abstract

The search of sustainable material to replace or partially replace petroleum-based polymer is increasing recently. Among them, lignin is the most promising biobased material that can be used for partially replacing petroleum-based polymer. The objective of this research was to develop high impact polystyrene (HIPS) and lignin biocomposite filaments for 3D printing. The thermal, mechanical, and morphological properties of filaments were examined to determine the effect of lignin in HIPS matrix. In this study, we demonstrated 20 wt% replacement of HIPS with lignin but with significant decrease in tensile strength and elongation at break. However, filament with 10 wt% lignin had no significant difference in mechanical properties as that of pure HIPS. Besides, flame test was carried out on HIPS-lignin composites to determine the flame-retardant capacity of lignin showed that adding unmodified lignin do not contribute in improvement of flame-retardant capacity of HIPS.

Keywords: HIPS, lignin, biocomposites, filament, 3D printing.

4.2 Introduction

Three-dimensional (3D) printing is a manufacturing technology in which a 3D object is created from 3D model data through depositing material layer by layer in a build platform [1]. Fused deposition modeling (FDM) is one of the widely used 3D printing techniques that requires solid thermoplastic filament as a feedstock. Most of the thermoplastic filaments used for FDM printing are acrylonitrile butadiene styrene (ABS), nylon, high impact polystyrene (HIPS) and are derived from petroleum based.

Among all the polymers, HIPS is one of the widely used polystyrenes for structural materials, and are prepared by adding polybutadiene during polymerization of polystyrene [2]. It is a thermoplastic resin widely used in several fields such as electronic and electrical industry, construction and automotive production because of its good mechanical properties, electrical character and ease of processing [3–5]. HIPS is also among the widely used polymer in 3D printing. Because of its solubility in chemical limonene, it is generally used to print supporting parts. However, its properties such as easy combustibility and smoke generation limit the application of HIPS in several fields.

Additionally, the excessive use of petroleum-based plastics has increased the growing concern of limited fossil resources as well as environmental pollution. This has driven the interest of scientific community towards the development of sustainable and ecofriendly material. Several studies are being carried out to replace or reduce the use of traditional plastics with green sustainable material.

Lignin is a bio-based amorphous polymer obtained abundantly as a by-(co-)product from pulp and paper and bioethanol industries [6]. Among the different biomaterials studied, lignin is considered one of the promising material for preparing composites because of its low cost, non-toxicity and biocompatibility, biodegradability and could provide multiple functionalities because of its complex structure [6–10]. Several studies regarding polymer-lignin composites were reported where lignin behaved as antioxidant [11,12], flame retardant [13] and nucleating agent [14].

In recent years, researches regarding incorporation lignin in different thermoplastic polymer have been increased which not only helps in reduction of excessive use of traditional polymer but also helps in reduction of cost of filament [15–17]. However, the effect of incorporating lignin in HIPS filament and its use in 3D printing has not been studied yet.

The main objective of this study was to develop HIPS-lignin composite filaments for 3D printing purpose. Lignin with the wt% of 5, 10, 15 and 20 was blended with HIPS and composite filaments were developed. The thermal, mechanical, and morphological properties of thus obtained filaments were studied using a number of analytical tools that are discussed in Section 4.3.

4.3 Materials and Methods

4.3.1 Materials

HIPS pellets were purchased from 3DXTECH (Grand Rapids, MI, USA) and the organosolv lignin was supplied by Attis Innovations, LLC (Milton, GA, USA). The properties of lignin used are mentioned in the Chapter 3 (Section 3.4.1, 3.4.2 and 3.4.3).

4.3.2 Sample preparation

HIPS pellets were oven dried at 80 °C for 8 hrs and lignin was oven dried at 50 °C for more than 24 hrs prior to processing. HIPS pellets and lignin were manually mixed first and then were extruded in twin extruder (Leistritz Mic 18/GL 40D, Nuremberg, Germany). The twin extruder used for extrusion is presented in Chapter 3 (Figure 3.2). Temperature of different zones of extruder were set at 160 ℃, 165 ℃, 170 ℃, 180 ℃, 191 ℃, 195 ℃, 198 ℃ from zone1 to zone 7, and the screw speed was set at 55 rpm. Temperature of different zones was selected based on extrusion temperature of HIPS, and trial and error within that temperature range to get filaments. The filaments obtained from twin extruder had varying diameter in the range of 1.3 to 2.5 mm. Those were coiled and stored in zip lock bags for further characterization.

Table 4.1 Samples prepared along with their sample codes

Sample code	HIPS (wt%)	Lignin (wt%)
HIPS	100	-
HIPS_L5	95	5

HIPS_L10	90	10
HIPS_L15	85	15
HIPS_L20	80	20

4.3.3 TGA

Q 500 (TA instruments, New Castle, DE, USA) was used to perform thermogravimetric analysis of all the samples. Samples of mass ranged from 6.5 to 10.4 mg were placed on platinum pan and were heated from room temperature to 600 ℃ at the heating rate of 10 ℃/min. All the runs were carried out under nitrogen atmosphere with the nitrogen flow rate of 60 mL/min.

4.3.4 DSC

To determine the thermal properties of HIPS and HIP-lignin filaments, DSC was performed using Q2000 (TA instruments, New Castle, DE, USA). Experiment was performed under nitrogen atmosphere with the nitrogen flow rate of 50mL/min. Sample with the mass ranged 3.6 to 4.3 was placed in Tzero aluminum pan and the sample was heated from room temperature to 250℃ and cooled down back to 40℃ with both heating and cooling rate of 10 ℃/min.

4.3.5 Mechanical testing

Instron 5565 (Norwood, MA, USA) was used to measure the mechanical properties of the filaments. The load cell of 1kN was used and the cross-head speed was set at 10 mm/min. The gauge length was fixed at 50 mm. The tensile test was carried out on 15 specimens for each case, and average values were reported.

4.3.6 SEM

Scanning electron microscopy was used to study the surface of cryogenically fractured filaments using Zeiss EVO50 (Carl Zeiss Microscopy, NY, USA). Samples were prepared by gold sputtering

using EMS 150R ES (Electron Microscopy Sciences, PA, USA) sputtering system. Accelerating voltage of 15 kV was used and specimen were studied at different magnification with a working distance of 8.5 to 10 mm approximately.

4.3.7 Flame test

Flame test was performed according to the ASTM D3801-19a to determine fire retardant properties of lignin. Samples were prepared according to the dimension mentioned in the standard by compression molding. CAD drawing of samples are presented in Figure 4.2. Five specimens for each case were subjected to the 20 mm flame for 10 sec and afterflame time for each specimen were noted after 10 sec of flame exposure.

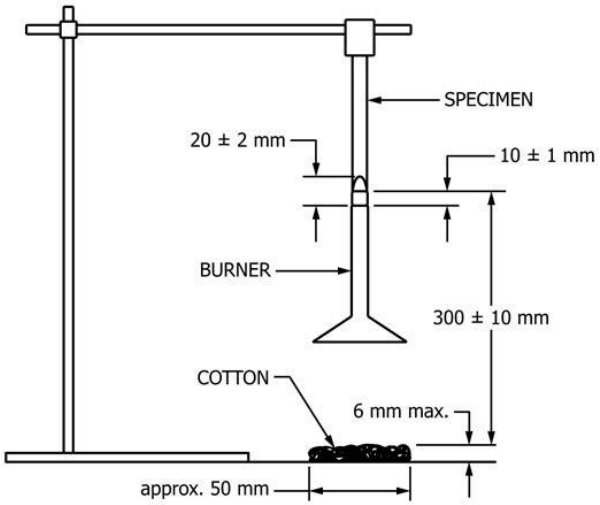

Figure 4.1 Experimental setup according to ASTM D3801-19a [18] (adopted for only illustration)

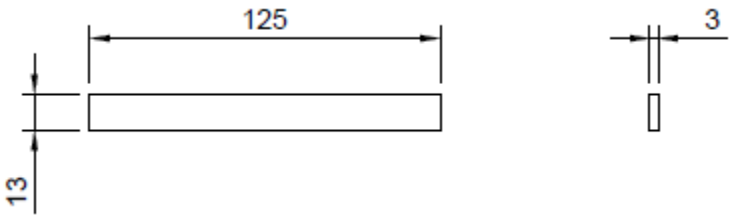

Figure 4.2 CAD drawing of flame test samples

4.3.8 FTIR

Nicolet 6700 FTIR (ThermoFisher Scientific, Madison, WI, USA) was used to perform FT-IR analysis of the sample. Two spectra were collected in the wavelength range from 400 - 4000 cm^{-1} for each sample and average spectrum was reported. Each spectrum was recorded for total of 64 scans with a resolution of $4cm^{-1}$.

4.3.9 3D printing

Filaments in the range of 1.6 to 1.9 mm were selected for 3D printing. 3D printer and all the printing parameters were kept same as Chapter 3 (Section 3.3.3) except extrusion temperature was set at 230 ℃. Dog bone samples according to ASTM D638 type V (CAD drawing shown in Chapter 3, Figure 3.3) were prepared.

4.4 Results

4.4.1 TGA

Thermal stability and degradation nature of a material is determined using the TGA. Figure 4.3 and 4.4 represent the TG and DTG curve of HIPS, lignin, and HIPS-lignin composites, respectively. Single step degradation of the composites can be observed from TG curve. The pure HIPS starts to degrade at 410 ℃ and its maximum degradation occurs at 429 ℃. Xia et al. [4] too found the initial degradation temperature of HIPS to be 410 ℃. With the addition of lignin in HIPS matrix, there was decrease in intial degradation temperature, which can be observed in TG curve below. This was because lignin starts degrading earlier. On incorportaing 20 wt% of lignin in HIPS matrix, intial degradtion temperature was shifted from 410 ℃ to 395 ℃ whereas there was slight change in maximum degradation temperature of HIPS from 429 ℃ to 424 ℃. However, there was increase in char residue from 1 to 9% with addition of 20 wt% lignin at 500 ℃. This shift in intial

degradation might help composite to decompose earlier to form char which acts as covering layer and block the transfer of heat and oxygen [13].

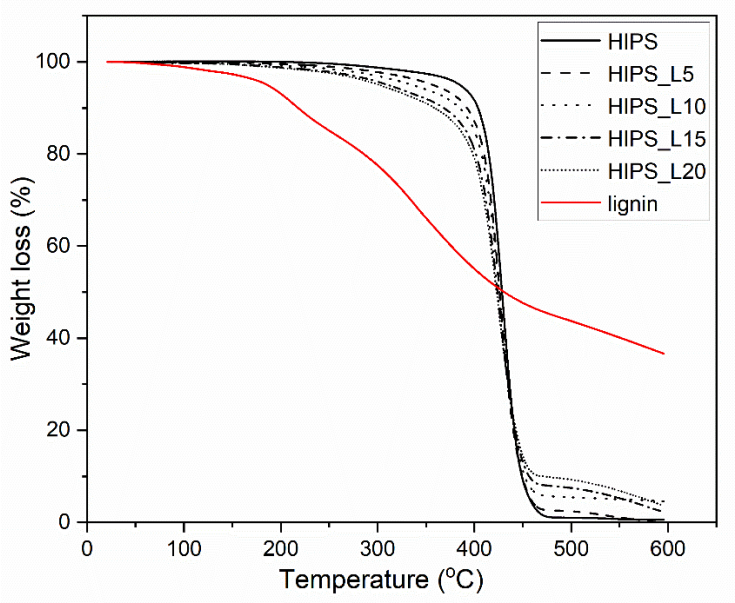

Figure 4.3 TG curve of HIPS and HIPS-lignin composites

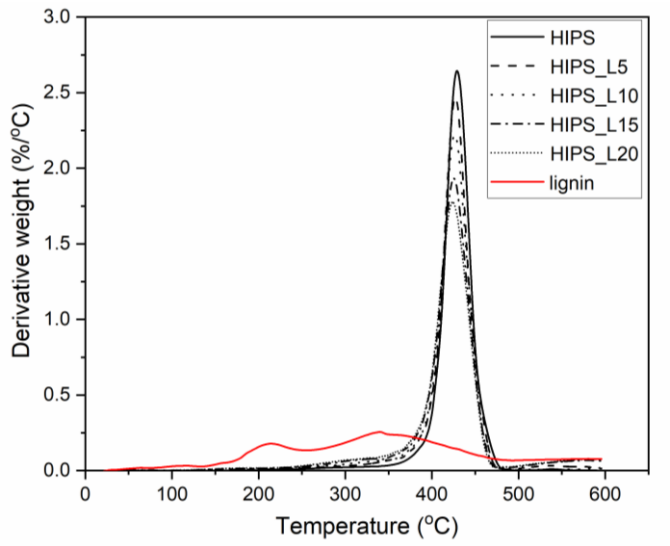

Figure 4.4 DTG curve of HIPS and HIPS-lignin composites

4.4.2 DSC

Heating cycle of DSC curve generally gives glass transition, cold crystallization and melting region. Since HIPS is an amorphous polymer, no clear melting temperature was observed in heating cycle of pure HIPS. However there was a visible change in the curve in the region of 100 ℃ representing the glass transition temperature (Tg) of the HIPS. However, Arraez et al.[19] mentioned slightly lower Tg of HIPS (in the range of 95.4 ℃). Figure 4.5 represents the enlarged section from 60 ℃ to 125 ℃ of heating curve of HIPS and HIPS-lignin composites. From the curve, it can be noted that with the addition of 20 wt% of lignin, there was a gradual shift in Tg from 100 ℃ to 92 ℃. This imples that on heating, HIPS turns out to be rubbery at lower tempertaure on adding lignin. The decrease in Tg with addition of lignin was due to the modification of molecular mobility of the HIPS matrix on adding lignin [20]. This decrease in Tg with addition of lignin and presence of single glass transition region in heating curve of HIPS-lignin composite implies that HIPS and lignin are compatible to certain extent [21]. At 10 ℃/min cooling rate, no notable change in cooling curve was observed on adding lignin.

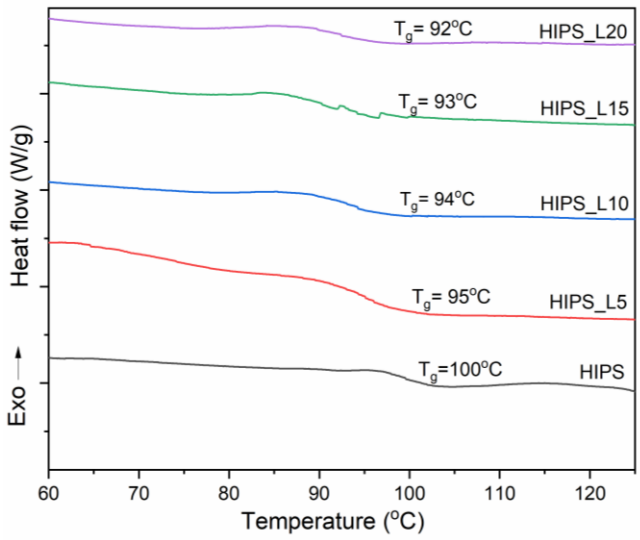

Figure 4.5 Enlarged section of heating curve

4.4.3 Mechanical testing

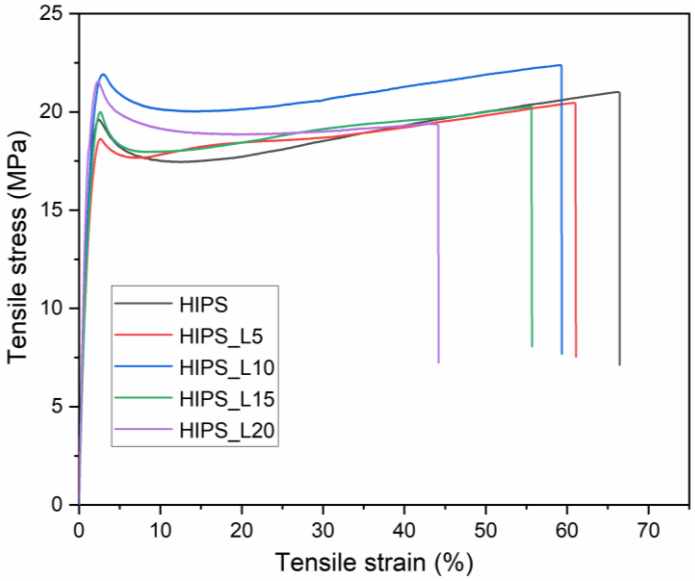

Figure 4.6 Tensile stress-strain curve of HIPS and HIPS-lignin composite filaments

From the tensile test of HIPS filament, tensile strength was found to be 21.73 MPa. Benini et al. [22] found the tensile strength of HIPS slightly higher i.e. 24.6 MPa. From the curve of neat HIPS (in Figure 4.6), it was found that, after filament reached the yield point, filament was still able to bear further increasing load and finally broke at higher value at tensile stress than at yield point. With the 20 wt% addition of lignin, there was change in nature of the curve. Curve reached maximum load condition at the yield point and on further stretching beyond the yield point, tensile stress of filament decreased and finally broke at lower tensile stress than that at yield point.

From the tensile results obtained, it was found that there was no significant difference in tensile strength among HIPS and HIPS-lignin filaments (with lignin content till 15 wt%) However, on increasing the lignin to 20 wt%, there was significant decrease in tensile strength by nearly 8%. Furthermore, there was no significant difference in modulus on adding 20wt% lignin in HIPS matrix. From the Figure 4.6 and Table 4.2, a gradual decrease in elongation at break on adding

lignin can be observed. There is no significant difference in elongation at break till 10 wt% addition of lignin in HIPS matrix; however, the difference turns out to be significant on further adding 15 and 20 wt% lignin. 20 wt% addition of lignin led to decrease in elongation at break of HIPS by 34%.

Table 4.2 Data presenting mean ± standard deviation of mechanical properties of HIPS and HIPS-lignin composite filaments

Sample	Tensile strength (MPa)	Modulus (GPa)	Elongation at break (%)
HIPS	$21.73 \pm 1.71^{a,b}$	$1.17 \pm 0.10^{a,b}$	64.69 ± 5.54^{a}
HIPS_L5	22.61 ± 1.22^{a}	1.03 ± 0.11^{b}	63.86 ± 7.10^{a}
HIPS_L10	$21.06 \pm 1.68^{b,c}$	1.06 ± 0.20^{b}	$58.75 \pm 7.32^{a,b}$
HIPS_L15	$22.06 \pm 1.50^{a,b}$	$1.13 \pm 0.14^{a,b}$	56.11 ± 5.85^{b}
HIPS_L20	20.06 ± 1.06^{c}	1.22 ± 0.15^{a}	42.65 ± 7.62^{c}

Any two means in the same column with different letters are significantly different ($p<0.05$) by the Tukey's HSD test.

4.4.4 SEM

Figure 4.7 a, b, c, d and e represents the SEM images of cryogenically fractured HIPS, HIPS_L5, HIPS_L10, HIPS_L15 and HIPS_L20 filaments, respectively. SEM image of neat HIPS has unidirectional fibrillar structure representing the ductile failure. Such fibrillar structure can also be observed in the SEM images of HIPS_L5 and HIPS_L10 composite. However, on increasing the lignin content, no such fibrillar structure were found in the SEM images (Figure 4.7d and e) which represents the change in nature of deformation from ductile to brittle. Akato et al.[23] observed the similar change in nature of failure from ductile to brittle on adding lignin in ABS matrix. From the SEM images below, it can also be noted that with the increase in lignin content, there is increase in the particle size of lignin which is basically due to coalescence phenomena [15].

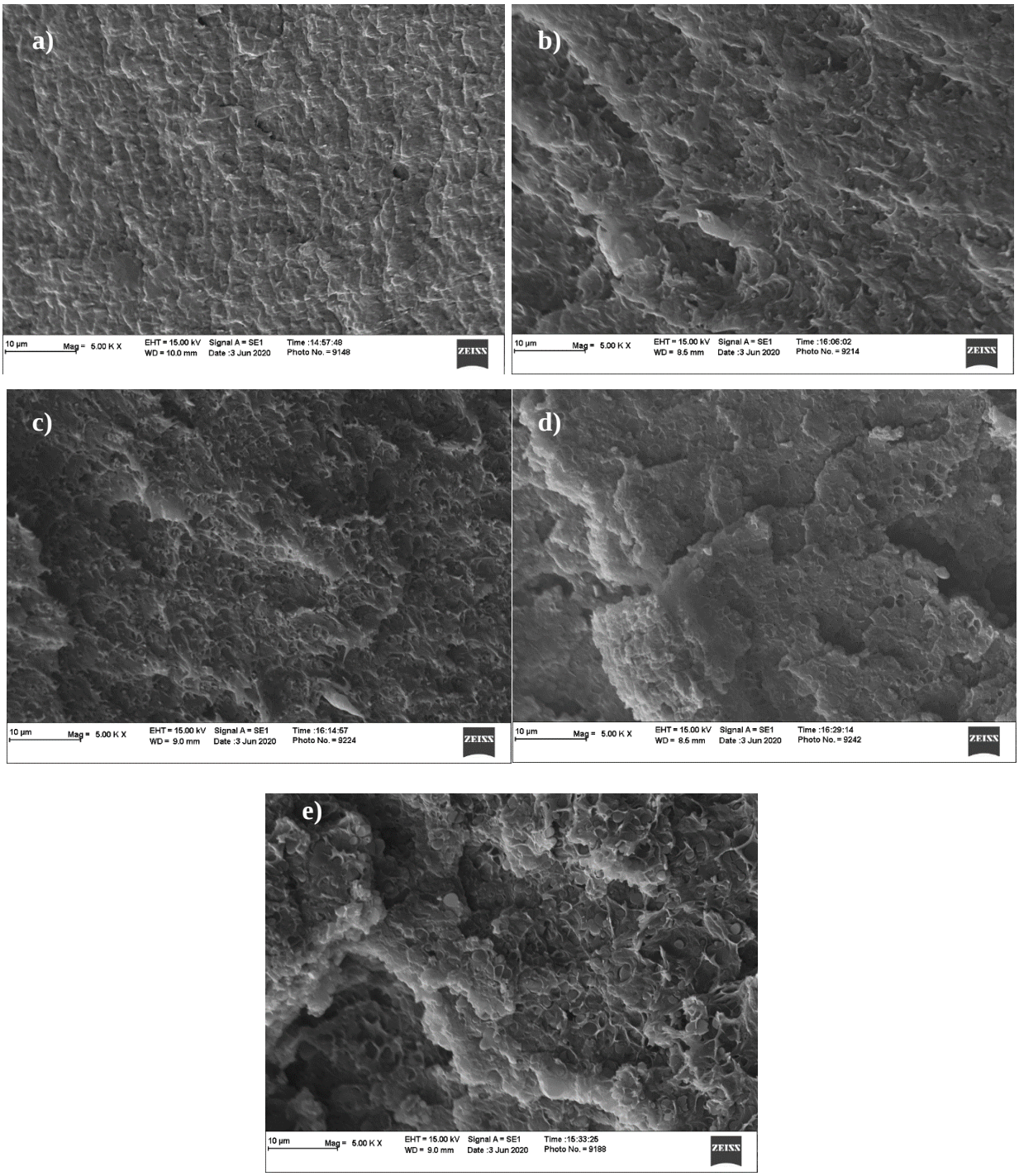

Figure 4.7 SEM images of a) HIPS b) HIPS_L5 c) HIPS_L10 d) HIPS_L15 and e) HIPS_L20 composite filaments

4.4.5 Flame test

Figure 4.8 presents the lab flame test done on the HIPS and HIPS_L20 composite according to the ASTM D3801-19a. After flame time for HIPS and HIPS_L20 was 212.9 ± 14.2 s and 113.1±9.7 s, respectively (data presented as average ± standard deviation). On adding lignin, composite burned faster than that without lignin. The flame burned up to the holding clamps for both HIPS and HIPS_L20 samples. During flaming, the molten flaming material dripped from the specimen on the cotton placed below the specimen and it ignited the cotton as well for all the cases. Specimens for both the cases burned all the way, and there was no need for second ignition. From the overall flame test, it was found that unmodified lignin in HIPS matrix did not show any flame-retardant property. Chen et al.[13] also hardly saw any improvement in UL94 test of polybutylene succinate (PBS) on adding 30wt% pure lignin in PBS. However, they found improvement in fire retardancy properties of lignin on grafting cyanuric chloride - 2,6,7-Trioxa-1-phosphabicyclo-[2,2,2]octane-4-methanol-1-oxide (CNC-PEPA).

Figure 4.8 Lab flame test of HIPS and HIPS-lignin composite samples

4.4.6 FTIR

Figure 4.9 represents the FTIR spectra of HIPS, lignin, and HIPS_L20. From the spectrum of neat HIPS, the peak at 3024 cm^{-1}, 2918-2849 cm^{-1} represents aromatic CH stretching and CH stretching in CH_3 and CH_2 respectively [24]. Lignin spectrum has similar peaks due to CH stretching at 2935 cm^{-1} and 2865 cm^{-1}. The absorption band at 1600 cm^{-1} and 1492 cm^{-1} in HIPS spectrum was due to aromatic ring stretching whereas the one at 1451 cm^{-1} was attributed by CH bend. The other peaks at 1027 cm^{-1}, 694 cm^{-1}, 537 cm^{-1} represented aromatic CH bend, aromatic CH out of plane bend, and aromatic ring out of plane bend respectively[25]. IR spectrum of lignin has peaks at O-H stretching of hydroxyl group of lignin, yielded a strong absorption band near 3400 cm^{-1} [26]. On adding lignin in HIPS matrix, absorption band near 3450 cm^{-1} was observed in HIPS_L20 spectra but the peak intensity was weak than that of lignin. This might be due to interaction between HIPS and lignin.

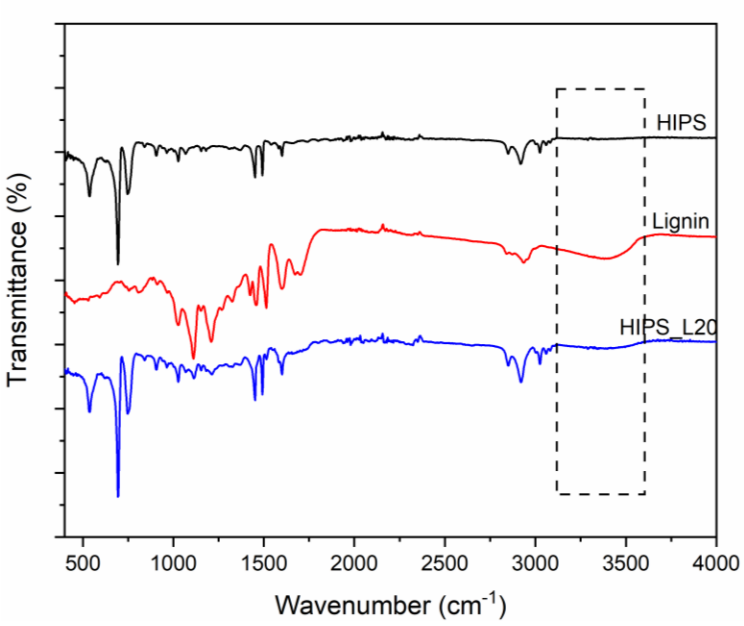

Figure 4.9 FTIR spectra of HIPS, lignin and HIPS_L20 composite

4.4.7 3D printing

The dog bone samples prepared from 3D printing were subjected to tensile testing. On performing the tensile test for all the HIPS as well as HIPS-lignin samples, problems such as failure of only half region of specimens and separation of layers of printed parts were observed, presented in Figure 4.10a and 4.10b. On analyzing, the main reason behind those problems were found to be poor layer adhesion and which was due to the lower bed temperature. It was found that bed temperature plays the crucial role in improving the mechanical properties of the printed parts [27]. The printer used for printing these dog bone samples had maximum bed temperature of 60 ℃, which was less than the glass transition region of HIPS. Generally, it is suggested to use the bed temperature in the glass transition region of the polymer used for 3D printing. Beside these problems, filament showed the good printability. Upon increasing the bed temperature and using the optimized printing parameters, better 3D printed parts can be obtained from the HIPS-lignin composite filaments.

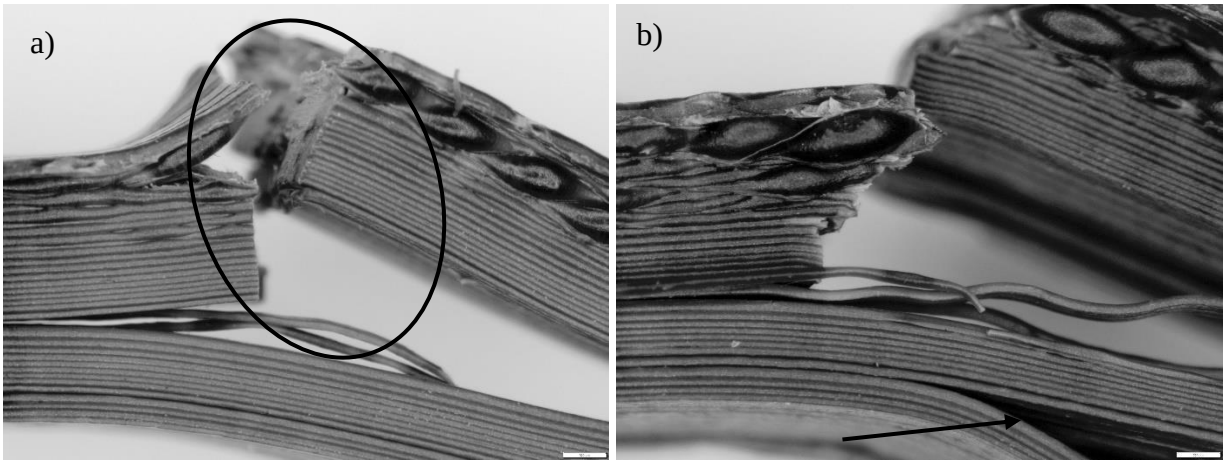

Figure 4.10 Microscopic images of tensile tested specimen, a) specimen failure in half region and b) layer separation

4.5 Conclusions

Bio composite filaments using HIPS and lignin were developed and their thermal, mechanical, and morphological properties were studied. Furthermore, flame-retardant properties of HIPS-lignin composites were also investigated. We were able to replace 20 wt% of HIPS with lignin but with significant decrease in tensile strength and elongation at break. On further increasing the lignin content to 25 wt%, filaments did not have enough flexibility to be rolled around the filament spooler. From mechanical testing, it was found that on replacing till 10 wt% HIPS with lignin, the filaments showed comparable properties to that of neat HIPS and had no significant difference in tensile strength, elongation at break and modulus. Besides, the obtained filaments exhibited good printability however due to the lower bed temperature of printer, there was poor layer adhesion between the adjacent printed layers. Additionally, from the flame test, it was found that adding 20 wt% unmodified lignin in HIPS did not exhibit any improvement in flame retardant capacity of HIPS.

4.6 References

[1] Wang X, Jiang M, Zhou Z, Gou J, Hui D. 3D printing of polymer matrix composites : A review and prospective. Compos Part B 2017;110:442–58. https://doi.org/10.1016/j.compositesb.2016.11.034.

[2] Bachtiar D, Sapuan SM, Khalina A, Zainudin ES, Dahlan KZM. The flexural, impact and thermal properties of untreated short sugar palm fibre reinforced high impact polystyrene (HIPS) composites. Polym Polym Compos 2012;20:493–502. https://doi.org/10.1177/096739111202000510.

[3] Wang L, Sun Q. Study on the flame retardancy of high impact polystyrene composites filled with organic-modified carbon nanotubes. Plast Rubber Compos 2020;8011. https://doi.org/10.1080/14658011.2020.1723316.

[4] Xia Y, Liu R, Lyu X, Zhang H, Wang Q, Guo J, et al. Study on kenaf flame retarded by halogen-free flame retardant/HIPS composites. Fibers Polym 2014;15:2181–5. https://doi.org/10.1007/s12221-014-2181-9.

[5] Yang D, Hu Y, Li H, Wang J, Song L, Xu H, et al. Flammability and carbonization of high-impact polystyrene/α-zirconium phosphate nanocomposites. Iran Polym J (English Ed 2015;24:1069–75. https://doi.org/10.1007/s13726-015-0394-4.

[6] Gordobil O, Egüés I, Llano-Ponte R, Labidi J. Physicochemical properties of PLA lignin blends. Polym Degrad Stab 2014;108. https://doi.org/10.1016/j.polymdegradstab.2014.01.002.

[7] Prieur B, Meub M, Wittemann M, Klein R, Bellayer S, Fontaine G, et al. Phosphorylation of lignin to flame retard acrylonitrile butadiene styrene (ABS). Polym Degrad Stab 2016;127:32–43. https://doi.org/10.1016/j.polymdegradstab.2016.01.015.

[8] Song P, Cao Z, Fu S, Fang Z, Wu Q, Ye J. Thermal degradation and flame retardancy properties of ABS/lignin: Effects of lignin content and reactive compatibilization. Thermochim Acta 2011;518:59–65. https://doi.org/10.1016/j.tca.2011.02.007.

[9] Barzegari MR, Alemdar A, Zhang Y, Rodrigue D. Thermal analysis of highly filled composites of polystyrene with lignin. Polym Polym Compos 2013;21:357–66. https://doi.org/10.1177/096739111302100604.

[10] Ghavidel N, Fatehi P. Synergistic effect of lignin incorporation into polystyrene for producing sustainable superadsorbent. RSC Adv 2019;9:17639–52. https://doi.org/10.1039/c9ra02526j.

[11] Kai D, Zhang K, Jiang L, Wong HZ, Li Z, Zhang Z, et al. Sustainable and antioxidant lignin-polyester copolymers and nanofibers for potential healthcare applications. ACS Sustain Chem Eng 2017;5:6016–25. https://doi.org/10.1021/acssuschemeng.7b00850.

[12] Domínguez-Robles J, Martin N, Fong M, Stewart S, Irwin N, Rial-Hermida M, et al. Antioxidant PLA composites containing lignin for 3D printing applications: a potential material for healthcare applications. Pharmaceutics 2019;11:165. https://doi.org/10.3390/pharmaceutics11040165.

[13] Chen S, Lin S, Hu Y, Ma M, Shi Y, Liu J, et al. A lignin-based flame retardant for improving fire behavior and biodegradation performance of polybutylene succinate. Polym Adv Technol 2018;29:3142–50. https://doi.org/10.1002/pat.4436.

[14] Bertini F, Canetti M, Cacciamani A, Elegir G, Orlandi M, Zoia L. Effect of ligno-derivatives on thermal properties and degradation behavior of poly(3-hydroxybutyrate)-based biocomposites. Polym Degrad Stab 2012;97:1979–87. https://doi.org/10.1016/j.polymdegradstab.2012.03.009.

[15] Gkartzou E, Koumoulos EP, Charitidis CA. Production and 3D printing processing of bio-based thermoplastic filament. Manuf Rev 2017;4:1. https://doi.org/10.1051/mfreview/2016020.

[16] Nguyen NA, Barnes SH, Bowland CC, Meek KM, Littrell KC, Keum JK, et al. A path for lignin valorization via additive manufacturing of high-performance sustainable composites with enhanced 3D printability. Sci Adv 2018;4:eaat4967. https://doi.org/10.1126/sciadv.aat4967.

[17] Nguyen NA, Bowland CC, Naskar AK. A general method to improve 3D-printability and inter-layer adhesion in lignin-based composites. Appl Mater Today 2018;12:138–52. https://doi.org/10.1016/j.apmt.2018.03.009.

[18] ASTM International. D3801-19a - Standard Test Method for Measuring the Comparative Burning Characteristics of Solid Plastics in a Vertical Position[1].

[19] Arráez FJ, Arnal ML, Müller AJ. Thermal degradation of high-impact polystyrene with pro-oxidant additives. Polym Bull 2019;76:1489–515. https://doi.org/10.1007/s00289-018-2453-4.

[20] Anwer MAS, Naguib HE, Celzard A, Fierro V. Comparison of the thermal, dynamic mechanical and morphological properties of PLA-Lignin & PLA-Tannin particulate green composites. Compos Part B Eng 2015;82:92–9. https://doi.org/10.1016/j.compositesb.2015.08.028.

[21] Pérez-Guerrero P, Lisperguer J, Navarrete J, Rodrigue D. Effect of modified Eucalyptus nitens lignin on the morphology and thermo-mechanical properties of recycled polystyrene. BioResources 2014;9:6514–26. https://doi.org/10.15376/biores.9.4.6514-6526.

[22] Benini KCCC, Voorwald HJC, Cioffi MOH. Mechanical properties of HIPS/sugarcane bagasse fiber composites after accelerated weathering. Procedia Eng 2011;10:3246–51. https://doi.org/10.1016/j.proeng.2011.04.536.

[23] Akato K, Tran CD, Chen J, Naskar AK. Poly(ethylene oxide)-assisted macromolecular self-assembly of lignin in ABS matrix for sustainable composite applications. ACS Sustain Chem Eng 2015;3:3070–6. https://doi.org/10.1021/acssuschemeng.5b00509.

[24] Thanh Truc NT, Lee BK. Combining ZnO/microwave treatment for changing wettability of WEEE styrene plastics (ABS and HIPS) and their selective separation by froth flotation. Appl Surf Sci 2017;420:746–52. https://doi.org/10.1016/j.apsusc.2017.04.075.

[25] Jung MR, Horgen FD, Orski S V., Rodriguez C. V, Beers KL, Balazs GH, et al. Validation of ATR FT-IR to identify polymers of plastic marine debris, including those ingested by marine organisms. Mar Pollut Bull 2018;127:704–16. https://doi.org/10.1016/j.marpolbul.2017.12.061.

[26] Kumar Singla R, Maiti SN, Ghosh AK. Crystallization, morphological, and mechanical response of poly(lactic acid)/lignin-based biodegradable composites. Polym - Plast Technol Eng 2016;55:475–85. https://doi.org/10.1080/03602559.2015.1098688.

[27] Benwood C, Anstey A, Andrzejewski J, Misra M, Mohanty AK. Improving the impact strength and heat resistance of 3D printed models: structure, property, and processing correlationships during fused deposition modeling (FDM) of poly(lactic acid). ACS Omega 2018;3:4400–11. https://doi.org/10.1021/acsomega.8b00129.

Chapter 5

Summary and future recommendations

5.1 Summary

The effect of lignin in PLA-lignin composite filaments were investigated. With the addition of lignin, gradual decrease in tensile stress and elongation at maximum load was observed. In order to improve mechanical properties, two plasticizers (PEG 2000 and struktol TR451) were added and their effect in thermal, mechanical and morphological properties of PLA_L20 filaments were observed. Among these plasticizers, 2 wt% PEG was significantly able to improve both tensile stress and elongation at maximum load of PLA_L20 filament and 0.5 wt% struktol was able to enhance only the elongation at maximum load. On 3D printed samples, the prepared filaments showed better printability and good layer adhesion.

Additionally, the effect of lignin in thermal, mechanical, morphological, and flame-retardant properties of HIPS were also studied. Adding up to 10 wt% lignin in HIPS showed similar mechanical properties as that of neat HIPS. However, on further adding lignin to 20 wt%, there was decrease in both tensile stress and elongation at break. Also, adding unmodified lignin in HIPS did not improve the flammability of HIPS.

From both the studies, it was found that lignin content and its distribution in polymer matrix greatly affects the properties of composites prepared.

5.2 Recommendations

Filament diameter greatly influence the properties of printed parts. So, it is recommended that in further studies, various strategies can be applied to obtain uniform filament diameter such as double extrusion using twin extruder first and then single screw extruder, maintaining uniform

feed rate, maintaining uniform extrusion and filament spooler speed. Beside this, in the Chapter 3, it was observed that PLA_L20_P2 filament had significantly lower tensile strength than net PLA. This could be improved in 3D printed object by altering various printing parameter. Therefore, it is recommended that future studies can be done on investigation of different 3D printing parameters to print the parts using PLA_L20_P2 biocomposite filaments.

In the study of HIPS-lignin filaments, no strategies were applied to enhance the mechanical properties and flame-retardance of HIPS_L20 composites. Thus, it is recommended that future work can be done on developing HIPS_L20 composite filaments having better mechanical and flame-retarding properties.

Appendix A

Supplementary data of Chapter 3

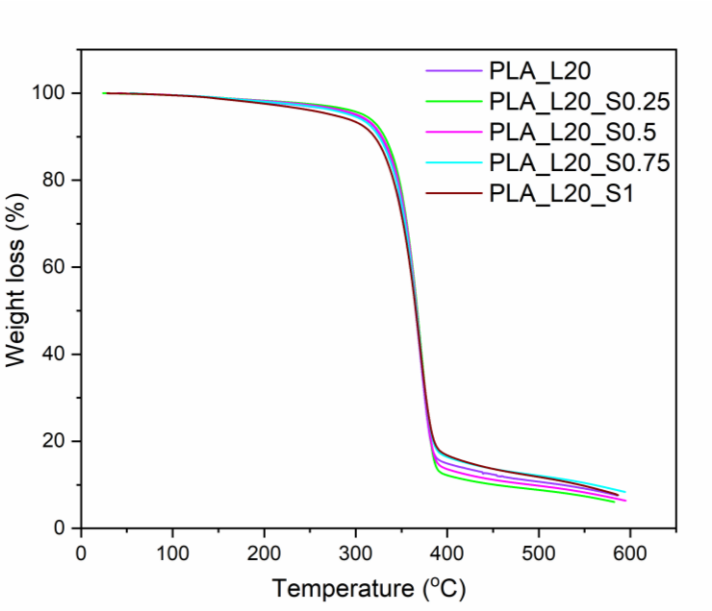

Figure A.1 TG curve of PLA-lignin-struktol composites

Table A.1: Transition temperatures of PLA, PLA-lignin, PLA-lignin-PEG and PLA-lignin-struktol composites

Sample	Tg (°C)	Tcc (°C)	Hcc (J/g)	Tm (°C)	Hm (J/g)
PLA	59.13	121.22	9.62	150.43	13.03
PLA_L5	58.57	120.48	16.56	149.49	17.16
PLA_L10	55.38	119.01	16.68	147.76	15.26
PLA _L15	53.71	119.04	12.83	147.73	14.31
PLA_L20	52.57	112.91	9.19	145.65	14.33
PLA_L20_P0.25	52.06	105.43	9.78	144.76	17.49
PLA_L20_P0.5	52.6	105.8	11.13	143.79	15.84
PLA_L20_P0.75	51.3	108.02	10.08	144.9	15.41
PLA_L20_P1	52.77	108.38	13.45	145.54	14.61
PLA_L20_P2	52.71	106.3	12.50	143.78	22.46
PLA_L20_P3	51.66	109.16	7.77	144.96	13.43
PLA_L20_P4	51.82	113.43	9.66	145.63	14.46
PLA_L20_P5	51.49	107.21	11.15	145.83	15.05
PLA_L20_S0.25	54.53	119.24	15.94	146.67	17.04

PLA_L20_S0.5	51.51	108.24	13.17	142.81	18.97
PLA_L20_S0.75	51.35	109.11	13.15	142.91	18.15
PLA_L20_S1	51.02	108.9	11.31	145.97	15.35

Table A.2: Data presenting mean ± standard deviation of mechanical properties of PLA-lignin composite filaments

Samples	Tensile stress at max. load	Tensile modulus	Elongation at max. load
PLA	57.18 ± 1.52^{a}	1.93 ± 0.21^{b}	4.14 ± 0.42^{a}
PLA_L5	54.93 ± 3.18^{a}	$2.19\pm0.25^{a,b}$	3.60 ± 0.30^{b}
PLA_L10	50.46 ± 3.87^{b}	$2.11\pm0.29^{a,b}$	$3.29\pm0.55^{b,c}$
PLA_L15	49.25 ± 2.77^{b}	2.28 ± 0.36^{a}	3.14 ± 0.32^{c}
PLA_L20	42.90 ± 3.59^{c}	2.26 ± 0.27^{a}	2.94 ± 0.32^{c}

Any two means in the same column with different letters are significantly different ($p<0.05$) by the Tukey's HSD test.

Table A.3: p values obtained from multiple comparison of tensile stress between the PLA-lignin composite filaments using Tukey's test

	PLA	PLA_L5	PLA_L10	PLA_L15	PLA_L20
PLA		0.2850	<0.0001	<0.0001	<0.0001
PLA_L5	0.2850		0.0017	<0.0001	<0.0001
PLA_L10	<0.0001	0.0017		0.8197	<0.0001
PLA_L15	<0.0001	<0.0001	0.8197		<0.0001
PLA_L20	<0.0001	<0.0001	<0.0001	<0.0001	

Table A.4: p values obtained from multiple comparison of modulus between PLA-lignin composite filaments using Tukey's test

	PLA	PLA_L5	PLA_L10	PLA_L15	PLA_L20
PLA		0.0974	0.4252	0.0100	0.0164
PLA_L5	0.0974		0.9309	0.9099	0.9575
PLA_L10	0.4252	0.9309		0.4664	0.5731
PLA_L15	0.0100	0.9099	0.4664		0.9998
PLA_L20	0.0164	0.9575	0.5731	0.9998	

Table A.5: p values obtained from multiple comparison of elongation at max. load between PLA-lignin composite filaments using Tukey's test

	PLA	PLA_L5	PLA_L10	PLA_L15	PLA_L20
PLA		0.0055	<0.0001	<0.0001	<0.0001
PLA_L5	0.0055		0.2528	0.0257	0.0003

PLA_L10	<0.0001	0.2528		0.8539	0.1365
PLA_L15	<0.0001	0.0257	0.8539		0.6510
PLA_L20	<0.0001	0.0003	0.1365	0.6510	

Table A.6: Data presenting mean ± standard deviation of mechanical properties of PLA-lignin-PEG composite filaments

Samples	Tensile stress at max. load	Tensile modulus	Elongation at max. load
PLA	57.18 ± 1.52^{a}	$1.93\pm0.21^{b,c,d}$	4.14 ± 0.42^{a}
PLA_L20	42.90 ± 3.59^{d}	2.26 ± 0.27^{a}	2.94 ± 0.32^{d}
PLA_L20_P0.25	43.32 ± 2.98^{d}	$1.76\pm0.31^{c,d}$	3.47 ± 0.34^{c}
PLA_L20_P0.5	$45.55\pm2.47^{c,d}$	$1.79\pm0.26^{b,c,d}$	$3.63\pm0.46^{b,c}$
PLA_L20_P0.75	$48.12\pm3.34^{b,c}$	$1.77\pm0.32^{b,c,d}$	$3.81\pm0.37^{a,b,c}$
PLA_L20_P1	49.43 ± 3.28^{b}	$1.97\pm0.32^{a,b,c}$	$3.61\pm0.43^{b,c}$
PLA_L20_P2	50.84 ± 4.01^{b}	$2.08\pm0.30^{a,b}$	$3.98\pm0.59^{a,b}$
PLA_L20_P3	50.40 ± 3.67^{b}	$1.96\pm0.25^{a,b,c}$	$3.89\pm0.41^{a,b,c}$
PLA_L20_P4	$47.30\pm2.41^{b,c}$	$1.88\pm0.21^{b,c,d}$	$3.74\pm0.44^{a,b,c}$
PLA_L20_P5	42.39 ± 4.09^{d}	1.62 ± 0.20^{d}	$3.95\pm0.34^{a,b,c}$

Any two means in the same column with different letters are significantly different ($p<0.05$) by the Tukey's HSD test.

Table A.7: p values obtained from multiple comparison of tensile stress between the PLA-lignin-PEG composite filaments using Tukey's test

	PLA	PLA_L20	PLA_L20_P0.25	PLA_L20_P0.5	PLA_L20_P0.75	PLA_L20_P1	PLA_L20_P2	PLA_L20_P3	PLA_L20_P4	PLA_L20_P5
PLA		<0.0001	<0.0001	<0.0001	<0.0001	<0.0001	<0.0001	<0.0001	<0.0001	<0.0001
PLA_L20	<0.0001		1.0000	0.4283	0.0008	<0.0001	<0.0001	<0.0001	0.0100	1.0000
PLA_L20_P0.25	<0.0001	1.0000		0.6741	0.0030	<0.0001	<0.0001	<0.0001	0.0314	0.9986
PLA_L20_P0.5	<0.0001	0.4283	0.6741		0.4740	0.0400	0.0006	0.0026	0.8970	0.1908
PLA_L20_P0.75	<0.0001	<0.0001	0.0030	0.4740		0.9829	0.3922	0.6481	0.9995	0.0001
PLA_L20_P1	<0.0001	<0.0001	<0.0001	0.0400	0.9829		0.9721	0.9982	0.7276	<0.0001

PLA_L20_P2	<0.0001	<0.0001	<0.0001	0.0006	0.3922	0.9721		1.0000	0.0885	<0.0001
PLA_L20_P3	<0.0001	<0.0001	<0.0001	0.0026	0.6481	0.9983	1.0000		0.2135	<0.0001
PLA_L20_P4	<0.0001	0.0100	0.0314	0.8970	0.9995	0.7276	0.0885	0.2135		0.0021
PLA_L20_P5	<0.0001	1.0000	0.9986	0.1908	0.0001	<0.0001	<0.0001	<0.0001	0.0021	

Table A.8: p values obtained from multiple comparison of modulus between the PLA-lignin-PEG composite filaments using Tukey's test

	PLA	PLA_L20	PLA_L20_P0.25	PLA_L20_P0.5	PLA_L20_P0.75	PLA_L20_P1	PLA_L20_P2	PLA_L20_P3	PLA_L20_P4	PLA_L20_P5
PLA		0.0297	0.7464	0.9078	0.8188	1.0000	0.8676	1.0000	0.9999	0.0598
PLA_L20_P0.25	0.0297		<0.0001	0.0001	<0.0001	0.0978	0.7093	0.0683	0.0047	<0.0001
PLA_L20_P0.5	0.7464	<0.0001		1.0000	1.0000	0.4573	0.0355	0.5517	0.9677	0.9340
PLA_L20_P0.75	0.8188	<0.0001	1.0000	1.0000		0.5445	0.0511	0.6395	0.9845	0.8911
PLA_L20_P1	1.0000	0.0978	0.4573	0.6829	0.5445		0.9811	1.0000	0.9927	0.0167
PLA_L20_P2	0.8676	0.7093	0.0355	0.0882	0.0511	0.9811		0.9599	0.5221	0.0003
PLA_L20_P3	1.0000	0.0683	0.5517	0.7691	0.6395	1.0000	0.9599		0.9976	0.0256
PLA_L20_P4	0.9999	0.0047	0.9677	0.9964	0.9845	0.9927	0.5221	0.9976		0.2311
PLA_L20_P5	0.0598	<0.0001	0.9340	0.7947	0.8911	0.0167	0.0003	0.0256	0.2311	

Table A.9: p values obtained from multiple comparison of elongation at max. load between the PLA-lignin-PEG composite filaments using Tukey's test

	PLA	PLA_L20	PLA_L20_P0.25	PLA_L20_P0.5	PLA_L20_P0.75	PLA_L20_P1	PLA_L20_P2	PLA_L20_P3	PLA_L20_P4	PLA_L20_P5
PLA		<0.0001	0.0010	0.0381	0.5174	0.0271	0.9900	0.8330	0.2282	0.9679
PLA_L20	<0.0001		0.0228	0.0005	<0.0001	0.0008	<0.0001	<0.0001	<0.0001	<0.0001
PLA_L20_P0.25	0.0010	0.0228		0.9884	0.4341	0.9949	0.0357	0.1707	0.7578	0.0618
PLA_L20_P0.5	0.0381	0.0005	0.9884		0.9727	1.0000	0.4083	0.8031	0.9994	0.5387
PLA_L20_P0.75	0.5174	<0.0001	0.4341	0.9727		0.9513	0.9850	1.0000	1.0000	0.9963
PLA_L20_P1	0.0271	0.0008	0.9949	1.0000	0.9513		0.3377	0.7364	0.9981	0.4605
PLA_L20_P2	0.9900	<0.0001	0.0357	0.4083	0.9850	0.3377		0.9999	0.8603	1.0000
PLA_L20_P3	0.8330	<0.0001	0.1707	0.8031	1.0000	0.7364	0.9999		0.9934	1.0000
PLA_L20_P4	0.2282	<0.0001	0.7578	0.9994	1.0000	0.9981	0.8603	0.9934		0.9320
PLA_L20_P5	0.9679	<0.0001	0.0618	0.5387	0.9963	0.4605	1.0000	1.0000	0.9320	

Table A.10: Data presenting mean ± standard deviation of mechanical properties of PLA-lignin-struktol composite filaments

Samples	Tensile stress at max. load	Tensile modulus	Elongation at max. load
PLA	57.18±1.52^{a}	1.93±0.21^{b,c}	4.14±0.42^{a}
PLA_L20	42.90±3.59^{b}	2.26±0.28^{a}	2.94±0.32^{c}
PLA_L20_S0.25	45.88±3.82^{b}	2.09±0.27^{a,b}	3.25±0.28^{b,c}
PLA_L20_S0.5	44.81±2.44^{b}	1.71±0.25^{c}	3.65±0.67^{b}
PLA_L20_S0.75	42.97±2.79^{b}	1.87±0.28^{b,c}	3.21±0.44^{b,c}
PLA_L20_S1	44.36±3.14^{b}	2.08±0.35^{a,b}	3.20±0.50^{b,c}

Any two means in the same column with different letters are significantly different ($p<0.05$) by the Tukey's HSD test.

Table A.11: p values obtained from multiple comparison of tensile stress between the PLA-lignin-struktol composite filaments using Tukey's test

	PLA	PLA_L20	PLA_L20_S0.25	PLA_L20_S0.5	PLA_L20_S0.75	PLA_L20_S1
PLA		<0.0001	<0.0001	<0.0001	<0.0001	<0.0001
PLA_L20	<0.0001		0.0779	0.5012	1.0000	0.7611
PLA_L20_S0.25	<0.0001	0.0779		0.9208	0.0920	0.7275
PLA_L20_S0.5	<0.0001	0.5012	0.9208		0.5460	0.9984
PLA_L20_S0.75	<0.0001	1.0000	0.0920	0.5460		1.0000
PLA_L20_S1	<0.0001	0.7611	0.7275	0.9984	0.7991	

Table A.12: p values obtained from multiple comparison of modulus between the PLA-lignin-struktol composite filaments using Tukey's test

	PLA	PLA_L20	PLA_L20_S0.25	PLA_L20_S0.5	PLA_L20_S0.75	PLA_L20_S1
PLA		0.0189	0.6424	0.2633	0.9919	0.7004
PLA_L20	0.0189		0.5150	<0.0001	0.0030	0.4562
PLA_L20_S0.25	0.6424	0.5150		0.0049	0.2878	1.0000
PLA_L20_S0.5	0.2633	<0.0001	0.0049		0.6101	0.0066
PLA_L20_S0.75	0.9919	0.0030	0.2878	0.6101		0.3363
PLA_L20_S1	0.7004	0.4562	1.0000	0.0066	0.3363	

Table A.13: p values obtained from multiple comparison of elongation at max. load between the PLA-lignin-struktol composite filaments using Tukey's test

	PLA	PLA_L20	PLA_L20_S0.25	PLA_L20_S0.5	PLA_L20_S0.75	PLA_L20_S1
PLA		<0.0001	<0.0001	0.0497	<0.0001	<0.0001

PLA_L20	<0.0001		0.4140	0.0007	0.5880	0.6296
PLA_L20_S0.25	<0.0001	0.4140		0.1690	0.9998	0.9994
PLA_L20_S0.5	0.0497	0.0007	0.1690		0.0922	0.0791
PLA_L20_S0.75	<0.0001	0.5880	0.9998	0.0922		1.0000
PLA_L20_S1	<0.0001	0.6296	0.9994	0.0791	1.0000	

Table A.14: Values of storage modulus and glass transition temperature of PLA, PLA-lignin, PLA-lignin-PEG and PLA-lignin-struktol composites

Sample	Storage modulus (GPa)	Glass transition (Tg)
PLA	2.19±0.16	64.96±0.11
PLA_L5	2.76±0.19	64.09±0.68
PLA_L10	2.77±0.25	64.43±0.47
PLA_L15	2.81±0.25	61.20±0.98
PLA_L20	2.65±0.36	61.08±2.35
PLA_L20_S0.25	2.61±0.32	59.44±1.08
PLA_L20_S0.5	2.18±0.04	61.67±0.2
PLA_L20_S0.75	2.16±0.43	59.34±0.49
PLA_L20_S1	2.02±0.23	60.92±0.56
PLA_L20_P0.25	2.58±0.10	60.56±1.59
PLA_L20_P0.5	2.57±0.12	60.42±0.36
PLA_L20_P0.75	2.43±0.07	60.75±0.34
PLA_L20_P1	2.39±0.19	59.20±0.59
PLA_L20_P2	2.56±0.39	59.12±0.86
PLA_L20_P3	2.33±0.17	60.36±0.59
PLA_L20_P4	1.58±0.09	60.43±0.02
PLA_L20_P5	2.03±0.11	60.83±0.69

Appendix B

Supplementary data of Chapter 4

Table B.1: p values obtained from multiple comparison of tensile strength between HIPS-lignin composite filaments using Tukey's test

	HIPS	HIPS_L5	HIPS_L10	HIPS_L15	HIPS_L20
HIPS		0.4346	0.7196	0.9715	0.0201
HIPS_L5	0.4346		0.0327	0.8109	<0.0001
HIPS_L10	0.7196	0.0327		0.3408	0.3334
HIPS_L15	0.9715	0.8109	0.3408		0.0031
HIPS_L20	0.0201	<0.0001	0.3334	0.0031	

Table B.2: p values obtained from multiple comparison of modulus between HIPS-lignin composite filaments using Tukey's test

	HIPS	HIPS_L5	HIPS_L10	HIPS_L15	HIPS_L20
HIPS		0.0854	0.2834	0.9639	0.8394
HIPS_L5	0.0854		0.9757	0.3179	0.0050
HIPS_L10	0.2834	0.9757		0.6770	0.0282
HIPS_L15	0.9639	0.3179	0.6770		0.4441
HIPS_L20	0.8394	0.0050	0.0282	0.4441	

Table B.3: p values obtained from multiple comparison of elongation at break between HIPS-lignin composite filaments using Tukey's test

	HIPS	HIPS_L5	HIPS_L10	HIPS_L15	HIPS_L20
HIPS		0.9972	0.1240	0.0074	<0.0001
HIPS_L5	0.9972		0.2418	0.0197	<0.0001
HIPS_L10	0.1240	0.2418		0.8196	<0.0001
HIPS_L15	0.0074	0.0197	0.8196		<0.0001
HIPS_L20	<0.0001	<0.0001	<0.0001	<0.0001	